

Beiträge zur Meereskunde

Contributions to Marine Scientific Research

Heft 56 · 1987

Contents

WOLFGANG FENNEL, DAVID HALPERN, HANS ULRICH LASS	
Current spectra at the Equator	3
ANDREAS IRMISCH	
Investigations on the dissolved carbohydrates in the Baltic Sea (in German)	19
HANS ULRICH LASS, REINHARD SCHWABE, WOLFGANG MATTHÄUS, EBERHARD FRANCKE	
On the dynamics of water exchange between Baltic and North Sea	27
DIETWART NEHRING et al.	
Results of oceanological studies in the Mozambique Channel in February—March 1980	51
HARTMUT PRANDKE, ADOLF STIPS	
To the effect of different pronounced micro-structure of temperature and salinity in thermo-haline discontinuity layers (in German)	65
HERBERT SIEGEL	
On the relationship between the spectral reflectance and inherent optical properties of oceanic water	73
<i>Scientific note</i>	81

Beiträge zur Meereskunde

Contributions to Marine Scientific Research

9 April 1987

Heft 56 · 1987



Akademie der Wissenschaften der DDR
Institut für Meereskunde

Beiträge zur Meereskunde

Contributions to Marine Scientific
Research

Die „Beiträge zur Meereskunde“ erscheinen in unregelmäßiger Folge und in fortlaufender Nummerierung ihrer Hefte. Publiziert werden Originalbeiträge zur wissenschaftlichen Meeresforschung, insbesondere zu meeresphysikalischen, -chemischen, -geologischen und -biologischen Problemen sowie zur Entwicklung der Meeresforschungstechnik. Manuskriptsendungen werden erbeten an den Herausgeber: Prof. Dr. sc. Klaus Voigt, Institut für Meereskunde, DDR-2530 Rostock-Warnemünde. Es können Originalarbeiten in deutscher, englischer und russischer Sprache eingereicht werden. Von jedem Beitrag werden 70 Sonderdrucke kostenfrei geliefert. Um Beachtung der Hinweise für Autoren auf der 3. Umschlagseite wird gebeten.

*

The “Beiträge zur Meereskunde” is published at irregular intervals and numbered consecutively. It is a medium for the publication of original articles on the marine scientific research: the physical and chemical oceanography, the marine geology and biology as well as the marine research technology. Manuscripts should be submitted to the editor: Prof. Dr. sc. Klaus Voigt, Institut für Meereskunde, DDR-2530 Rostock-Warnemünde,

Begründet von ERICH BRUNS

Herausgegeben von KLAUS VOIGT

unter Mitwirkung von HANS-JÜRGEN BROSEN,
LUTZ BRÜGMANN, DIETER LANGE, WOLFGANG
MATTHÄUS, DIETWARD NEHRING, KLAUS STRIGGOW
und MANFRED STURM (Schriftleitung)

German Democratic Republic. Original contributions are accepted in German, English or Russian. 70 reprints of each article published will be supplied free of charge. See the last page for Note to Contributors which will be printed alternately in English and Russian.

*

Журнал „Beiträge zur Meereskunde“ не является периодическим изданием, но с порядковой нумерацией. В журнале публикуются оригинальные статьи, посвященные научным исследованиям морей и океанов, в частности физическим, химическим, геологическим и биологическим проблемам моря, а также развитию технических средств исследования морей. Авторские рукописи просим высыпать в адрес издателя: Prof. Dr. sc. Klaus Voigt, Institut für Meereskunde, DDR-2530 Rostock-Warnemünde, Германская Демократическая Республика. Статьи принимаются на немецком, английском или русском языках. Автору высылается бесплатно 70 отдельных экземпляров оттисков. Просим обратить внимание на инструкцию для авторов, находящуюся на последней странице. Инструкция печатается попеременно на английском и русском языках.



Akademie der Wissenschaften der DDR
Institut für Meereskunde

Beiträge zur Meereskunde

Contributions to Marine Scientific Research

Akademie der Wissenschaften der DDR
Institut für Meereskunde
Heft 56 · 1987
253 Warnemünde
Deutsche Demokratische Republik
7987.373

Inhalt

WOLFGANG FENNEL, DAVID HALPERN, HANS ULRICH LASS Strömungsspektren am Äquator (in Englisch)	3
ANDREAS IRMISCH Untersuchungen über die gelösten Kohlenhydrate in der Ostsee	19
HANS ULRICH LASS, REINHARD SCHWABE, WOLFGANG MATTHÄUS, EBERHARD FRANCKE Zur Dynamik des Wasseraustausches zwischen Ost- und Nordsee (in Englisch)	27
DIETWARD NEHRING u. a. Ergebnisse ozeanologischer Untersuchungen im Moçambique-Kanal im Februar/März 1980 (in Englisch)	51
HELMUT PRANDKE, ADOLF STIPS Zur unterschiedlichen Ausprägung der Mikrostruktur von Temperatur und Salzgehalt in thermohalinen Sprungschichten	65
HERBERT SIEGEL Zum Zusammenhang zwischen dem spektralen Remissionskoeffizienten und den inhärenten optischen Eigenschaften des Ozeanwassers (in Englisch)	73
<i>Wissenschaftliche Kurzmitteilung</i>	81

WOLFGANG FENNEL, DAVID HALPERN, HANS ULRICH LASS	
Current spectra at the Equator	
ANDREAS IRMISCH	
Investigations of the dissolved carbohydrates in the Baltic Sea (in German)	
HANS ULRICH LASS, REINHARD SCHWABE, WOLFGANG MATTHÄUS, EBERHARD FRANCKE	
On the dynamics of water exchange between Baltic and North Sea	
DIETWART NEHRING et al.	
Results of oceanological studies in the Mozambique Channel in February—March 1980	
HARTMUT PRANDKE, ADOLF STIPS	
To the effect of different pronounced microstructure of temperature and salinity in thermo-haline discontinuity layers (in German)	
HERBERT SIEGEL	
On the relationship between the spectral reflectance and inherent optical properties of oceanic water	
<i>Scientific note</i>	

ISBN 3-05-500264-4
ISSN 0067-5148

Erschienen im Akademie-Verlag Berlin, DDR-1086 Berlin, Leipziger Straße 3—4
© Akademie-Verlag Berlin 1987
Lizenznummer: 202 · 100/441/87
Printed in the German Democratic Republic
Gesamtherstellung: VEB Druckerei „Thomas Müntzer“, 5820 Bad Langensalza
Lektor: Dipl.-Phys. Helga Müller
Umschlaggestaltung: Michael Schmidt
LSV 1465
Bestellnummer: 763 681 5 (2105/56)

Beitr. Meereskd., Berlin 56 (1987) S. 3—18

WOLFGANG FENNEL, DAVID HALPERN, and HANS ULRICH LASS

Current spectra at the Equator

With 13 figures and 1 table

ВОЛЬФГАНГ ФЕННЕЛЬ, ДАВИД ХАЛПЕРН, ХАНС УЛЬРИХ ЛАСС	
3 Спектры течения на экваторе (на английском языке)	3
АНДРЕАС ИРМИШ	
19 Исследования о растворенных углеводах в Балтийском море (на немецком языке)	19
ХАНС УЛЬРИХ ЛАСС, РАЙНХАРД ШВАБЕ, ВОЛЬФГАНГ МАТТЕУС, ЭБЕРХАРД ФРАНКЕ	
27 О динамике водообмена Балтийского моря с Северным (на английском языке)	27
ДИТВАРТ НЕРИНГ и другие	
51 Результаты океанологических исследований в Мозамбикском проливе с февраля до марта 1980-го года (на английском языке)	51
ХАРТМУТ ПРАНДКЕ, АДОЛЬФ ШТИПС	
65 О различном проявлении микроструктуры температуры и солености в термохалинных слоях скачков (на немецком языке)	65
ХЕРБЕРТ ЗИГЕЛЬ	
73 О связи между коэффициентом диффузного отражения и собственными оптическими характеристиками океанской воды (на английском языке)	73
81 Научное сообщение	81

Abstract: We discuss spectra of the zonal and meridional current component derived from two years long time series measured at the equator in the eastern Pacific (111° W) in 15 and 100 m depth. These spectra are compared with theoretically calculated spectra.

The theory is based on the linear, hydrostatic Boussinesq-equations for a continuously stratified, unbounded ocean on the equatorial β -plane. Dissipation is accounted for in terms of Rayleigh friction and Newtonian cooling with the same relaxation parameter. The stratification is governed by a constant Brunt Väisälä Frequency (BVF) in the upper layer and an exponentially decreasing BVF below.

On the model acts a wind considered as a volume force evenly distributed within the upper layer. The wind is sinusoidal in zonal direction and Gaussian distributed perpendicular to the equator. The time behaviour of the wind is modelled by means of a step function.

The solution theory is based on a Green's-function technique. We find a good resemblance of measured and theoretically estimated spectra for the dissipation parameter $r = 2\pi/1$ years, and for a wind with the zonal wave number $k_0 = -2\pi/(3000 \text{ km})$ and a meridional scale $L_a = 1000 \text{ km}$.

Zusammenfassung: Es werden Spektren der zonalen und meridionalen Strömungskomponenten, die aus zweijährigen Zeitreihen im östlichen Pazifik (111° W) am Äquator in 15 und 100 Metern Tiefe gewonnen wurden, diskutiert und mit theoretisch ermittelten Spektren verglichen.

Die Theorie basiert auf den linearen, hydrostatischen Boussinesq-Gleichungen für einen geschichteten, unberandeten Ozean auf der äquatorialen β -Ebene. Als Dissipationsmechanismus wird Rayleigh-Reibung und Newtonsche Abkühlung mit gleicher Relaxationskonstante verwendet. Die Schichtung wird durch eine konstante Brunt-Väisälä-Frequenz (BVF) in der Deckschicht und eine exponentiell abnehmende BVF in der unteren Schicht modelliert.

Der auf das Modell wirkende Wind wird als Volumenkraft angenommen, die gleichmäßig über die Deckschicht verteilt ist. Das Windfeld sei zonal periodisch und habe meridional die Form einer Gauß-Verteilung. Das zeitliche Verhalten des Windes wird durch eine Einschaltfunktion simuliert.

Als Lösungskonzept wird eine Green-Funktions-technik verwendet. Eine sehr gute Übereinstimmung der gemessenen und theoretischen Spektren ergibt sich mit einem Dissipationsparameter $r = 2\pi/(1 \text{ Jahr})$, für ein Windfeld mit der zonalen Wellenzahl $k_0 = -2\pi/(3000 \text{ km})$ und einer meridionalen Skale $L_a = 1000 \text{ km}$.

Резюме: В статье обсуждаются спектры зональных и меридиональных компонент течения в восточном Тихом Океане, которые получились из ряда с длительностью больше двух лет в глубинах 15 м и 100 м. Измеренные спектры сравниваются с теоретическими.

Теория основана на линейных квазистационарных уравнениях Буссинеска для океана с неизменной стратификацией и с плоским дном на неограниченной β -плоскости. В качестве механизма диссипации мы применяем трение Рэлея и охлаждение по Ньютону с одинаковой постоянной диссипацией. Мы обсуждаем модель двух слоев с постоянной частотой Вайссала-Брента в поверхностном слое и с падающей по показательной функции частотой Вайссала-Брента в низком слое.

На эту модель действует ветер в виде силы по объему, которая распространяется одинаково в поверхностном слое океана. Поведение ветра по времени изображается функцией включения. Поле ветра в зональном направлении является периодическим и в меридиональном направлении описывается функцией Гаусса.

Концепция решения основана на функции Грина. Измеренные и теоретические спектры показывают очень хорошее совпадение при параметре

диссипации $r = 2\pi/\text{год}$, для поля с зональным числом волн $k_0 = 2\pi/3000 \text{ км}$ и с меридиональным масштабом $L_a = 1000 \text{ км}$.

1. Introduction

From March 1980 to April 1982 continuous current measurements have been conducted on the equator in the eastern Pacific at 111° W . The technical details of the measurements can be found in HALPERN (1983). In the present paper we consider spectra which are derived from these time series.

A choice of spectra of the zonal and meridional current components at 15 m, and 100 m depth are displayed in Figs. 1 to 4. Near the surface, i.e. at 15 m, the zonal-current spectrum depicted in Fig. 1 increases continuously with decreasing frequency. In 100 m depth, however, the spectrum shows some saturation for periods larger than about 100 days, see Fig. 2.

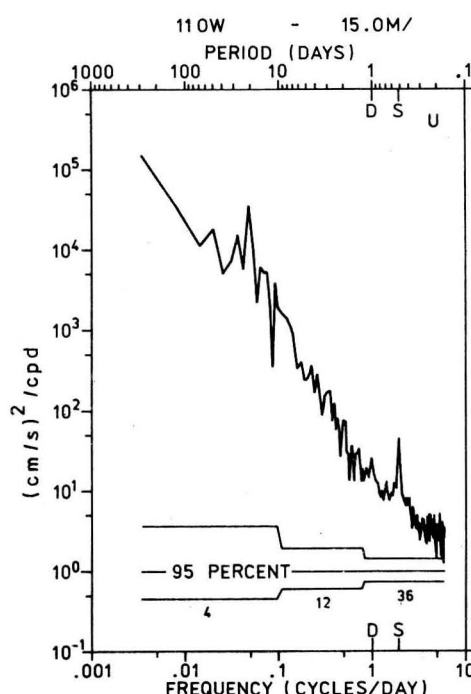


Fig. 1
Spectrum of the zonal current at the equator in the Eastern Pacific at 111° W in the upper mixed, $z = -15 \text{ m}$

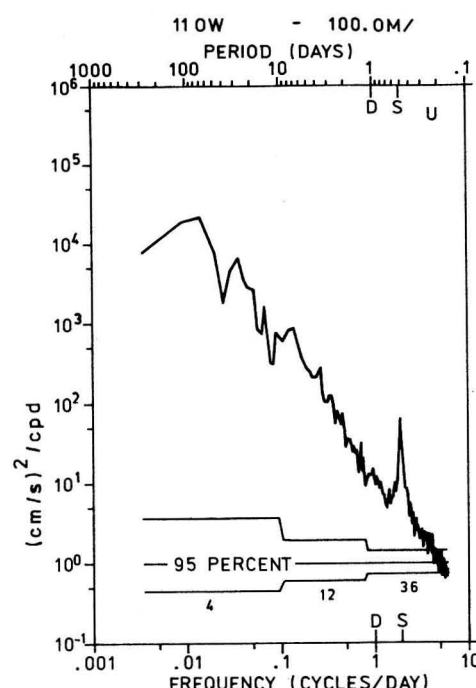


Fig. 2

Spectrum of the zonal current at the equator in the Eastern Pacific at 111° W within the thermocline, $z = -100 \text{ m}$

The meridional spectra appear to be saturated in the low frequency domain in both 15 m and 100 m depth, as can be seen from Figs. 3 and 4. All spectra exhibit various peaks in the range of periods less than, say, 50 days. A predominant peak can be observed around 20 days. This peak is prominent in particular in the near surface meridional spectrum.

The overall structure of the near surface zonal spectrum resembles sea level spectra found at near equatorial islands in the Pacific, see WUNSCH and GILL (1976), and LUTHER (1980).

In order to compare these findings with theoretical results we consider in Section 2 the forcing problem for an unbounded, linear, stratified ocean on the equatorial β -plane. The theory is based on a Green's-function technique and is an extension of a first approach of FENNEL and LASS (1983). Though the general results can be transformed in the formulas given by CANE and SARACHIK,

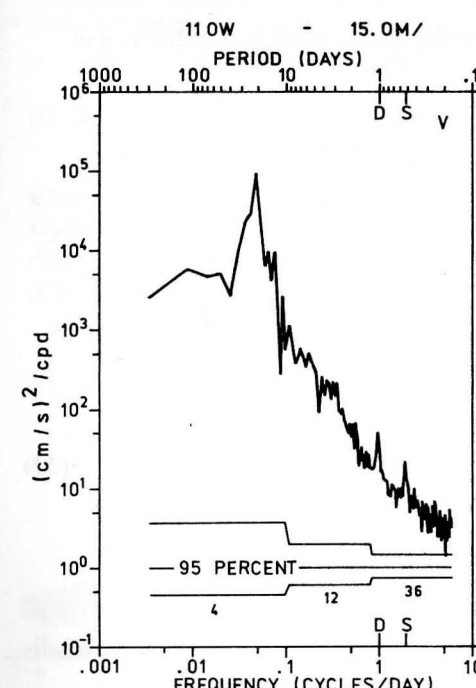


Fig. 3

Spectrum of the meridional current at the equator in the Eastern Pacific at 111° W in the upper mixed layer, $z = -15 \text{ m}$

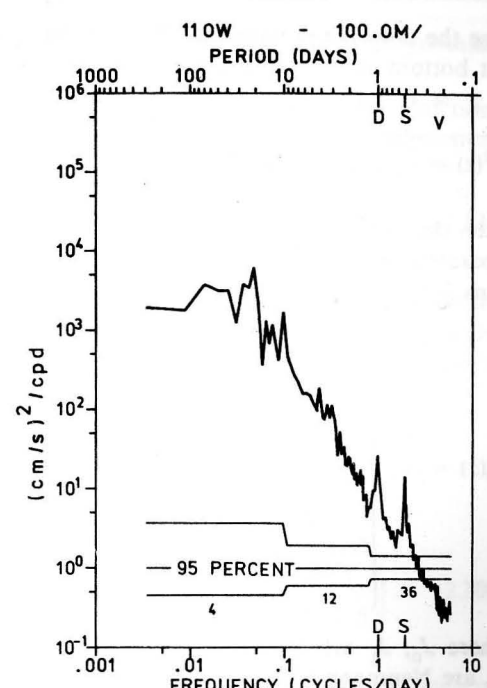


Fig. 4

Spectrum of the meridional current at the equator in the Eastern Pacific at 111° W within the thermocline, $z = -100 \text{ m}$

(1976), it seems that the Green's-function concept provides the most general and compact formulation of the formal solution of the forcing problem.

In Section 3 and 4 we apply the general results for examples of meridional and zonal volume forces Gaussian distributed in meridional direction around the equator. The properties of the forcing in the frequency-wave number domain have been chosen in accordance with the spectral properties of the wind fields reported by LUTHER (1980). In Section 5 and 6 we discuss the theoretically obtained spectra, and we compare the results with the measured spectra in Section 7.

2. The general formal solution

In this section we give a detailed description how a compact formulation of the general

solution of the equatorial forcing problem can be obtained on the basis of the Green's-function concept. We start with the linear Boussinesq equations on the unbounded equatorial β -plane

$$u_t + ru - \beta y v + p_x = X \quad (2.1)$$

$$v_t + rv + \beta y u + p_y = Y \quad (2.2)$$

$$u_x + v_y - \left(\frac{1}{N^2} (p_{tz} + rp_z) \right)_z = 0. \quad (2.3)$$

The subscripts x , y , z and t denote partial derivatives, p is the perturbation pressure divided by a standard density, and X , Y are the wind forces which are considered to act through the upper mixed layer of thickness h like body forces, see e.g. LIGHTHILL (1969). As dissipation mechanism Rayleigh friction and Newtonian cooling with the same relaxation parameter r has been assumed. Other-

wise the notation is standard. We consider a flat bottom at $z = -H$ and a rigid surface at $z = 0$, and adopt an exponential BVF

$$N^2(z) = \begin{cases} N_1^2 & \text{for } 0 \geq z \geq -h \\ N_2^2 e^{2a(h+z)} & \text{for } -h \geq z \geq -H \end{cases} \quad (2.4)$$

Then the z -dependence of u , v , and p can be separated in terms of the vertical eigenfunctions $F_m(z)$:

$$F_m(z) = A_m \begin{cases} \frac{N_1 \cos(N_1 \lambda_m z)}{\sin N_1 \lambda_m (H-h)} \left[J_0\left(\frac{\lambda_m}{a} N_2\right) - \frac{J_0\left(\frac{\lambda_m}{a} N(-H)\right)}{Y_0\left(\frac{\lambda_m}{a} N(-H)\right)} Y_0\left(\frac{\lambda_m}{a} N_2\right) \right] & 0 \geq z > -h \\ N(z) \left[J_1\left(\frac{\lambda_m}{a} N(z)\right) - \frac{J_0\left(\frac{\lambda_m}{a} N(-H)\right)}{Y_0\left(\frac{\lambda_m}{a} N(-H)\right)} Y_1\left(\frac{\lambda_m}{a} N(z)\right) \right] & -h \geq z > -H \end{cases} \quad (2.5)$$

where J_0 , J_1 are Bessel functions, and Y_0 , Y_1 are Neumann functions which should not be confused with the meridional forcing component. A_m is a normalization constant of the m -th mode, and the λ_m 's are the vertical eigenvalues, see FENNEL, LASS (1979) for more detail.

We expand u , v , p , X , and Y in terms of the vertical eigenfunctions

$$(u, v, p, X, Y) = \sum_m (u_m, v_m, p_m, X_m, Y_m) F_m(z). \quad (2.6)$$

Then with (2.6) we obtain after Fourier transformation of (2.1) to (2.3) with respect to x and t the set

$$-i\bar{\omega}u_m - \beta yv_m + ikp_m = X_m, \quad (2.7)$$

$$-i\bar{\omega}v_m + \beta yu_m + p_{my} = Y_m, \quad (2.8)$$

$$iku_m + v_{my} - i\bar{\omega}\lambda_m^2 p_m = 0 \quad (2.9)$$

with $\bar{\omega} = \omega + ir$. From the above set we find in the usual manner the following equation for v_m alone

$$v_{ss}(\omega, k, y) + \left(q + \frac{1}{2} - \frac{s^2}{4} \right) v(\omega, k, y)$$

$$= i \frac{(\bar{\omega}^2 \lambda^2 - k^2)}{2\lambda\beta\bar{\omega}} Y + \sqrt{\frac{\lambda}{2\beta}} \frac{s}{2} X + \frac{k}{\bar{\omega} \sqrt{2\lambda\beta}} X_s \quad (2.10)$$

where the abbreviation $s = \sqrt{2\lambda\beta} y$, and

$$2q + 1 = \frac{(\bar{\omega}^2 \lambda^2 - k^2)}{\lambda\beta} - \frac{k}{\lambda\bar{\omega}} \quad (2.11)$$

have been introduced. The vertical mode index m has been dropped. We note that for integer q , i.e. $q = 0, 1, 2, 3, \dots$ (2.11) yields the well-known dispersion relation of free ETW's,

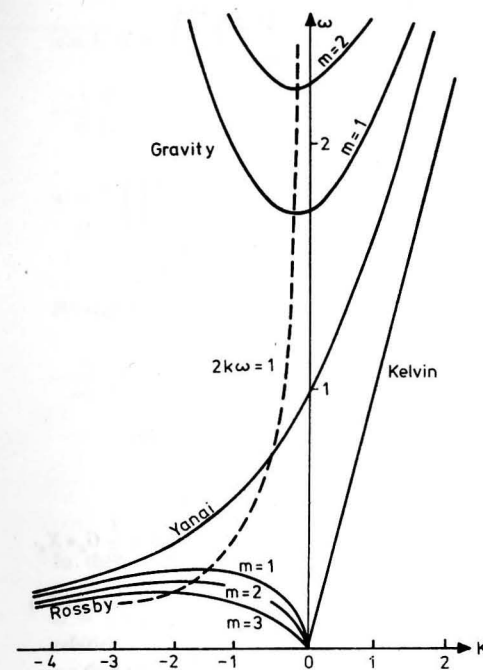


Fig. 5
Dispersion diagram of free equatorially trapped waves showing the different roots of the dispersion relation (2.11) in the ω - k -plane. In this figure ω and k are scaled with $\sqrt{\lambda/\beta}$ and $1/\sqrt{\lambda/\beta}$, respectively

where $\Gamma(-q)$ is Euler's Gamma function. Now we can construct the Green's function and obtain

$$G(q, s; s') = \theta(s - s') G^>(q, s; s') + \theta(s' - s) G^<(q, s; s') \quad (2.16)$$

with

$$\begin{aligned} G^>(q, s; s') &= -\frac{\Gamma(-q)}{\sqrt{2\pi}} D_q(s) D_q(-s') \\ &= G^<(q, s'; s). \end{aligned} \quad (2.17)$$

Here $\theta(s - s')$ is the step function. We note that for integer q , it follows

$$D_n(s) = \frac{e^{-s^2/4}}{2^{n/2}} H_n\left(\frac{s}{\sqrt{2}}\right) \quad (2.18)$$

where $H_n\left(\frac{s}{\sqrt{2}}\right)$ is the Hermite polynomial of n -th order. Moreover, the gamma function $\Gamma(-q)$ has poles at $q = n$, with the expansion

$$\Gamma(-q) \rightarrow \frac{(-1)^n}{n!(n-q)} \quad (2.19)$$

in the vicinity of the poles. Therefore, a partial fraction expansion of (2.16) and (2.17) yields a bilinear representation of the Green's function in terms of Hermite functions

$$G(q, s; s') = \sum_{n=0}^{\infty} \frac{e^{-\frac{s^2+s'^2}{4}}}{\sqrt{2\pi}(q-n)n! \cdot 2^n} \times H_n\left(\frac{s}{\sqrt{2}}\right) H_n\left(\frac{s'}{\sqrt{2}}\right). \quad (2.20)$$

Obviously, the poles of the Green's function at $q = n$ define the dispersion relation of free ETW's, compare (2.11). With (2.16), (2.17) or equivalently, with (2.20) we obtain the formal solution of (2.10) in terms of a source representation

$$\begin{aligned} v(\omega, k, s) &= i \frac{(\bar{\omega}^2 \lambda^2 - k^2)}{2\lambda\beta\bar{\omega}} G * Y \\ &+ \sqrt{\frac{\lambda}{2\beta}} G * \frac{s'}{2} X + \frac{k}{\bar{\omega} \sqrt{2\lambda\beta}} G * X_{s'}. \end{aligned} \quad (2.21)$$

Here the following convolution integrals have been introduced

$$G * Y = \int_{-\infty}^{+\infty} ds' G(s; s') Y(s') \quad (2.22)$$

$$G * s' X = \int_{-\infty}^{+\infty} ds' s' G(s; s') X(s') \quad (2.23)$$

$$G * X_{s'} = \int_{-\infty}^{+\infty} ds' G(s; s') \frac{\partial}{\partial s'} X(s'). \quad (2.24)$$

Now we may express the remaining quantities u and p in terms of v , and of the external forcing, and obtain with (2.21)

$$\begin{aligned} u(\omega, k, s) &= \sqrt{\frac{\lambda}{2\beta}} \left(\frac{k}{\lambda\bar{\omega}} \frac{\partial}{\partial s} - \frac{s}{2} \right) G * Y \\ &+ \frac{i\bar{\omega}^2\lambda^2}{\bar{\omega}^2\lambda^2 - k^2} \left[X - \left(\frac{k}{\lambda\bar{\omega}} \frac{\partial}{\partial s} - \frac{s}{2} \right) \right. \\ &\times \left. \left(G * \left(\frac{s'}{2} X \right) + \frac{k}{\bar{\omega}\lambda} G * X_{s'} \right) \right] \end{aligned} \quad (2.25)$$

$$\begin{aligned} p(\omega, k, s) &= \frac{1}{\sqrt{2\lambda\beta}} \left(\frac{\partial}{\partial s} - \frac{k}{\lambda\bar{\omega}} \frac{s}{2} \right) G * Y \\ &+ \frac{ik}{\bar{\omega}^2\lambda^2 - k^2} \left[X - \left(\frac{\lambda\bar{\omega}}{k} \frac{\partial}{\partial s} - \frac{s}{2} \right) \right. \\ &\times \left. \left(G * \frac{s'}{2} X + \frac{k}{\bar{\omega}\lambda} G * X_{s'} \right) \right]. \end{aligned} \quad (2.26)$$

The set (2.21) to (2.26) represents already a general formal solution of the forcing problem of an unbounded equatorial ocean. The physics of the response is governed by the analytical properties of the above expressions in the complex ω -plane. The poles near the origin of the ω -plane correspond to steady, or eventually, to accelerating motion, the poles of the Green's function take the set of the ETW's into account, and the poles at $\omega = k/\lambda$, which occurs only in (2.25) and (2.26), correspond to the equatorial Kelvin wave. Thus this formulation covers the whole catalog of possible response patterns. Ultimately it depends on the structure of the forcing which of these possibilities will be realized.

We may show explicitly, that the poles at $\omega = -k/\lambda$, which also appear in (2.25) and (2.26) do not contribute, because the corresponding residues vanish. To this end we discuss some relations and properties of the general solution and of the Green's function, which may also be useful for further applications of this technique. Using the identities

$$\begin{aligned} \frac{\bar{\omega}}{\bar{\omega}^2 - \left(\frac{k}{\lambda} \right)^2} &= \frac{1}{2} \left(\frac{1}{\bar{\omega} - \frac{k}{\lambda}} + \frac{1}{\bar{\omega} + \frac{k}{\lambda}} \right), \\ \frac{1}{\bar{\omega}^2 - \left(\frac{k}{\lambda} \right)^2} &= \frac{\lambda}{2k} \left(\frac{1}{\bar{\omega} - \frac{k}{\lambda}} - \frac{1}{\bar{\omega} + \frac{k}{\lambda}} \right) \end{aligned}$$

and

$$\begin{aligned} \frac{1}{\bar{\omega} \left(\bar{\omega}^2 - \left(\frac{k}{\lambda} \right)^2 \right)} \\ = - \left(\frac{\lambda}{k} \right)^2 \left(\frac{1}{\bar{\omega}} - \frac{1}{2} \left(\frac{1}{\bar{\omega} - \frac{k}{\lambda}} + \frac{1}{\bar{\omega} + \frac{k}{\lambda}} \right) \right) \end{aligned}$$

we may rewrite the zonal portion of the expressions (2.25), (2.26):

$$\begin{aligned} u(\omega, k, s) &= \sqrt{\frac{\lambda}{2\beta}} \left(\frac{k}{\lambda\bar{\omega}} \frac{\partial}{\partial s} - \frac{s}{2} \right) G * Y \\ &+ \frac{iX *}{2 \left(\bar{\omega} - \frac{k}{\lambda} \right)} (\delta(s - s') + A^-(s) A^-(s') G) \\ &+ \frac{iX *}{2 \left(\bar{\omega} + \frac{k}{\lambda} \right)} (\delta(s - s') + A^+(s) A^+(s') G) + \frac{i}{\bar{\omega}} G_s * X_{s'} \end{aligned} \quad (2.27)$$

$$\begin{aligned} p(\omega, k, s) &= \frac{1}{\sqrt{2\lambda\beta}} \left(\frac{\partial}{\partial s} - \frac{k}{\lambda\bar{\omega}} \frac{s}{2} \right) G * Y \\ &+ \frac{iX *}{2 \left(\bar{\omega} - \frac{k}{\lambda} \right)} (\delta(s - s') + A^-(s) A^-(s') G) \\ &- \frac{iX *}{2 \lambda \left(\bar{\omega} + \frac{k}{\lambda} \right)} (\delta(s - s') + A^+(s) A^+(s') G) + \frac{i}{\bar{\omega}\lambda} G_{s'} * X \end{aligned} \quad (2.28)$$

Here the creation and annihilation operators $A^\pm(s)$

$$A^\pm(s) = \frac{d}{ds} \pm \frac{s}{2}$$

have been introduced. Using well-known identities of the parabolic cylinder functions

$$A^-(s) D_q(\pm s) = \pm D_{q+1}(\pm s)$$

$$A^+(s) D_q(\pm s) = \pm q D_{q-1}(\pm s)$$

we may easily verify, that

$$\begin{aligned} A^-(s) A^-(s') G(q, s; s') &= -\delta(s - s') \\ &+ (q + 1) G(q + 1, s; s') \end{aligned} \quad (2.29)$$

$$\begin{aligned} A^+(s) A^+(s') G(q, s; s') &= -\delta(s - s') \\ &+ q G(q - 1, s; s') \end{aligned} \quad (2.30)$$

Inserting (2.29), (2.30) in (2.27) and (2.28) we find an equivalent formulation for u and p

$$\begin{aligned} u(\omega, k, s) &= \sqrt{\frac{\lambda}{2\beta}} \left(\frac{k}{\lambda\bar{\omega}} \frac{\partial}{\partial s} - \frac{s}{2} \right) G * Y \\ &+ \frac{i}{\bar{\omega}} \frac{\partial}{\partial s} G(q, s; s') * X_{s'} + \frac{i}{2} \left[\frac{(q + 1) G(q + 1, s; s') * X}{\bar{\omega} - \frac{k}{\lambda}} \right. \\ &\left. + \frac{q}{\bar{\omega} + \frac{k}{\lambda}} G(q - 1, s; s') * X \right] \end{aligned} \quad (2.31)$$

$$\begin{aligned} p(\omega, k, s) &= \frac{1}{\sqrt{2\lambda\beta}} \left(\frac{\partial}{\partial s} - \frac{k}{\lambda\bar{\omega}} \frac{s}{2} \right) G * Y \\ &- \frac{i}{\lambda\bar{\omega}} \frac{s}{2} G(q, s; s') * X_{s'} + \frac{i}{2\lambda} \left[\frac{(q + 1) G(q + 1, s; s') * X}{\bar{\omega} - \frac{k}{\lambda}} \right. \\ &\left. - \frac{q G(q - 1, s; s') * X}{\bar{\omega} + \frac{k}{\lambda}} \right]. \end{aligned} \quad (2.32)$$

In these expressions the poles at $\omega = 0$, and at $\omega = \pm k/\lambda$ are separated. For the Kelvin pole $\omega = k/\lambda$ it follows from (2.11) $q = -1$. Taking the relation $-(q + 1) \Gamma(-q - 1) = \Gamma(-q)$ into account we find with (2.16), (2.17)

$$(q + 1) G(q + 1, s; s') * X \xrightarrow{q \rightarrow -1} \Gamma(1) D_0(s) D_0(s') * X = e^{-\frac{s^2+s'^2}{4}} * X.$$

Thus the Kelvin pole corresponds in fact to a forced equatorially trapped wave. By contrast, for the pole at $\omega = -k/\lambda$ it follows $q = 0$, and therefore the corresponding residue vanishes.

Because the Kelvin poles occur only in those term which are due to the zonal forcing X we may conclude that only zonal forcing is able to excite Kelvin waves in the unbounded, linear, equatorial ocean.

Finally we note that the general formal solution given above is equivalent to the formalism of CANE, SARACHIK (1976). This can be seen if we use the bilinear expansion (2.20) of the Green's function. Then the calculation of the convolution, e.g. $G * X$, reduces to the estimation of the coefficients of the Hermite expansion of the forcing functions, and the expressions given by CANE and SARACHIK follow.

3. Solution on the equator

Now we use the results of the previous section in order to estimate spectra on the equator,

i.e. $s = y = 0$. We assume the forcing X and Y to have the following structure

$$\begin{pmatrix} X(\omega, k, s) \\ Y(\omega, k, s) \end{pmatrix} = \begin{pmatrix} X^{(0)}(\omega, k) \\ Y^{(0)}(\omega, k) \end{pmatrix} \Psi_0(s)$$

$$+ \begin{pmatrix} X^{(1)}(\omega, k) \\ Y^{(1)}(\omega, k) \end{pmatrix} \Psi_1(s) \quad (3.1)$$

where Ψ_0 and Ψ_1 are the atmospheric Hermite functions

$$\Psi_0(s) = e^{-\zeta \frac{s^2}{4}} \quad (3.2)$$

$$\Psi_1(s) = \sqrt{2\zeta} s \Psi_0(s) \quad (3.3)$$

and ζ is the squared ratio of the meridional scale L_a of the atmospheric forcing and the oceanic equatorial Rossby radius $\zeta = (L_a/L_R)^2$, $L_R = (\lambda\beta)^{-1/2}$. Inserting (3.1) to (3.3) into (2.21) to (2.26), and putting then $s = 0$ in the resulting expressions we may realize that the meridional portion of the problem amounts to the estimation of the following convolutions of G and Ψ_0

$$\begin{aligned} G * \Psi_0 &= \left(\frac{2}{\zeta + 1} \right)^{1/2} \frac{1}{q} {}_2F_1 \\ &\times \left(-\frac{q}{2}, \frac{1}{2}; 1 - \frac{q}{2}; \frac{\zeta - 1}{\zeta + 1} \right), \end{aligned} \quad (3.4)$$

$$G * s\Psi_0 = 0 \quad (3.5)$$

$$\begin{aligned} G * s' \Psi_0 &= \left(\frac{2}{\zeta + 1} \right)^{3/2} \frac{2}{q(q - 2)} {}_2F_1 \\ &\times \left(-\frac{q}{2}, \frac{3}{2}; 2 - \frac{q}{2}; \frac{\zeta - 1}{\zeta + 1} \right), \end{aligned} \quad (3.6)$$

$$\frac{\partial}{\partial s} G * \Psi_0 = 0 \quad (3.7)$$

$$\begin{aligned} \frac{\partial}{\partial s} G * s' \Psi_0 &= \left(\frac{2}{\zeta + 1} \right)^{3/2} \frac{1}{q - 1} {}_2F_1 \\ &\times \left(-\frac{q}{2}, \frac{3}{2}; \frac{3 - q}{2}, \frac{\zeta - 1}{\zeta + 1} \right), \end{aligned} \quad (3.8)$$

$$\frac{\partial}{\partial s} G * s'^2 \Psi_0 = 0 \quad (3.9)$$

where ${}_2F_1(a, b; c; x)$ is the hypergeometric function

$$\begin{aligned} {}_2F_1(a, b; c; x) &= \frac{\Gamma(c)}{\Gamma(a)\Gamma(b)} \\ &\times \sum_{l=0}^{\infty} \frac{\Gamma(a+l)\Gamma(b+l)x^l}{\Gamma(c+l)l!} \end{aligned}$$

The expressions (3.4) to (3.9) are taken at $s = 0$. These results may be derived from the basic integral

$$\begin{aligned} &\int_0^{\infty} e^{-\zeta s^2/4} D_q(s) ds \\ &= \frac{\sqrt{\pi}}{2^{q/2}(\zeta+1)^{1/2}} \Gamma\left(-\frac{q}{2}+1\right) {}_2F_1\left(-\frac{q}{2}, \frac{1}{2}; \frac{2-q}{2}, \frac{\zeta-1}{\zeta+1}\right) \end{aligned}$$

and using standard identities of the parabolic cylinder functions, and of the hypergeometric function. (Compare, e.g., GRADSTEIN, RYSHIK (1971).) For u , v and p we obtain on the equator

$$\begin{aligned} u(\omega, k, 0) &= \frac{i\bar{\omega}\lambda^2 X^{(0)}(\omega, k)}{\bar{\omega}^2\lambda^2 - k^2} \\ &+ \left[\frac{k}{\bar{\omega}} \left(\frac{\zeta}{\lambda\beta} \right)^{1/2} Y^{(1)}(\omega, k) + \frac{iX^{(0)}(\omega, k)}{\bar{\omega}^2\lambda^2 - k^2} \right. \\ &\quad \left. \times \left(\frac{k^2\zeta}{2\bar{\omega}} - \frac{k\lambda}{2} \right) \right] \left(\frac{2}{\zeta+1} \right)^{3/2} \frac{1}{q-1} \\ &\times {}_2F_1\left(\frac{1-q}{2}, \frac{3}{2}; \frac{3-q}{2}, \frac{\zeta-1}{\zeta+1}\right) \quad (3.10) \end{aligned}$$

$$\begin{aligned} v(\omega, k, 0) &= \left[\frac{i(\bar{\omega}^2\lambda^2 - k^2)}{2\beta\lambda\bar{\omega}} Y^{(0)} + \frac{k}{\bar{\omega}} \sqrt{\frac{\zeta}{\lambda\beta}} X^{(1)} \right. \\ &\times \left(\frac{2}{\zeta+1} \right)^{1/2} \frac{1}{q} {}_2F_1\left(-\frac{q}{2}, \frac{1}{2}; \frac{1-q}{2}, \frac{\zeta-1}{\zeta+1}\right) \\ &+ \sqrt{\frac{\lambda}{\beta}} \left(\frac{1}{\zeta} - \frac{k}{2\bar{\omega}\lambda} \right) X^{(1)} \left(\frac{2\zeta}{\zeta+1} \right)^{1/2} \frac{1}{q(q-2)} \\ &\times {}_2F_1\left(-\frac{q}{2}, \frac{3}{2}; \frac{2-q}{2}, \frac{\zeta-1}{\zeta+1}\right) \quad (3.11) \end{aligned}$$

$$\begin{aligned} p(\omega, k, 0) &= \frac{i\bar{\omega}X^{(0)}}{\bar{\omega}^2\lambda^2 - k^2} \\ &+ \left[\sqrt{\frac{\zeta}{\lambda\beta}} Y^{(1)} - \frac{i(\bar{\omega}\lambda - k\zeta)}{\bar{\omega}^2\lambda^2 - k^2} \frac{1}{2} X^{(0)} \right] \left(\frac{2}{\zeta+1} \right)^{3/2} \\ &\times \frac{1}{q-1} {}_2F_1\left(\frac{1-q}{2}, \frac{3}{2}; \frac{3-q}{2}, \frac{\zeta-1}{\zeta+1}\right) \quad (3.12) \end{aligned}$$

Obviously, u and p are forced by the even zonal and the odd meridional component of the wind, and v is forced by the odd zonal and the even meridional forcing. We note that u , v , p , $X^{(0)}$, $Y^{(0)}$, $X^{(1)}$, $Y^{(1)}$, λ , q , and ζ are implicitly indexed with respect to the vertical mode number m .

4. Calculation of spectra

In order to calculate frequency spectra from (3.10) to (3.11) we have to specify the zonal, and temporal behaviour of the wind forcing. Unfortunately, few is known about the frequency-wave number spectra of the equatorial wind field. Some frequency spectra of the wind components recorded at several near equatorial sites appear to be approximately "red", i.e. they vary like ω^{-1} to $\omega^{-1/2}$, as reported by LUTHER (1980), and GARZOLI and KATZ (1984). Moreover, some peaks have been detected at periods of 4 to 5 days.

We may model the gross behavior of those wind spectra in the time domain by functions such as $\theta(t)$ or $\theta(t)t^{-1/2}$, whose Fourier transformed vary like ω^{-1} or $\omega^{-1/2}$, respectively. We adopt the step function $\theta(t)$ to describe the time behaviour of the forcing, but being aware that this choice may exaggerate the overall slope of the response spectra.

According to LUTHER (1980) the zonal wave-number spectra of the wind components are concentrated in a small band in the vicinity of $k = 0$. While the energy maxima of the zonal wind spectra are nearly symmetrically distributed around $k = 0$, the most energetic part of the meridional wind spectra appear to be shifted into the domain of small negative wave numbers. The zonal scales of the wind

ranging from about 3000 km to one circumference of the earth. Thus we try to model the wave-number spectra of the forcing by Dirac's delta function, which is peaked at a small wave number k_0 . Let us assume

$$(X(x, y, z, t), Y(x, y, z, t))$$

$$= \frac{1}{h} (u_*^2, v_*^2) \theta(t) e^{ik_0 x} e^{-\frac{y^2}{2L_a}} \theta(z+h) \quad (4.1)$$

where u_* and v_* are the friction velocities

$$(u_*^2, v_*^2) = \left(\frac{\tau^x}{\rho_0}, \frac{\tau^y}{\rho_0} \right),$$

with τ^x and τ^y being the zonal and meridional wind stress components, respectively, and ρ_0 is a standard density of the ocean. Moreover, h is the thickness of the wind mixed layer. The expansion of (4.1) in terms of the vertical eigenfunction (2.5) amounts to the expansion of the step function $\theta(z+h)$:

$$\theta(z+h) = \sum_{m=1}^{\infty} b_m F_m(z) \quad (4.2)$$

with

$$\begin{aligned} b_m &= \frac{1}{H} \int_{-H}^0 dz \theta(z+h) F_m(z) \\ &= + \frac{A_m}{\lambda_m} \left[J_0\left(\frac{\lambda_m}{a} N_1\right) \right. \\ &\quad \left. - \frac{J_0\left(\frac{\lambda_m}{a} N(-H)\right)}{Y_0\left(\frac{\lambda_m}{a} N(-H)\right)} Y_0\left(\frac{\lambda_m}{a} N_1\right) \right]. \quad (4.3) \end{aligned}$$

In order to obtain nondimensional eigenfunctions the following normalization has been chosen

$$\frac{1}{H} \int_{-H}^0 F_m^2(z) dz = 1.$$

We adopt the following numerical values of the parameters $H = 4000$ m, $h = 75$ m,

$a^{-1} = 1400$ m, $N_1 = 5.8 \cdot 10^{-3}$ s $^{-1}$, and $N_2 = 1.6 \cdot 10^{-3}$ s $^{-1}$, which reasonably fit for the equatorial oceans (see e.g. FENNEL, LASS 1979). The corresponding eigenvalues, and the projection coefficients are listed in Table 1 for the first ten modes. Moreover, the values of the vertical eigenfunctions within ($z = -10$ m), and below ($z = -300$ m) the thermocline have been included in Table 1.

Obviously, the projection coefficients of the step function i.e. those of the body force (4.1) converge rather slowly. Using Parseval's theorem

$$\frac{h}{H} = \frac{1}{H} \int_{-H}^0 \theta^2(z+h) dz = \sum_{m=1}^{\infty} b_m^2 \approx \sum_{m=1}^M b_m^2 \quad (4.4)$$

we find that the sum of the first ten coefficients ($M = 10$) reproduce almost 70% of the forcing function, see Table 1. Clearly, the step function is a rather localized function, closely trapped at the surface, and those functions are known to converge slowly. On the other hand the response of the equatorial ocean can be expected to be less sharply surface trapped than the external body force. Hence the projection coefficients of the response should converge more rapidly. In our numerical examples discussed below we take into account only the first ten modes.

Now we Fourier transform (4.1) with respect to x and t and use the expansion (4.2), and obtain in the notation of (3.1) and (3.2)

$$\begin{aligned} &(X(\omega, k, y, z), Y(\omega, k, y, z)) \\ &= \sum_m (X_m^{(0)}(\omega, k), Y_m^{(0)}(\omega, k)) \Psi_0(s_m) F_m(z) \quad (4.5) \end{aligned}$$

with

$$\begin{aligned} &(X_m^{(0)}(\omega, k), Y_m^{(0)}(\omega, k)) \\ &= \left(\frac{u_*^2}{h}, \frac{v_*^2}{h} \right) b_m \frac{2\pi i}{\omega} \delta(k - k_0). \quad (4.6) \end{aligned}$$

Inserting (4.6) in (3.10) and (3.11), and estimating the inverse Fourier transformation with

Table 1

The first ten vertical eigenvalues λ_m , projections coefficients b_m , approximated Parseval's sums, and eigenfunctions F_m above ($z = -10$ m) and below ($z = -300$ m) the thermocline. Here the following numerical values were adopted: $H = 4$ km, $h = 75$ m, $a^{-1} = 1400$ m, $N_1 = 5.8 \cdot 10^{-3}$ s $^{-1}$, and $N_2 = 1.6 \cdot 10^{-3}$ s $^{-1}$.

mode	λ_m s/m	$100 b_m$	$\frac{H}{h} \sum_{n=1}^m b_n^2$	$F_m(-10$ m)	$F_m(-300$ m)
1	0.36	4.64	0.11	2.47	2.10
2	0.76	-4.43	0.22	-2.37	-0.91
3	1.15	4.17	0.31	2.23	-0.54
4	1.55	-3.88	0.39	-2.01	1.71
5	1.95	-3.58	0.46	-1.92	2.23
6	2.35	3.29	0.52	1.78	-1.98
7	2.75	-3.02	0.57	-1.64	1.09
8	3.16	2.78	0.61	1.52	0.13
9	3.56	-2.56	0.64	-1.42	-1.29
10	3.97	2.37	0.67	1.32	2.07

respect to k , and performing the vertical mode sum we obtain explicitly

$$u(x, 0, z, \omega) = \frac{u_*^2}{\beta h} \frac{e^{-ik_0x}}{\omega} \sum_m b_m F_m(z) \\ \times \beta \left[\frac{\bar{\omega} \lambda_m^2}{\bar{\omega}^2 \lambda_m^2 - k_0^2} + \frac{k_0}{2\bar{\omega}} \frac{(k_0 \zeta - \bar{\omega} \lambda_m)}{\bar{\omega}^2 \lambda_m^2 - k_0^2} \right] \\ \times \left(\frac{2}{\zeta_m + 1} \right)^{3/2} \frac{1}{q_m - 1} \\ \times {}_2F_1 \left(\frac{1 - q_m}{2}, \frac{3}{2}; \frac{3 - q_m}{2}, \frac{\zeta_m - 1}{\zeta_m + 1} \right) \quad (4.7)$$

$$v(x, 0, z, \omega) = \frac{v_*^2}{\beta h} \frac{e^{-ik_0x}}{\omega} \sum_m \frac{b_m F_m(z)}{\lambda_m} \\ \times \frac{\lambda_m^2 \bar{\omega}^2 - k_0^2}{2\bar{\omega}} \left(\frac{2}{\zeta_m + 1} \right)^{1/2} \frac{1}{q_m} \\ \times {}_2F_1 \left(-\frac{q_m}{2}, \frac{1}{2}, \frac{1 - q_m}{2}, \frac{\zeta_m - 1}{\zeta_m + 1} \right). \quad (4.8)$$

The expressions (4.7), (4.8) represent the spectral functions of the horizontal current components on the equator which respond to the forcing (4.1). We may define the spectra S_u and S_v to be the modulus of (4.7) and (4.8), respectively. Taking the square root of the

sum of the squared real and imaginary part of u and v it follows

$$S_u(k_0, z, \omega) = \frac{h\beta}{u_*^2} [(\text{Re } u)^2 + (\text{Im } u)^2]^{1/2} \quad (4.9)$$

$$S_v(k_0, z, \omega) = \frac{h\beta}{v_*^2} [(\text{Re } v)^2 + (\text{Im } v)^2]^{1/2} \quad (4.10)$$

where the spectra have been normalized by the strength of the volume force components, and by the β parameter.

Generally, the expressions (4.7), (4.8), and therefore (4.9), (4.10) have poles in the lower half plane of the complex ω -plane. These poles correspond to peaks of finite height on the real ω -axis. The peak frequencies follow from the transsections of the line $k = k_0$ and the dispersion curves in the dispersion diagram of free equatorially trapped waves. For the meridional component only the even, for the zonal component only the odd equatorial trapped modes contribute to the spectra right on the equator. For positive k_0 the inertia-gravity, and the Yanai wave are excited, while for negative k_0 also the Rossby waves contribute. Moreover, in the zonal

current spectra a jet, which for $k_0 = 0$ is confined to the upper mixed layer, and in case of positive k_0 the equatorial Kelvin wave may occur. Therefore the zonal spectrum should be expected to be more energetic in the low frequency range than the meridional spectrum, where these portion of the response is absent.

In the following two sections we estimate the spectra at the depths $z = -10$ m, and $z = -300$ m, i.e. within and below the upper mixed layer, and vary the friction parameter r , the meridional wind scale L_a , and the zonal wave number within certain intervals.

5. Spectra of the meridional current component

In the following sections we deal with numerical examples of current spectra right on the equator which can be derived from the theory outlined in the previous sections. We start with the spectra of the meridional current component. First we fix the dissipation parameter r , the depth z , and the meridional scale L_a of the forcing, where $r = 2\pi/(1 \text{ year})$, $z = -10$ m, and $L_a = 1000$ km has been adopted, and we vary the zonal wave number k_0 in the interval from zero to $-2\pi/(3000 \text{ km})$. The results are shown in Fig. 6. Moreover, in Fig. 7 we show the spectra for $k_0 = \pm 2\pi/(3000 \text{ km})$. We recognize both striking similarities and differences between these spectra. The similarities can be found in the range of periods smaller than ten days, which corresponds to the excitation of inertia-gravity waves. In this range the spectra appear to consist of a continuum of spikes which may be attributed to the interference of various different vertical and meridional modes.

The differences occur for periods larger than, say, 20 days. For zero and negative wave numbers the spectra are almost constant or lightly increasing. This indicates the effect of the excitation of Rossby waves. Generally these spectra depend only weakly on the magnitude of k_0 . By contrast, for positive wave number the low frequency part of the

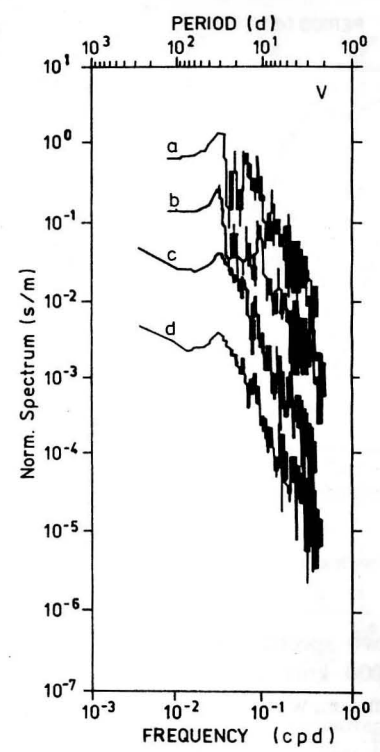


Fig. 6

Theoretical spectra of the meridional current at the equator at 10 m depth with $r = 2\pi/(1 \text{ year})$, $L_a = 10^3$ km for different zonal wave numbers: a) $k_0 = 0$, b) $k_0 = -2\pi/(6L_a)$, c) $k_0 = -2\pi/(4L_a)$, d) $k_0 = -2\pi/(3L_a)$. The curves are subsequently displaced downward by one decade

spectrum has changed dramatically, see Fig. 7. In this case a well developed spectral gap occurs in the low frequency range, which has not been observed in measured equatorial spectra. The best resemblance of measured and theoretical spectra can be found for negative zonal wave numbers of the wind field. This is consistent with the preference of the range of small negative wave numbers in wave-number spectra of the meridional wind, as mentioned by LUTHER (1980) (note that according to (4.8) only the meridional wind component appears in the spectral function).

The most prominent peak occurs in the period range of 10 to 20 days and may be attributed to the excitation of the Yanai wave.

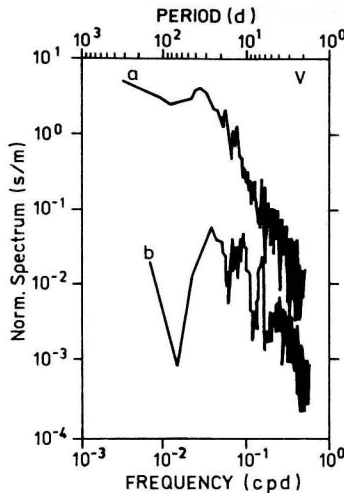


Fig. 7

Same as Fig. 6 with a) $k_0 = -2\pi/(3L_a)$ and b) $k_0 = 2\pi/(3L_a)$

In Fig. 8 two spectra are displayed for $k_0 = -2\pi/(3000 \text{ km})$ at $z = -10 \text{ m}$, and $z = -300 \text{ m}$, i.e., within and below the upper mixed layer. The general shape of both spectra is quite similar, the magnitude however appears to be somewhat reduced below the thermocline.

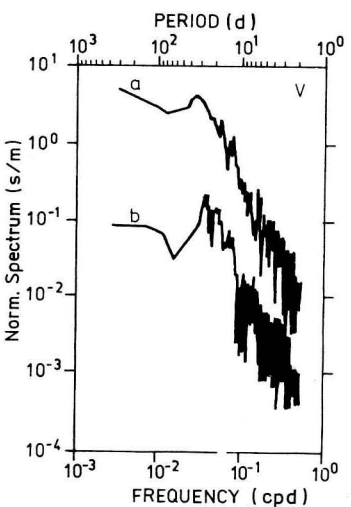


Fig. 8

Theoretical spectra of the meridional current at the equator with $r = 2\pi/(1 \text{ year})$, $L_a = 10^3 \text{ km}$, $k_0 = -2\pi/(3L_a)$ for a) $z = -10 \text{ m}$, b) $z = -300 \text{ m}$. The lower curve is displaced downward by one decade.

The influence of the variation of the meridional scale L_a has been shown in Fig. 9. A threefold increase of L_a enhances slightly the level of the spectrum, and makes it somewhat more spiky. A reduction of L_a to one third suppresses the spectral level, and reduces somewhat the heights of the peaks.

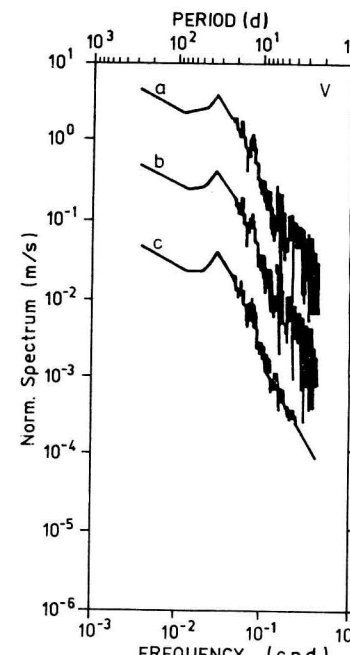


Fig. 9

Theoretical spectra of the meridional current at the equator with $r = 2\pi/(1 \text{ year})$, $k_0 = -2\pi/(3 \cdot 10^3 \text{ km})$, $z = -10 \text{ m}$, for different meridional scales of the forcing: a) $L_a = 3 \cdot 10^3 \text{ km}$, b) $L_a = 10^3 \text{ km}$, and c) $L_a = 3000 \text{ km}$. The curves are subsequently shifted downward by one decade.

Finally, the sensitivity of the spectra to changes of the friction parameter r is shown in Fig. 10. In case of a threefold enhanced r the spectrum becomes unreasonably smoothed, while for $r/2$ the spectrum becomes more spiky in the inertia-gravity range, and has an enhanced magnitude for low frequencies. Thus, the choice of $r = 2\pi/(1 \text{ year})$ seems to be a reasonable order of magnitude of the dissipation parameter.

Generally the theoretical spectra appear to be not very sensitive to small changes of the involved parameters.

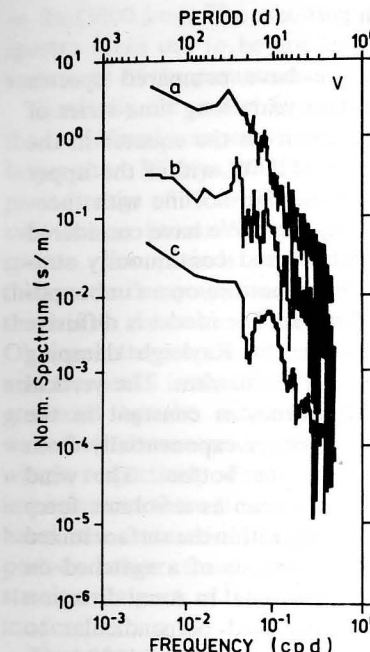


Fig. 10

Theoretical spectra of the meridional current at the equator with $L_a = 10^3 \text{ km}$, $k_0 = -2\pi/(3L_a)$, $z = -10 \text{ m}$, for different dissipation parameter: a) $r = 2\pi/(1 \text{ year})$, b) $r = \pi/(1 \text{ year})$, and c) $r = 6\pi/(1 \text{ year})$. The curves are subsequently shifted downward by one decade.

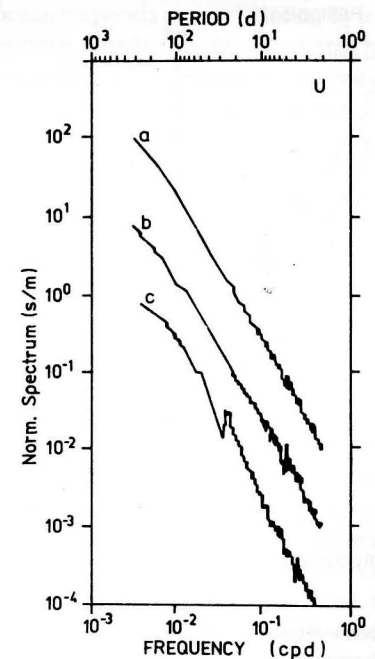


Fig. 11

Theoretical spectra of the zonal current at the equator at 10 m depth with $r = 2\pi/(1 \text{ year})$, $L_a = 10^3 \text{ km}$ for different zonal wave numbers: a) $k_0 = 0$, b) $k_0 = -2\pi/(6L_a)$, c) $k_0 = 2\pi/(6L_a)$. The curves are subsequently shifted downward by one decade.

The main difference between the spectra for $k_0 = \pm 2\pi/(6000 \text{ km})$, which both exhibit some marginal peaks corresponding to ETW's consists in the occurrence of a slight peak in the positive wave number case, which may be attributed to the Kelvin-wave pole at $\bar{\omega} = k_0/\lambda$, compare (4.7).

In Fig. 12 spectra for $k_0 = -2\pi/(3000 \text{ km})$ within and below the upper mixed layer are compared with. Due to the enhanced zonal wave number these spectra are more spiky in the inertia-gravity range and, moreover, we observe some slight indications of Rossby waves. In the low-frequency range the spectral slope appears to be somewhat weakened below the thermocline, i.e. at $z = -300 \text{ m}$. This weakening of the low-frequency slope can also be observed in Fig. 13 where the zonal spectra are shown for $k_0 = \pm 2\pi/(3000 \text{ km})$ at $z = -300 \text{ m}$. For positive wave number we

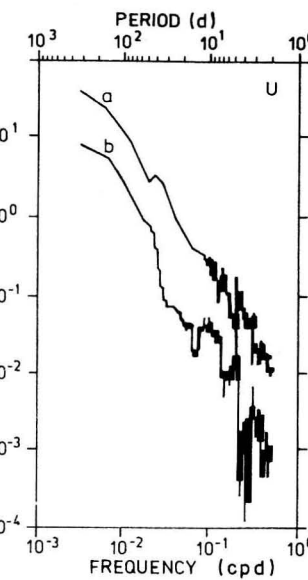


Fig. 12

Theoretical spectra of the zonal current at the equator with $r = 2\pi/(1 \text{ year})$, $L_a = 10^3 \text{ km}$, $k_0 = -2\pi/(3L_a)$ for different depths: a) $z = -10 \text{ m}$, and b) $z = -300 \text{ m}$. The lower curve is displaced by one decade.

find again the Kelvin-wave peak mentioned above.

7. Discussion

In this paper we have compared spectra estimated from two years long time series of the horizontal current on the equator in the eastern Pacific at 111° W within the upper mixed layer and the thermocline with theoretically derived spectra. We have considered a linear, hydrostatic and continuously stratified model with flat bottom on an unbounded equatorial β -plane. The model is diffusive in the interior due to Rayleigh damping Newtonian cooling mechanism. The vertical Brunt-Väisälä frequency is constant in the mixed layer and decays exponentially from the thermocline to the bottom. The wind forcing acts on the ocean as a volume force distributed uniformly within the surface mixed layer. The forcing consists of a switched on pattern which is sinusoidal in zonal direction and Gaussian distributed perpendicular to the equator with a length scale of 1000 km.

Our theoretical concept is based on the Green's-function technique. The response of the meridional current component at the equator is described by a superposition of even equatorially trapped inertia-gravity waves, Yanai- and Rossby waves. The response of the zonal current component is similar in its vertical structure but the amplitudes of the vertical modes consist of odd equatorially trapped waves and additionally of both eastward propagating equatorially trapped Kelvin waves and accelerating surface jets.

Amplitude density frequency spectra have been calculated theoretically for periods ranging from 2 to 300 days for an equatorial site at different depths located within the mixed layer and in the thermocline, taking into account the first ten vertical modes. These theoretical spectra have been compared with spectra estimated from the above mentioned time series.

The best resemblance between observed

and calculated spectra could be achieved by choosing a friction parameter $r = 2\pi/(1 \text{ year})$, the meridional scale of the forcing $L_a = 1000 \text{ km}$ and its zonal wave number $k_0 = 2\pi/(3000 \text{ km})$. The resulting shape of the spectra turns out to be not very sensitive to variations of the parameters.

Generally the model frequency spectra of the meridional component are flat for periods larger than 30 days, and have a peak in the period range of 10 to 30 days, which is, however not as pronounced as in the observed spectra. For periods smaller than 10 days the spectra decay approximately like ω^{-1} and there is an ensemble of superimposed peaks. Obviously the prominent peak at some 10 days and the peaks in the high-frequency part are governed by the excitation of the Yanai wave and the even modes of the inertia-gravity waves, respectively. Friction seems to be less important at these time scales. On the other hand the saturation of the spectrum at periods longer than 30 days indicates the stronger impact of friction on the Rossby modes.

There is no essential difference between the v -spectra within the surface mixed layer and the thermocline suggesting a radiation of the excited waves into the deeper parts of the ocean.

Contrary to the v -spectra both the observed and the modelled u -spectra are red in the low frequency range, i.e. for periods larger than 30 days, at least in the surface mixed layer. This behaviour corresponds to the occurrence of low frequency zonal jets which drain much more energy from the wind field into the ocean than the Rossby waves. The decay of the low frequency part of the u -spectrum with depth, significantly in the observed and but only marginally in the modelled spectra, suggests that these jets are confined to the surface area but may radiate partly into the deep ocean.

The main result of this paper consists in the good agreement of the general shape of observed and modelled near surface current component spectra at the equator. This suggests that in a first order the equatorial

ocean responds to wind forcing by a dynamical pattern which can be described by a linear superposition of inertia-gravity waves, Yanai- and Rossby waves, Kelvin waves, and surface jets.

Finally we note two differences between the observed and the theoretical spectra. In the high-frequency range the decay of the model spectra appears to be exaggerated. As mentioned in Section 4 this is due to the chosen switch on of the wind, i.e. forcing proportional $\theta(t)$. In accordance with the observed wind spectra, e.g. LUTHER (1980), the wind would be better modelled by $\theta(t) t^{-1/2}$ with the Fourier transformed proportional to $\omega^{-1/2}$. In the other words a wind which decays after its 'switch on' would feed more energy into the high-frequency part of the spectrum. This seems to be a more realistic description of the observed wind fields than a simple switch on of a steady wind.

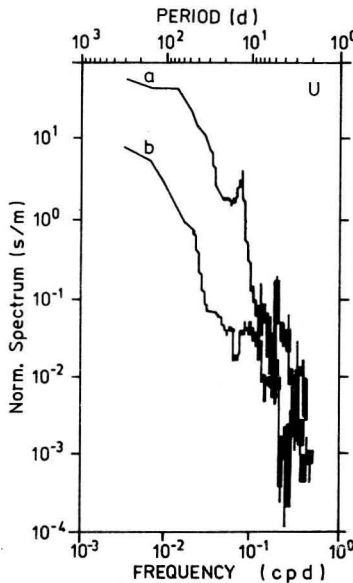
The second difference is the more pronounced peak at the 20 days period in the observed spectra within the surface mixed layer. This may be due to instabilities caused by the large horizontal and vertical current shear of the equatorial mean currents in the surface layer which are not considered in our linear model.

References

- CANE, M. A.; SARACHIK, E. S.: Forced baroclinic ocean motions. I. The linear equatorial unbounded case. — J. Marine Research, Vol. 34 (1976), 629–665.
- FENNEL, W.; LASS, H. U.: On the vertical eigenvalue problem of equatorial trapped waves. — Gerlands Beitr. Geophys., Vol. 88 (1977), 279–293.
- FENNEL, W.; LASS, H. U.: Theory of frequency spectra of equatorial trapped waves, pp. 319–338. In: Hydrodynamics of the equatorial ocean (edited by J. NIHOUL). — Amsterdam/Oxford/New York: Elsevier 1983. 368 pp.
- GARZOLI, S. L.; KATZ, E. J.: Winds at St. Peter and St. Paul Rocks during the first SEQUAL year. — Geophys. Res. Letters, Vol. 11 (1984), 715–718.
- GRADSTEIN, I. S.; RYSHIK, I. M.: Tables of series, products and integrals (in Russ.). — Moscow 1971.

Fig. 13

Same as Fig. 11 but at 300 m depth and for a) $k_0 = 2\pi/(3L_a)$ and b) $k_0 = -2\pi/(3L_a)$.



HALPERN, D.: Variability of the Cromwell Current at 110° W before and during the 1982–83 warm event. — Tropical ocean atmosphere newsletter, No. 21 (1983), 31–34.

LIGHTHILL, M. J.: Dynamics response of the Indian Ocean to onset of the south west monsoon. — Philos. Trans. royal Soc. London, Ser. A., Vol. 265 (1969), 45–92.

LUTHER, O. S.: Observations of long period waves in the tropical oceans and atmosphere. — Techn. Report W.H.O.I. 80-17 Woods Hole 1980, 210 pp.

WUNSCH, C.; GILL, A. E.: Observations of equatorially trapped waves in the Pacific sea level variations. — Deep Sea Research, Vol. 23 (1976), 371–390.

Addresses of the authors:

Dr. sc. WOLFGANG FENNEL, Dr. sc. HANS ULRICH LASS
Akademie der Wissenschaften der DDR
Institut für Meereskunde
DDR-2530 Rostock-Warnemünde

Dr. DAVID HALPERN
School of Oceanography
University of Washington
Seattle, WA 98195
USA

Received: December 5, 1985

Accepted: January 31, 1986

Beitr. Meereskd., Berlin 56 (1987) S. 19–26

ANDREAS IRMISCH

Untersuchungen über die gelösten Kohlenhydrate in der Ostsee

Mit 4 Abbildungen und 3 Tabellen

Zusammenfassung: In der Oberflächenschicht (0 bis 1 m) der Ostsee beträgt die Konzentration der gelösten Kohlenhydrate im Mittel der Jahre 1978, 1980, 1982, 1983 und 1984 0,72–0,84 mg/dm³. Die Einzelwerte schwanken im Bereich von 0,14–1,65 mg/dm³.

Die Kohlenhydratkonzentrationen unterliegen einer jahreszeitlichen Veränderlichkeit, die dem Gang der Phytoplanktonentwicklung ähnelt. Maxima der Kohlenhydratkonzentrationen treten im Sommer auf. Experimente mit eingeschlossenen Planktongemeinschaften erbrachten Hinweise darauf, daß die Zersetzung der Phytoplanktonbiomasse wesentlich am Zustandekommen der sommerlichen Kohlenhydratmaxima in der Ostsee beteiligt sein kann.

In den gelösten Kohlenhydraten ist ein beträchtlicher Energiegehalt gespeichert — nahezu achtmal mehr als in der Phytoplanktonbiomasse.

Abstract: According to investigations in the years 1978, 1980, 1982, 1983 and 1984 the average concentrations of dissolved carbohydrates vary in the surface layer of the Baltic Sea between 0,72 and 0,84 mg/dm³, single values in the range of 0,14 and 1,65 mg/dm³.

The carbohydrate concentrations show seasonal fluctuations, which are similar to the seasonal variations in the phytoplankton productivity. There are experimental evidences, that the carbohydrate maximum in August is caused by the decay of phytoplankton.

In the dissolved carbohydrates eight times more energy can be storaged than in phytoplankton biomass.

Резюме: В 1978, 1980, 1982, 1983 и 1984 годах проводились исследования о растворенных углеводах в Балтийском море. В поверхностном слое (0—1 м) концентрации колеблются в пределах 0,14—1,65 мг/л, средняя концентрация составляет 0,72—0,84 мг/л.

Концентрации углеводов показывают сезонную изменчивость, которая похожа на вариации развития фитопланктона. Максимумы концентраций

углеводов наблюдаются летом. Существуют указания на то, что распад биомассы фитопланктона имеет важное значение при возникновении летнего максимума концентрации углеводов.

В растворенных углеводах накоплено значительное содержание энергии — почти восемь раз больше, чем в биомассе фитопланктона.

1. Einleitung

Die gelösten Kohlenhydrate liegen im Meerwasser in Form eines Gemisches, bestehend hauptsächlich aus Mono- und Oligosacchariden sowie geringen Mengen an Polysacchariden, vor. Diese Substanzen sind im wesentlichen Exsudationsprodukte des Phytoplanktons, gelangen aber auch zu einem nicht unbedeutenden Teil infolge der Autolyse und der mikrobiellen Zersetzung alternder beziehungsweise abgestorbener Algenzellen in Lösung. Eine weitere Quelle für gelöste Kohlenhydrate sind Festlandsabflüsse und atmosphärische Niederschläge.

Kohlenhydrate sind energiereiche Verbindungen und werden größtenteils durch die heterotrophen marinen Mikroorganismen, vor allem Bakterien, verwertet. Die dabei entstehende Biomasse ist ein Nahrungsbestandteil des Zooplanktons. Auf diese Weise sind die gelösten Kohlenhydrate in die Nahrungs-kette des Meeres einzbezogen.

Die Konzentration der gelösten Kohlenhydrate im freien Ozean beträgt durchschnittlich 0,1—0,5 mg/dm³ (ROMANKEVIČ 1984 und die dort referierte Literatur).

Angaben über die Kohlenhydratkonzentrationen in der Ostsee wurden in der zugäng-

lichen Literatur nicht vorgefunden. Es muß jedoch mit höheren Werten als im Ozean gerechnet werden. Grund zu dieser Annahme geben die in der Ostsee zwei- bis dreimal höheren Konzentrationen des gelösten organischen Kohlenstoffs. Hier sind 2 mg C/dm³ charakteristisch (IRMISCH 1984), wohingegen für den Ozean ein Mittelwert von 0,7 mg C/dm³ angenommen wird (WILLIAMS 1975; WANGERSKY 1978).

Ziel der hier vorgestellten Untersuchungen war es, Aufschlüsse über die raum-zeitliche Verteilung der gelösten Kohlenhydrate in der Ostsee zu gewinnen und daraus Kenntnisse über ihre Einbeziehung in den biologisch-chemischen Stoffkreislauf abzuleiten.

Die Probenentnahme erfolgte während der Terminfahrten des Instituts für Meereskunde der AdW der DDR im Januar/Februar,

März/April, Mai, August und Oktober/November der Jahre 1978, 1980, 1982, 1983 und 1984. Abb. 1 zeigt die Lage der bearbeiteten Stationen. Im Jahre 1978 wurden alle verzeichneten Stationen beprobt, um einen möglichst breiten Überblick über die Kohlenhydratverteilung in der Ostsee zu erhalten. In der Folgezeit wurden für einzelne Seengebiete typische Stationen ausgewählt. Dies waren: Stat. 012 — westliche Ostsee, Stat. 113 — Arkonasee, Stat. 213(5A) — Bornholmsee und Stat. 271(15A) — Gotlandsee.

Kohlenhydratmessungen erfolgten auch im Rahmen der Ökologischen Experimente 1981 (ÖKEX 1981), in deren Verlauf die Veränderlichkeit biologischer und chemischer Größen innerhalb eingeschlossener Wasserkörper verfolgt wurde (SCHULZ u. a. 1985).

Die Proben wurden nach der Entnahme

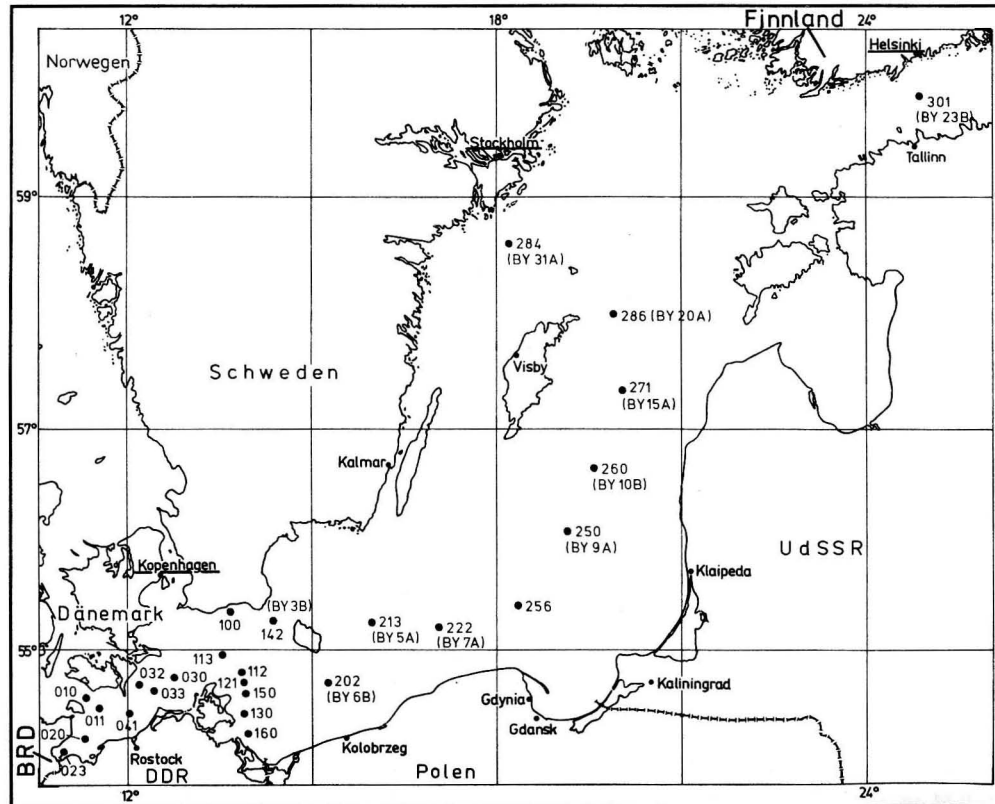


Abb. 1
Stationskarte

Tabelle 1
Mittelwerte der Konzentration der gelösten Kohlenhydrate (mg/dm³) in der Oberflächenschicht (0—1 m) ausgewählter Stationen in der Ostsee

Seengebiet und Stationsbezeichnung	1978			1980			1982		
	m	min	max	m	min	max	m	min	max
westl. Ostsee									
010	0,77	0,47	0,95						
012	0,50	0,14	0,82	0,84	0,60	1,02	0,67	0,46	0,80
023	0,58	0,18	0,80						
Arkonasee									
033	0,52	0,23	1,09						
130	0,88	0,39	1,12						
160	1,00	0,63	1,25						
113	0,66	0,40	0,98	0,79	0,40	1,20	0,75	0,43	1,05
150	0,71	0,23	1,14						
Bornholmsee									
213 (5A)	0,53	0,25	0,92	0,78	0,54	1,01	0,82	0,53	1,10
östl. Gotlandsee									
250 (9A)	0,59	0,19	1,13						
271 (15A)	0,70	0,39	1,17	0,78	0,37	1,08	0,75	0,58	0,98

m — Mittelwert

n — Anzahl der Werte

s — Standardabweichung

Fortsetzung der Tabelle auf S. 22!

über geglättete Glasfaserfilter GF/C filtriert und tiefgefroren aufbewahrt (-20°C). Die Analysen fanden im Labor an Land statt, wobei die Anthronmethode nach LEWIS und RAKESTRAW (1955) zur Anwendung kam. Als Eichsubstanz diente Glucose.

Eine genaue Beschreibung des Analysenganges findet sich bei IRMISCH (1979).

2. Ergebnisse

In Tab. 1 sind die mittleren jährlichen Kohlenhydratkonzentrationen in der Oberflächenschicht der bearbeiteten Ostseestationen zusammengestellt. Die Angaben lassen weder Unterschiede zwischen den einzelnen Stationen noch zwischen den Seengebieten erkennen.

Die Konzentration der gelösten Kohlenhydrate in der Oberflächenschicht der Ostsee unterliegt jahreszeitlichen Schwankungen, die

durch Maximalwerte im Sommer gekennzeichnet sind (Abb. 2). Aus Abb. 2 geht weiterhin hervor, daß die Veränderlichkeiten der Kohlenhydratkonzentration und der Primärproduktion des Phytoplanktons einen gleichsinnigen Verlauf aufweisen.

Die Vertikalverteilung der gelösten Kohlenhydrate soll am Beispiel der Station 271 (15A) im Gotlandtief erläutert werden (Tab. 2). Im Winter und im Spätherbst sind keine eindeutigen vertikalen Konzentrationsunterschiede der gelösten Kohlenhydrate zu erkennen.

Im Frühjahr und Sommer steigen die Kohlenhydratkonzentrationen in der Wasserschicht der oberen 20—30 m ihrer jahreszeitlichen Veränderlichkeit entsprechend an (vgl. Abb. 2). Diese Schicht unterscheidet sich dann durch höhere Kohlenhydratwerte von der übrigen Wassersäule, in der weiterhin keine eindeutige Abhängigkeit dieser Größe von der Wassertiefe besteht.

Tabelle 1 (Fortsetzung)

Seegebiet und Stationsbezeichnung	1983			1984			Mittel über die Jahre					
	m	min	max	m	min	max	m	min	max	s	n	
westl. Ostsee												
012	1,21	0,68	1,65	0,96	0,65	1,38	0,83	0,14	1,65	0,36	25	
Arkonasee												
113	0,82	0,55	1,06	0,72	0,38	0,89	0,75	0,40	1,20	0,22	25	
Bornholmsee												
213 (5A)	0,74	0,46	1,03	0,77	0,60	1,17	0,72	0,25	1,17	0,23	25	
östl. Gotlandsee												
271 (15A)	0,95	0,66	1,28	1,03	0,63	1,32	0,84	0,37	1,32	0,28	23	

Auch eine Besonderheit in der vertikalen Verteilung des gelösten organischen Kohlenstoffs und des Harnstoffs, erhöhte Konzentrationen im anoxischen Milieu (IRMISCH

1984, 1986), konnte im Falle der gelösten Kohlenhydrate nicht beobachtet werden.

Die Untersuchungen mit in durchsichtigen Plastbehältern eingeschlossenen Wasserproben während der Ökologischen Experimente 1981 gaben Gelegenheit, die Konzentrationsänderungen der gelösten Kohlenhydrate von Beginn der Phytoplanktonentwicklung bis zu deren Ende zu verfolgen (Abb. 3 und 4). Während der exponentiellen Entwicklungsphase des Phytoplanktons veränderte sich die Kohlenhydratkonzentration nur wenig. Danach stieg sie stark an, während die Primärproduktion rasch abnahm.

3. Diskussion

Verglichen mit den Konzentrationen der gelösten Kohlenhydrate im Ozean, die überwiegend im Bereich von 0,1–0,5 mg/dm³ liegen (ROMANKEVIĆ 1984), weist die Ostsee

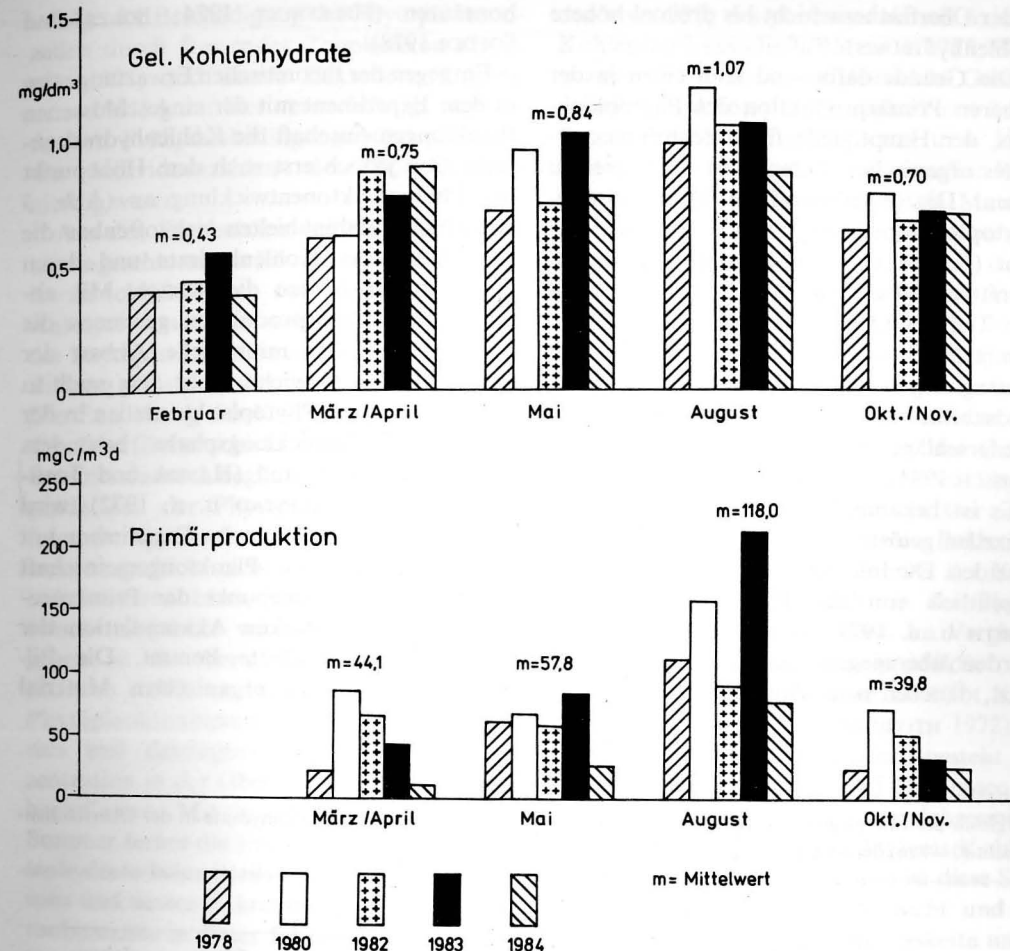


Abb. 2

Die Konzentration der gelösten Kohlenhydrate sowie die Primärproduktion des Phytoplanktons zu verschiedenen Jahreszeiten in der Oberflächenschicht (0–1 m) der Station 113 im Arkonabecken (Primärpr. nach Daten aus dem Inst. f. Meereskunde)

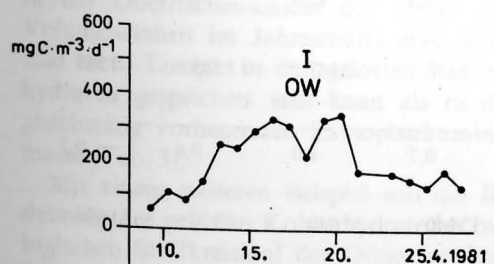


Abb. 3

Die Primärproduktion des Phytoplanktons in Experiment I von ÖKEX 1981 in der Ostsee

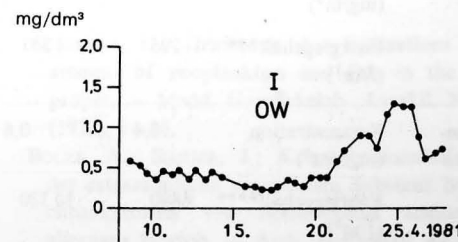


Abb. 4

Die Konzentration der gelösten Kohlenhydrate in Experiment I von ÖKEX 1981 in der Ostsee

in der Oberflächenschicht bis dreimal höhere Kohlenhydratwerte auf.

Die Gründe dafür sind zum einen in der höheren Primärproduktion des Phytoplanktons, der Hauptquelle für autochthones gelöstes organisches Material, in der Ostsee zu sehen. Die Primärproduktion des Ostsee-phytoplanktons beträgt $90-100 \text{ g C m}^{-2}$ pro Jahr (KAISER u. a. 1981) gegenüber durchschnittlich 50 g C m^{-2} /Jahr im überwiegenden Teil des Ozeans (RYTHER 1969). Hinzu kommt, daß die Ostsee einem relativ starken Eintrag organischen Materials durch Festlandsabflüsse und in Form atmosphärischer Niederschläge unterliegt (FONSELIUS 1972; IRMISCH 1984).

Es ist bekannt, daß gesunde Phytoplanktonzellen gelöste organische Substanzen ausscheiden. Die Intensität der Exsudation hängt wesentlich von der Photosyntheserate ab (SMITH u. a. 1977; MAGUE u. a. 1980). Es werden überwiegend Kohlenhydrate freigesetzt, daneben u. a. Aminosäuren und Kar-

bonsäuren (HELLEBUST 1974; BOLZE und SOEDER 1978).

Entgegen der theoretischen Erwartung stieg in dem Experiment mit der eingeschlossenen Planktongemeinschaft die Kohlenhydratkonzentration jedoch erst nach dem Höhepunkt der Phytoplanktonentwicklung an (Abb. 3 und 4). Bis dahin hielten sich offenbar die Freisetzung der Kohlenhydrate und deren heterotropher Abbau die Waage. Mit abnehmender Primärproduktion gewinnen die Autolyse und der mikrobielle Abbau der Algenzellen an Gewicht. Zieht man noch in Betracht, daß die Phytoplanktonzellen in der stationären Entwicklungsphase besonders kohlenhydratreich sind (HANDA und TOMINAGA 1969; MYKLESTAD u. a. 1972), wird verständlich, weshalb es im Experiment mit der eingeschlossenen Planktongemeinschaft erst nach dem Höhepunkt der Primärproduktion zu der starken Akkumulation der gelösten Kohlenhydrate kommt. Die Bildung von gelöstem organischem Material

infolge der Beschädigung der Phytoplanktonzellen durch fressendes Zooplankton (LAMPERT 1978) und dessen Exkretion (BURNETT u. a. 1981) kann hier vernachlässigt werden, da den Frühjahrsbedingungen entsprechend die Individuenzahlen des Zooplanktons niedrig waren.

Aus den Ergebnissen der Untersuchungen an eingeschlossenen Planktongemeinschaften ist zu schlußfolgern, daß in der Ostsee die Autolyse sowie die mikrobielle Zersetzung der Phytoplanktonbiomasse wesentlich an der Bildung gelöster Kohlenhydrate beteiligt sind. Die Entstehung der Kohlenhydratmaxima in der Oberflächenschicht der Ostsee wird im Sommer dadurch begünstigt, daß der überwiegende Teil der Phytoplanktonbiomasse infolge der sperrenden Wirkung der Temperaturprungschicht nicht in größere Tiefen aus sedimentieren kann, sondern in der Deckschicht abgebaut wird. Im Frühjahr hingegen ist die thermische Schichtung noch nicht so stabil, so daß größere Mengen der Phytoplanktonbiomasse tiefer absinken können und deswegen die Kohlenhydratkonzentration in der Oberflächenschicht weniger beeinflussen. Mit zu berücksichtigen ist im Sommer ferner die Freisetzung gelöster Kohlenhydrate beim Freßvorgang des Zooplanktons und dessen Exkretion, da die Zooplanktonbiomasse in dieser Jahreszeit die höchsten Werte erreicht (KAISER und SCHULZ 1985).

Neben der guten Verwertbarkeit durch heterotrophe Mikroorganismen weisen die Kohlenhydrate einen hohen Energiegehalt auf. Überschlagsrechnungen ergeben, daß in der Oberflächenschicht der Ostsee pro Volumeneinheit im Jahresmittel etwa achtmal mehr Energie in den gelösten Kohlenhydraten gespeichert sein kann als in der gleichzeitig vorliegenden Phytoplanktonbiomasse (Tab. 3).

Mit einem weiteren Beispiel soll die Bedeutung der gelösten Kohlenhydrate im biologischen Stoffkreislauf der Ostsee verdeutlicht werden. Es wurde bereits darauf hingewiesen, daß die Exsudationsprodukte des Phytoplanktons hauptsächlich aus Kohlenhydraten bestehen können. Insgesamt wer-

den etwa 20 % des photosynthetisch fixierten Kohlenstoffs exsudiert (WILLIAMS 1975; WANGERSKY 1978). Bei einer jährlichen Gesamtprimärproduktion des Phytoplanktons in der Ostsee von $50 \cdot 10^6 \text{ t C}$ (KAISER u. a. 1981) sind das $10 \cdot 10^6 \text{ t}$ gelöster organischer Kohlenstoff pro Jahr. Das freigesetzte Material besteht überwiegend aus niedermolekularen Verbindungen und wird vor allem durch Bakterien nahezu vollständig abgebaut (ITURRIAGA 1981; LARSSON und HAGSTRÖM 1981). Beträgt die Effizienz, mit der die Bakterien die aufgenommenen organischen Substanzen in Biomasse umwandeln 60 % (LARSSON und HAGSTRÖM 1979), so werden in der Ostsee aus den Exsudationsprodukten des Phytoplanktons jährlich $6 \cdot 10^6 \text{ t}$ partikulärer organischer Kohlenstoff in Form von Bakterienbiomasse erzeugt, fast ein Zehntel der Kohlenstoffmenge, die pro Jahr in der Phytoplanktonbiomasse fixiert wird. Im Vergleich dazu beläuft sich die Jahresproduktion des Ostseezooplanktons auf etwa $1 \cdot 10^6 \text{ t}$ Kohlenstoff (ACKEFORS und HERNROTH 1972).

Bezogen auf den Kohlenstoff, besteht das in der Deckschicht (0–30 m) der Ostsee gelöste organische Material im Jahresmittel zu 9 % bis 14 % (maximal 23 %) aus Kohlenhydraten (IRMISCH 1984). Somit ist diese Substanzklasse aus quantitativer Sicht und infolge ihrer Rolle in der Nahrungskette unbedingt bei Untersuchungen über den biologischen Stoff- und Energiefluß in der Ostsee zu berücksichtigen.

Literatur

- ACKEFORS, H.; HERNROTH, L.: Estimations of the amount of zooplankton and fish in the Baltic proper. — Medd. Havsfiskelab., Lysekil, No. 139 (1972), 1–16.
- BOLZE, A.; SOEDER, J.: Konzentrationsänderungen der extrazellulären organischen Substanz bei Synchronkulturen von *Scenedesmus acutus* var. *alternans* Hortob. — Arch. Hydrobiol. **82** (1978), 142–154.
- BURNETT, C. M.; KENNETH, M. J.; LAVOIE, D. M.; SIEBURTH, J. MCN.: Dissolved carbohydrates and microbial ATP in the north Atlantic: concentrations

Tabelle 3

Vergleich der Energiegehalte der Phytoplanktonbiomasse und der gelösten Kohlenhydrate in der Oberflächenschicht (0–1 m) der Station 113 (Arkonabecken)

	1978					
	Febr.	April	Mai	Aug.	Okt./Nov.	Jahresmittel
Phytoplankton	Chl.a (mg/m ³)*	0,4	1,8	3,8	2,9	1,6
	Kohlenstoff** (mg/m ³)	6,2	27,9	58,9	45,0	24,8
	Energiegehalt*** (J/m ³)	296	1331	2810	2147	1183
						1555
Kohlenhydrate	Konzentration (mg/dm ³)	0,4	0,6	0,7	1,0	0,6
	Energiegehalt**** (J/m ³)	6880	10320	12040	17040	10320
						11696

* Unveröffentlichte Werte des Instituts für Meereskunde, Rostock-Warnemünde

** Umrechnung des Chl.a in Phytoplanktonkohlenstoff nach CUSHING (1958)

*** Umrechnung des Phytoplanktonkohlenstoffs in Energiegehalte nach PLATT und IRWIN (1973)

**** Berechnung des Energiegehaltes der gelösten Kohlenhydrate nach OSTAPENJA und SERGEJEW (1963)

- and interactions. — Deep-Sea Research **26** (1979), 1267—1290.
- CUSHING, D. H.: The estimation of carbon in phytoplankton. — Rapp. Proc. Verb. Reun. Cons. perm. intern. Expl. Mer **114** (1958), 32—33.
- FONSELIUS, S. H.: On biogenic elements and organic matter in the Baltic. — Ambio Special Report, No. 1 (1972), 29—38.
- HELLEBUST, J. A.: Extracellular products. In: W. D. P. STEWART (Hrsg.): Algal physiology and biochemistry. Botanical Monographs, Vol. 10. — Oxford u. a.: Blackwell Scientific Publications 1974, S. 838—863.
- HANDA, N.; Tominaga, H.: A detailed analysis of carbohydrates in marine particulate matter. — Marine Biology **2** (1969), 228—235.
- IRMISCH, A.: Die Bestimmung der gelösten Kohlenhydrate. In: ROHDE, K.-H.; NEHRING, D. (Hrsg.): Ausgewählte Methoden zur Bestimmung von Inhaltsstoffen im Meer- und Brackwasser. — Geod. Geoph. Veröff. R. IV, H. 27 (1979), 52—54.
- IRMISCH, A.: Untersuchungen über den gelösten organischen Kohlenstoff, die gelösten Kohlenhydrate und den Harnstoff in der Ostsee. — Dissertation, Wilhelm-Pieck-Universität Rostock, 1984.
- IRMISCH, A.: Untersuchungen über den gelösten Harnstoff in der Ostsee. — Beitr. Meereskunde, H. 55 (1986), 29—37.
- ITURRIAGA, R.: Phytoplankton assimilated extracellular products, heterotrophic utilisation in marine environment. — Kielner Meeresforschungen, Sonderheft 5 (1981), 318—324.
- KAISER, W.; RENK, H.; SCHULZ, S.: Phytoplankton und Primärproduktion in der Ostsee. — Geod. Geoph. Veröff. R. IV, H. 33 (1981), 27—52.
- KAISER, W.; SCHULZ, S.: Analyse der ozeanologischen Bedingungen in der zentralen Ostsee im Jahre 1984. 2. Biologische Bedingungen. — Unveröff. Bericht des Instituts für Meereskunde, Warnemünde, 1985.
- LAMPERT, W.: Release of dissolved organic carbon by grazing zooplankton. — Limnol. Oceanogr. **23** (1978), 831—834.
- LARSSON, U.; HAGSTRÖM, A.: Phytoplankton exudate release as an energy source for growth of pelagic bacteria. — Marine Biology **52** (1979), 199—206.
- LARSSON, U.; HAGSTRÖM, A.: Fractionated phytoplankton primary production, exudate release, and bacterial production in a Baltic eutrophication gradient. — ICES, Council Meeting 1981/L:13.
- LEWIS, G. J.; RAKESTRAW, N. W.: Carbohydrate in seawater. — J. Marine Research **14** (1955), 253—258.
- MAGUE, T. H.; FRIBERG, E.; HUGHES, D. J.; MORRIS, I.: Extracellular release of carbon by marine phytoplankton; a physiological approach. — Limnol. Oceanogr. **25** (1980), 262—279.
- MYKLESTAD, S.; HAUG, A.; LARSEN, B.: Production of carbohydrates by the marine diatoms *Chaetoceros affinis* var. *willei* (Gran) Hustadt. II. Preliminary investigation of the extracellular polysaccharide. — J. exp. mar. Biol. Ecol. **9** (1972), 137—144.
- OSTAPENJA, A. P.; SERGEEV, A. U.: Der Kaloriengehalt des getrockneten Futters von Wasserevertebraten (russ.). — Voprosy ichtiologii **3** (1963), 177—193.
- PLATT, T.; IRWIN, B.: Caloric content of phytoplankton. — Limnol. Oceanogr. **18** (1973), 306—310.
- ROMANKEVIČ, E. A.: Geochemistry of organic matter in the ocean. — Berlin (West) u. a.: Springer-Verlag 1984.
- RYTHER, J. H.: Phytosynthesis and fish production in the sea. — Science **166** (1969), 72—76.
- SCHULZ, S.; BREUEL, G.; IRMISCH, A.; JOST, G.; SIEGEL, H.: Ergebnisse ökologischer Untersuchungen an eingeschlossenen Planktongemeinschaften der Arkonasee im Frühjahr 1981. — Geod. Geoph. Veröff. R. IV, H. 41 (1985), 1—66.
- SMITH, W. O., Jr.; BARBER, R. T.; HUNTSMAN, S. A.: Primary production off the coast of NW-Africa: excretion of dissolved organic matter and its heterotrophic uptake. — Deep-Sea Research **24** (1977), 35—47.
- WANGERSKY, P. J.: Production of dissolved organic matter. In: KINNE, O. (Hrsg.): Marine Ecology, Bd. 4. — Chichester u. a.: Wiley & Sons 1978, S. 115—200.
- WILLIAMS, P. J. LEB.: Biological and chemical aspects of dissolved organic matter in sea water. In: RILEY, J.; SKIRROW, G. (Hrsg.): Chemical Oceanography, Bd. 2, 2. Aufl. — London: Academic Press 1975, S. 301—363.

Anschrift des Autors:

Dr. ANDREAS IRMISCH

Akademie der Wissenschaften der DDR
Institut für Meereskunde
DDR-2530 Rostock-Warnemünde

Eingereicht: 19. September 1985

Zur Veröffentlichung angenommen: 31. Januar 1986

HANS ULRICH LASS, REINHARD SCHWABE, WOLFGANG MATTHÄUS, and EBERHARD FRANCKE

On the dynamics of water exchange between Baltic and North Sea

With 23 figures and 1 table

Abstract: Subinertial current fluctuations have been observed in the Darss Sill area (Baltic Sea) with time scales of 10—20 days, amplitudes of 40 cm/s and being coherent over distances of at least 150 km simultaneously with baroclinic current fluctuations having time scales of 2—3 days, amplitudes of 60 cm/s and spatial scales of less than 60 km. The currents with shorter time scales were associated with eddy like pattern of the salinity fields.

The low frequency current fluctuations at time scales of 10—20 days change between outflow and inflow regularly near the surface and are directed into the Baltic most of the time close to the bottom.

Evidence for a cross circulation has been found turning clockwise when looking in downstream direction near the surface and being in agreement with the observed up- and down-welling pattern near the coasts.

Transport fluctuations of $1.5 \cdot 10^5 \text{ m}^3/\text{s}$ associated with the current fluctuations of 10—20 days determine the mass balance of the Baltic essentially at these time scales and cause variations of the mean sea level of the Baltic of 10 cm.

The currents at the 10 day time scale in the Darss Sill area are driven by the longitudinal pressure gradient associated with sea level and density differences between the Kattegat and the Baltic. The transverse pressure gradient decreasing always from the surface to the bottom in magnitude adjusts geostrophically within two days to the driving longitudinal pressure gradient.

Zusammenfassung: Subinertiale Strömungsschwankungen mit Amplituden von 40 cm/s und Perioden von 10—20 Tagen, kohärent über mehr als 150 km, überlagert von baroklinen Fluktuationen mit Amplituden von 60 cm/s und Perioden von 2—3 Tagen, kohärent über weniger als 60 km, wurden in der Belt-See im Bereich der Darßer Schwelle beobachtet. Die kurzperiodischen Fluktuationen der Strömung waren

mit dem Auftreten wirbelartiger Strukturen des Massenfeldes verbunden.

Die longitudinale Komponente der 10—20tägigen Strömungsschwankungen wechselt in Oberflächennähe zwischen Ein- und Ausstrom, während in Bodennähe bei geringerer Amplitude der Schwankungen vorwiegend Einstrom beobachtet wird. Mit der zugehörigen transversalen Komponente bildet die longitudinale Komponente eine Querzirkulation in der Belt-See im Sinne einer Rechtsschraube. Die beobachtete Querzirkulation ist konsistent mit dem im Massenfeld beobachteten Wechsel von Auftriebs- und Downwelling-Prozessen an den Küsten der Belt-See.

Mit den beobachteten 10—20tägigen Strömungsfluktuationen sind Transportschwankungen von $1.5 \cdot 10^5 \text{ m}^3/\text{s}$ in der Belt-See verbunden, die die Massenbilanz der Ostsee wesentlich bestimmen und zu Schwankungen des mittleren Wasserstandes der Ostsee von ungefähr 10 cm führen.

Die Überlagerung der barotropen und baroklinen Anteile der longitudinalen Komponente des Druckgradienten korreliert gut mit den beobachteten langperiodischen Strömungsschwankungen, die wiederum mit den transversalen Komponenten des Druckgradienten in der Belt See in geostrophischem Gleichgewicht steht. Damit in Übereinstimmung ist die beobachtete enge Korrelation zwischen longitudinaler und transversaler Wasserstandsdifferenz in der Belt-See, wobei die longitudinale Differenz in der Phasenlage mit annähernd 2 Tagen führt. Eine enge Korrelation besteht auch zwischen transversaler Wasserstandsdifferenz und transversalen baroklinen Druckgradienten bei einer Phasenverschiebung von 180° .

Eine der treibenden Kräfte für den Wasseraustausch zwischen Nord- und Ostsee bei Zeitskalen von 10 bis 20 Tagen sind die Wasserstandsvariationen im Kattegat mit gleichen Zeitskalen.

Резюме: В Балтийском море в районе Дарсского порога наблюдались субинерционные колебания течения амплитудами 40 см/сек и периодами

10—20 суток, которые явились когерентными по длине больше чем 150 км и наложенными бароклинными флюктуациями амплитудами 60 см/сек и периодами 2—3 суток, которые были когерентны по длине меньше чем 60 км. Краткопериодические флюктуации течения были связаны с появлением вихревых структур поля массы.

При продольной компоненте 10—20 суточных колебаний течения в приповерхностном слое чередуют приток и поток, в то время как в придонном слое при меньшей амплитуде колебаний в большинстве случаев наблюдается приток. Вместе с относящейся к ней поперечной компонентой продольная компонента образует попутечную циркуляцию в Балтском море, врачающуюся на поверхности в направлении течения по движению часовой стрелки. Наблюдаемая поперечная циркуляция прочно связана с наблюдаемым в поле массы чередованием апвеллинга и даунвеллинга у берегов Балтского моря.

В связи с обнаруженными 10—20 суточными флюктуациями течения выступают колебания транспорта в Балтском море величиной $1,5 \cdot 10^5 \text{ m}^3/\text{сек}$, значительно определяющие водный баланс Балтийского моря и приводящие к колебаниям среднего уровня моря величиной около 10 см.

Наложение баротропной и бароклинной частей продольной компоненты градиента давления находится в хорошей корреляции с наблюдениями, охарактеризованными длинными периодами колебания течения, которое с другой стороны сохраняет геострофическое равновесие с поперечными компонентами градиента давления в Балтском море.

С упомянутым наложением согласуется наблюдаемая тесная корреляция между продольной и поперечной разностями уровня моря в Балтском море, причем ведущую роль имеет продольная разность с фазой волн около двух дней. Тесная корреляция имеется и между поперечной разностью уровня моря и поперечными градиентами давления при сдвиге фаз в 180° .

Одной из двух сил при обмене водами Северного и Балтийского морей с шкалами времени 10—20 суток являются вариации уровня моря в Каттегатском районе.

1. Introduction

The Baltic can be considered as a large fjord with a characteristic length of 1000 km, typical width of 300 km and a mean depth of 53 m. It is connected with the North Sea via

Kattegat through a system of three straits: first the Little Belt, second the Great Belt both merging into Fehmarn Belt and continuing into Mecklenburg Bight and third the Sound. About 70% of the water exchange between the Baltic and the North Sea takes place through the Belts and the adjacent straits (further on denoted as Belt Sea). The remaining water passes the Sound. North Sea water of high salinity mixed with the outflowing low salinity Baltic water moves more or less continuously along the bottom of the Belt Sea, passes the Darss Sill and penetrates into the deeper parts of the Baltic. However, this water is usually not sufficiently dense to replace the bottom water of the deep basins. The bottom water of the deep basins is replaced by water of high salinity at intervals of several years only. This replacement of stagnant bottom water is essential for the entire ecosystem of the Baltic because it reduces the negative trend in the oxygen conditions of the Baltic deep water. In order to understand the natural and anthropogenic parts of the observed negative oxygen trend it is necessary to understand the physics of the water exchange between the Baltic and the North Sea. This task has attracted oceanographers since the beginning of this century.

KNUDSEN (1899) pointed out that the barotropic part of the water exchange is determined by the large scale wind and air pressure field over the Baltic and the Kattegat which set up the driving sea level differences for the transport through the straits. The baroclinic part of the water exchange he assumed to be driven by the density differences between the saline North Sea and the brackish Baltic. Taking the salt- and massbalance into account he derived his famous theorem and applied it to estimate in- and outflow of the Baltic (KNUDSEN 1900).

WITTING (1918) estimated the terms of the water balance equation of the Baltic due to river inflow, evaporation and precipitation on a time scale of more than a month.

HELA (1944) investigated the daily volume fluctuations of the Baltic and found a typical time scale of ten to twenty days which he

could account for by transport fluctuations through the Danish straits at the same time scale with an order of magnitude of $10^5 \text{ m}^3/\text{s}$ which are about the tenfold of the transport fluctuations on a yearly time scale.

THIEL (1938) and HELA (1944) revealed that in spite of a changing flow direction in the upper layer of the Belt Sea the flow in the bottom layer is directed into the Baltic most of the time.

JENSEN and SINDING (1945) could reveal a semigeostrophic balance between the sea level difference Slipshavn-Korsör and the surface at the Halskov Rev lightship based on monthly mean values.

In several case studies WYRTKI (1953, 1954a, b) investigated the longitudinal momentum balance in the Fehmarn Belt. He found the inertia of the longitudinal current component and the longitudinal pressure gradient due to sea level and density differences between the Kattegat and the Baltic to be essential. Friction he took into account in order to explain phase differences between the observed currents and pressure gradients and to get a stationary momentum balance. Advection of longitudinal momentum was comparable to the other terms of the balance occasionally only.

WYRTKI (1954b) analyzed the dynamical

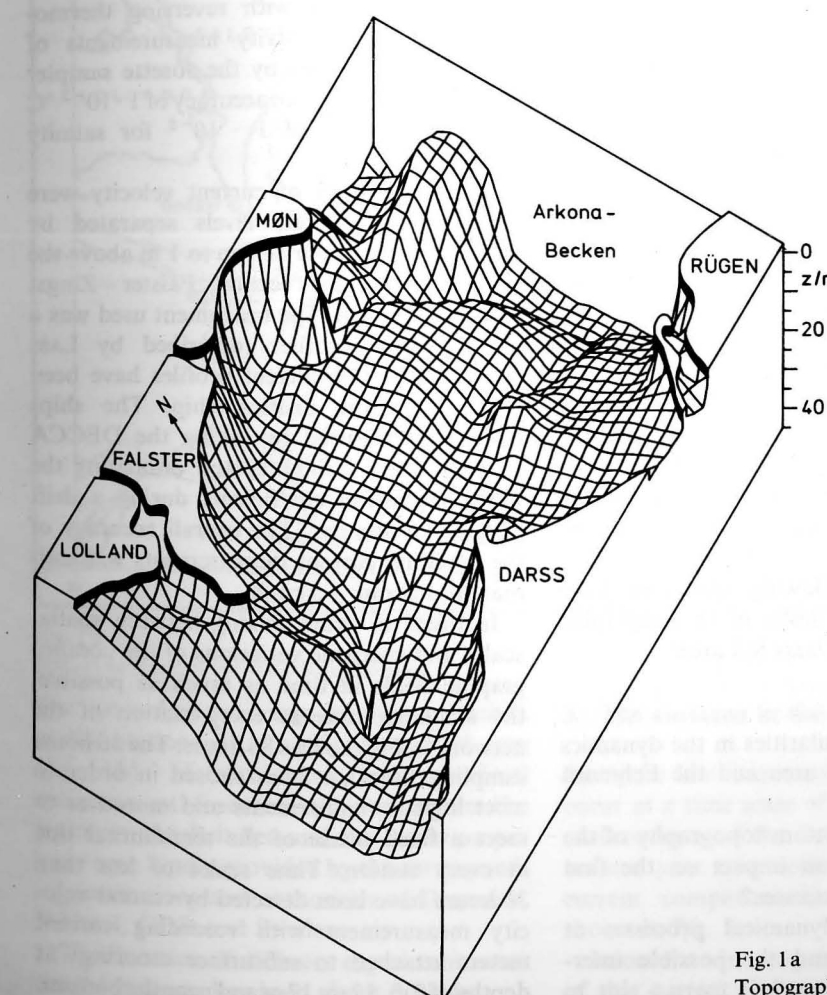


Fig. 1a
Topography of the Darss Sill area

water balance of the Baltic over several years considering the fresh water sources and sinks and the water exchange through the Danish straits. Assuming the inflow into the Baltic to be proportional to the sea level difference between Kattegat and Baltic in his model the Baltic sea level was driven by the sea level in the Kattegat and the fresh water sources in the Baltic.

LANGE (1975) showed that the longitudinal current component in the Fehmarn Belt on a time scale of two days is determined by corresponding fluctuations of the east component of the wind over the Baltic proper. Further he revealed the longitudinal current component to be nearly in geostrophic balance with the transverse pressure gradient. Showing that the transverse baroclinic pressure gradient has the opposite sign to that one at the surface he pointed out that the surface pressure gradient is compensated by the baroclinic pressure gradient in the bottom layer.

In spite of the knowledge on the dynamics of the Fehmarn Belt area few is known on the dynamics of the Darss Sill area. Because the Darss Sill is the last and most shallow sill the water masses have to pass it in order to enter the Baltic proper and because the bottom topography exhibits some special feature (Fig. 1a) it seems necessary to investigate the dynamics of the Darss Sill area and to understand whether it plays a special role in the water exchange between the North Sea and the Baltic or not.

Therefore the following questions have been addressed in a series of oceanographic observations in the Darss Sill area:

- What are the similarities in the dynamics of the Darss Sill area and the Fehmarn Belt?
- Does the local bottom topography of the Darss Sill have an impact on the first order dynamic processes?
- What are the dynamical processes at different scales and the possible interactions between them?

2. The data basis

In order to meet the objectives derived in the preceding section hydrographic and current measurements have been conducted at stations in the Darss Sill area shown in Fig. 1b during different seasons of the year. A detailed description of the experiments has been given elsewhere (MATTHÄUS et al. 1982) therefore we present a summary of the conducted measurements only.

Continuously vertical temperature and conductivity profiles were taken from the surface to the bottom on board the research vessels at every hydrographic station by means of a CTD-OM 75 (MÖCKEL 1980). Intercomparison measurements with reversing thermometers and conductivity measurements of water samples taken by the rosette sampler of the CTD revealed an accuracy of $1 \cdot 10^{-2}^{\circ}\text{C}$ for temperature and $1 \cdot 10^{-5}$ for salinity respectively.

Vertical profiles of current velocity were measured at discrete levels separated by 2 m between a depth of 7 m to 1 m above the bottom along the section Falster-Zingst (stations 72–76). The instrument used was a WPS current profiler (described by LASS et al. 1980). The current profiles have been taken from the drifting ship. The ship's drift was measured by taking the DECCA position every 2 minutes and estimating the linear regression coefficients during a drift time of 20 minutes. The overall accuracy of the profiling current measurements was estimated as about $\pm 5 \text{ cm/s}$.

In order to avoid mixing between spatial scales and energetic variations of the oceanographic fields in time as much as possible, the sampling time at every station of the network in Fig. 1b was 36 hours. The 36 hours sampling time has been chosen in order to meet logistic requirements and moreover to meet a fixed phase of the semidiurnal tide at every station. Time scales of less than 36 hours have been detected by current velocity measurement with recording current meters attached to subsurface moorings at depths of 7 m, 12 m, 17 m and near the bottom.

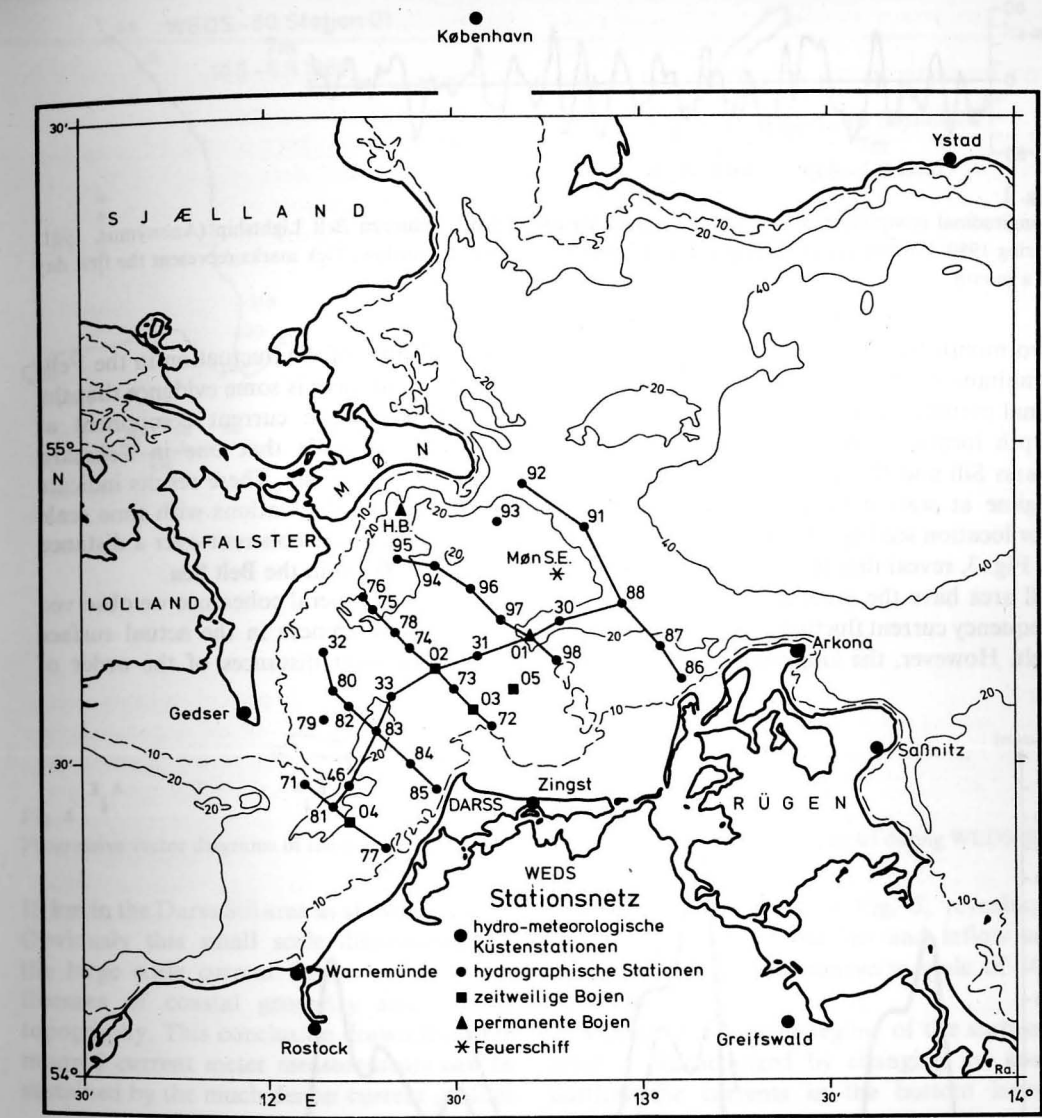


Fig. 1b
Station network of the WEDS-experiments

The subsurface moorings have been located at the stations 01, 02, 03, 04 and 05 (see Fig. 1b). Meteorological and sea level measurement from coastal stations in the Kattegat, the Belt Sea and the Baltic proper have been kindly provided by the corresponding institutions and authorities of Denmark, Finland, GDR and Sweden.

The duration of different experiments conducted hitherto has been about 3 weeks.

3. The currents in the Belt Sea

Energetic low frequency current fluctuations occur at a time scale of 10 to 20 days in the surface layer of the Belt Sea as revealed by an one year time series of the longitudinal current component in the Fehmarn Belt shown in Fig. 2.

In order to investigate the horizontal scale of this current fluctuations we compared a

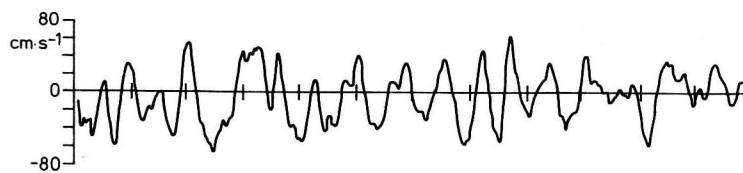


Fig. 2

Longitudinal component of the surface current measured from Fehmarn Belt Lightship (Anonymus, 1981) during 1980. Positive values correspond to inflow, negative ones to outflow. Tick marks represent the first day of a month.

two month fraction of this record with both simultaneous measurements of the longitudinal current component of station 02 in 7 m depth located near the saddle point of the Darss Sill and the times of changing current regime at station 01 east of the Darss Sill (for location see Fig. 1b). The results depicted in Fig. 3, reveal that the currents in the Darss Sill area have the same time scale as the low frequency current fluctuations in the Fehmarn Belt. However, the amplitude of the fluctua-

tion is half that of the fluctuation in the Fehmarn Belt and there is some evidence that the longitudinal surface current component at the Darss Sill leads that one in Fehmarn Belt by about one day. These results indicate that the current fluctuations with time scale of 10 to 20 days are coherent over a distance of at least 100 km in the Belt Sea.

Despite this general coherence we observed remarkable differences in the actual surface current field over distances of the order of

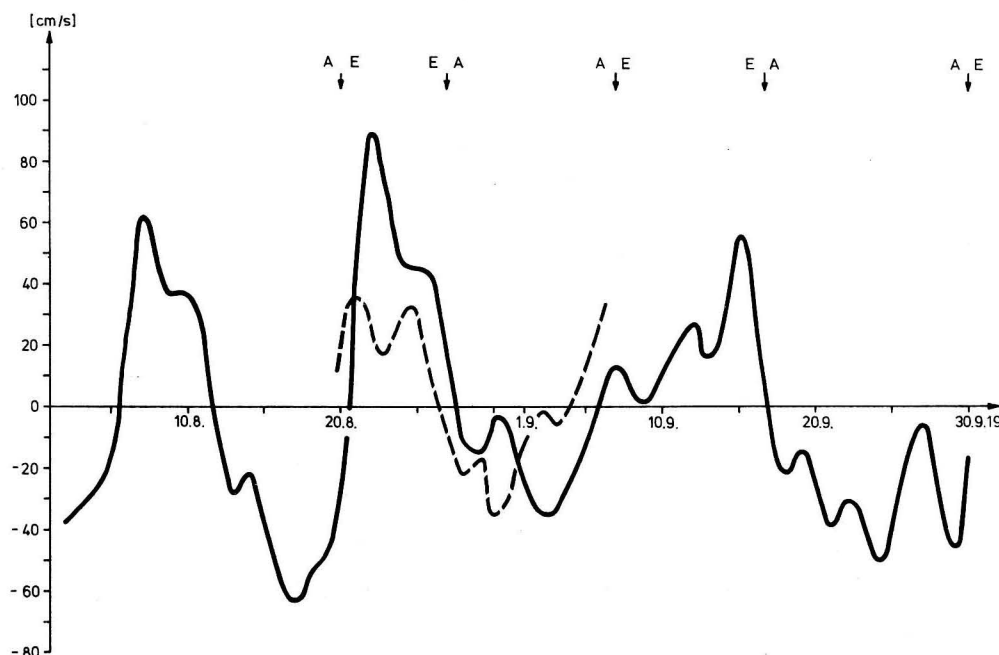


Fig. 3

Longitudinal surface current component of the Fehmarn Belt Lightship (solid line) and at the Darss Sill, station 02, (dashed line). Arrows above the record denote times at which the surface current at station 01 is changing from outflow (A) to inflow (E) and vice versa.

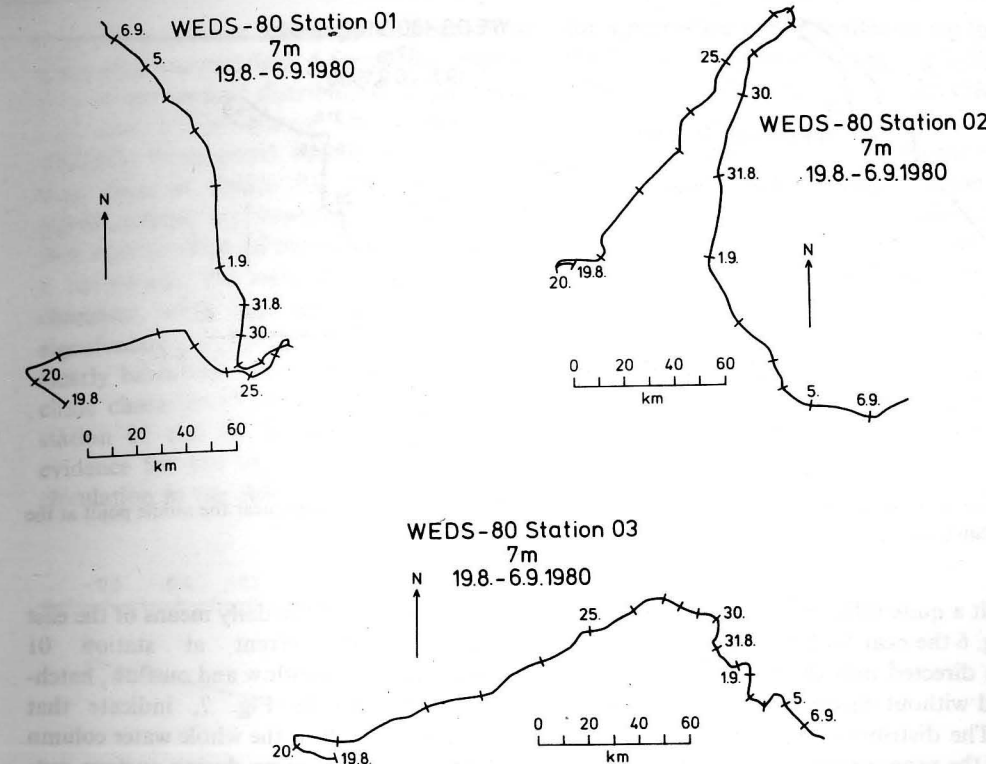


Fig. 4

Progressive vector diagrams of the current at 7 m depth at the mooring stations 01, 02 and 03 during WEDS-80

10 km in the Darss Sill area as shown in Fig. 4. Obviously this small scale disturbances of the large scale current field are due to influences of coastal geometry and bottom topography. This conclusion drawn from the moored current meter measurements can be sustained by the much denser current profiler

measurements depicted in Fig. 5, revealing alternating bands of outflow and inflow at the Darss Sill with a transverse scale of 10 to 20 km.

Whereas the current regime of the surface layer is characterized by changing in- and outflow the currents in the bottom layer

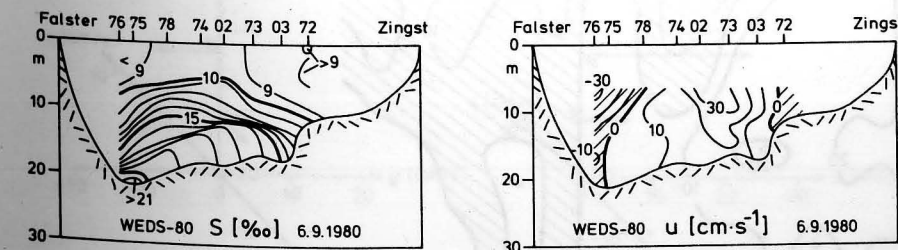


Fig. 5

Sections of salinity and longitudinal current component at the Darss Sill. Positive values indicate currents directed into the Baltic

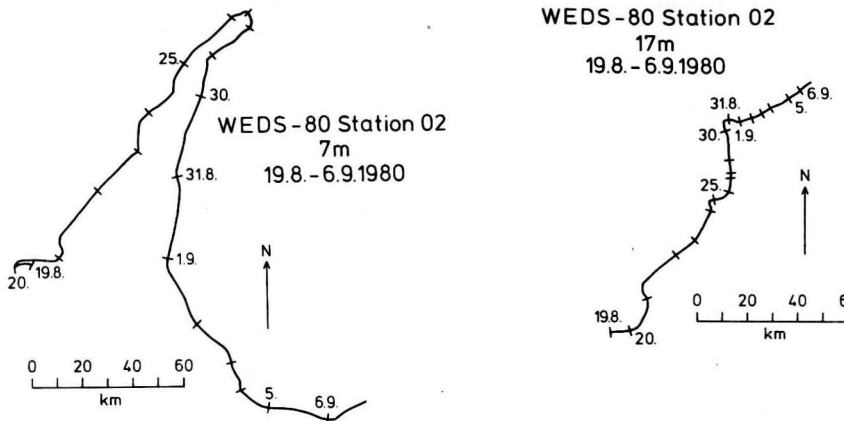


Fig. 6
Progressive vector diagrams of the current at 7 m depth and 1 m above the bottom near the saddle point at the Darss Sill (station 02)

exhibit a quite different behaviour. As shown in Fig. 6 the near bottom current at the Darss Sill is directed into the Baltic over a 10 day period without changing its direction essentially. The distribution of the daily tickmarks along the progressive vector diagram indicate that the inflow is enhanced during surface inflow and suppressed during surface outflow. Occasionally only the near bottom inflow turns into outflow during times of surface outflow.

The isopleths of the daily means of the east component of current at station 01 (representative for inflow and outflow, hatched area), shown in Fig. 7, indicate that during surface inflow the whole water column exhibits inflow whereas during surface outflow only an upper part flows out and the lower part of the water column flows in. The lower boundary of the inflowing fraction of the water varies in time between about 12 m depth and the bottom, indicating an

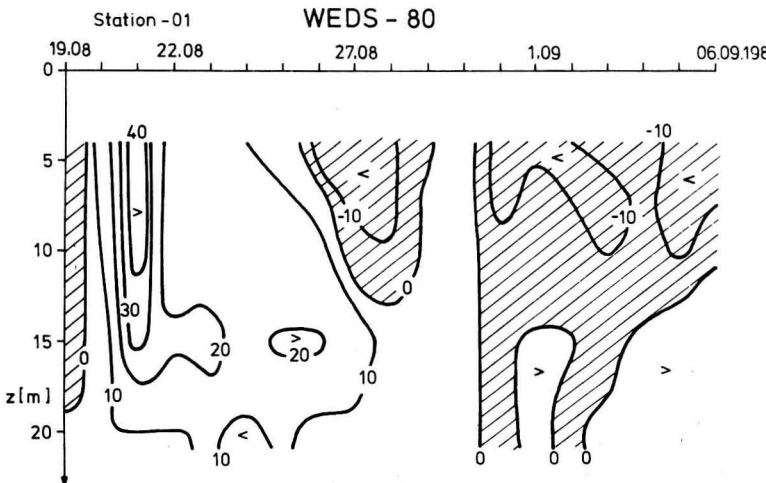


Fig. 7
Isopleths of daily mean values of the east component of current east of the Darss Sill (station 01) during WEDS-80

interaction between barotropic and baroclinic parts of the current field. A formal decomposition of the vertical distribution of the north and east component of the current into empirical orthogonal functions (EOF) has been done at station 01. The two gravest eigenfunctions are depicted in Fig. 8. The first eigenfunction of the east component has a barotropic, the second one a baroclinic character, while both the first and second eigenfunction of the north component have clearly baroclinic character. The pure baroclinic character of the north component at station 01 can be considered as a certain evidence for the baroclinicity of the cross-circulation in the Belt Sea. Further evidence

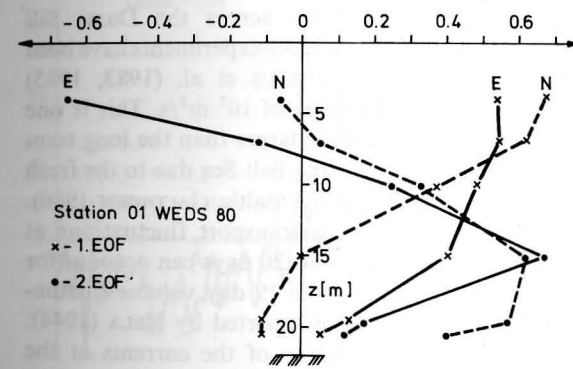


Fig. 8
First (crosses) and second (dots) eigenfunctions of the EOF decomposition of the east (E) and north (N) components of the current east of the Darss Sill at station 01

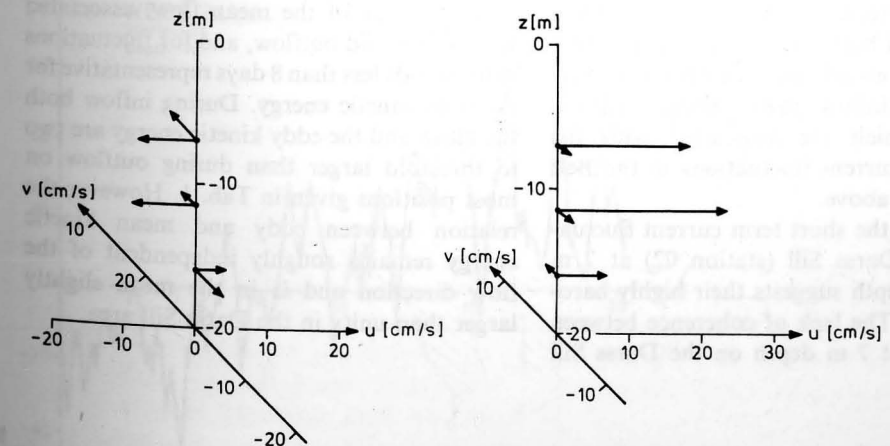


Fig. 9
Longitudinal (u') and transverse (v') current components at the Darss Sill (station 02) during WEDS-84

period of about 1 to 2 days. However, a similar type of cross circulation has been found at neighbouring moorings and moreover the observed displacements in the mass-field at the Darss Sill are consistent with the observed type of cross circulation. So we consider this observation of the cross circulation in the Belt Sea as a first guess which needs confirmation by further measurements under different conditions.

Moreover, these observations of the cross circulation are in agreement with theory (e.g. GILL, 1982) which predicts for a channel whose width is smaller than the barotropic Rossby radius and larger than the baroclinic Rossby radius (as it is the case in the Belt Sea) a vanishing barotropic and a full developed baroclinic subinertial cross circulation in the center of the channel.

It is interesting to find a baroclinic subinertial longitudinal current component near the channel axis of the Belt Sea. Obviously the baroclinic part of the longitudinal current component is not restricted to within one baroclinic Rossby radius of deformation at the coast. The baroclinic Rossby radius is about 5 km in the Belt Sea after FENNEL et al. (1984).

Besides the energetic current fluctuations with a time scale of 10 to 20 days we also observed energetic currents with a time scale of 1 to 2 days as shown in Fig. 10. Obviously there is an interaction between the current fluctuations of both scales, because the short term fluctuations are significantly more energetic during inflow than during outflow-situations, which are associated with the 10–20 days current fluctuations in the Belt Sea described above.

Comparing the short term current fluctuations at the Darss Sill (station 02) at 7 m and 11.5 m depth suggests their highly baroclinic nature. The lack of coherence between the currents at 7 m depth on the Darss Sill

(station 02) and at the same depth on a position about 50 km west of the Darss Sill (station 06) indicates a typical length scale of this short term current fluctuations of less than 50 km. It has been shown by LASS et al. (1984) that these energetic small scale current fluctuations are associated with baroclinic eddies located in the Darss Sill area and a horizontal scale of some 10 kilometers.

This interaction of energetic large and small scale fluctuations can make estimates of the mass transport in the Darss Sill area from current measurements at a single point very incorrect. The current measurements along the section Falster-Zingst at the Darss Sill have been sufficient dense sampled in order to avoid aliasing. Typical fluctuations of the volume transport associated with 10 to 20 day fluctuations across the Darss Sill during different WEDS-experiments have been reported by MATTHÄUS et al. (1983, 1985) and are of the order of $10^5 \text{ m}^3/\text{s}$. This is one order of magnitude larger than the long term masstransport in the Belt Sea due to the fresh water surplus of the Baltic (JACOBSEN 1980). The observed masstransport fluctuations at a time scale of 10 to 20 days can account for the amplitude of the 19 day volume fluctuations of the Baltic reported by HELA (1944).

The kinetic energy of the currents at the Darss Sill has been estimated for fluctuations with periods larger than 8 days as a kind of kinetic energy of the mean flow, associated with inflow and outflow, and for fluctuations with periods less than 8 days representative for the eddy kinetic energy. During inflow both the mean and the eddy kinetic energy are two to threefold larger than during outflow on most positions given in Tab. 1. However the relation between eddy and mean kinetic energy remains roughly independent of the flow direction and is in the mean slightly larger than unity in the Darss Sill area.

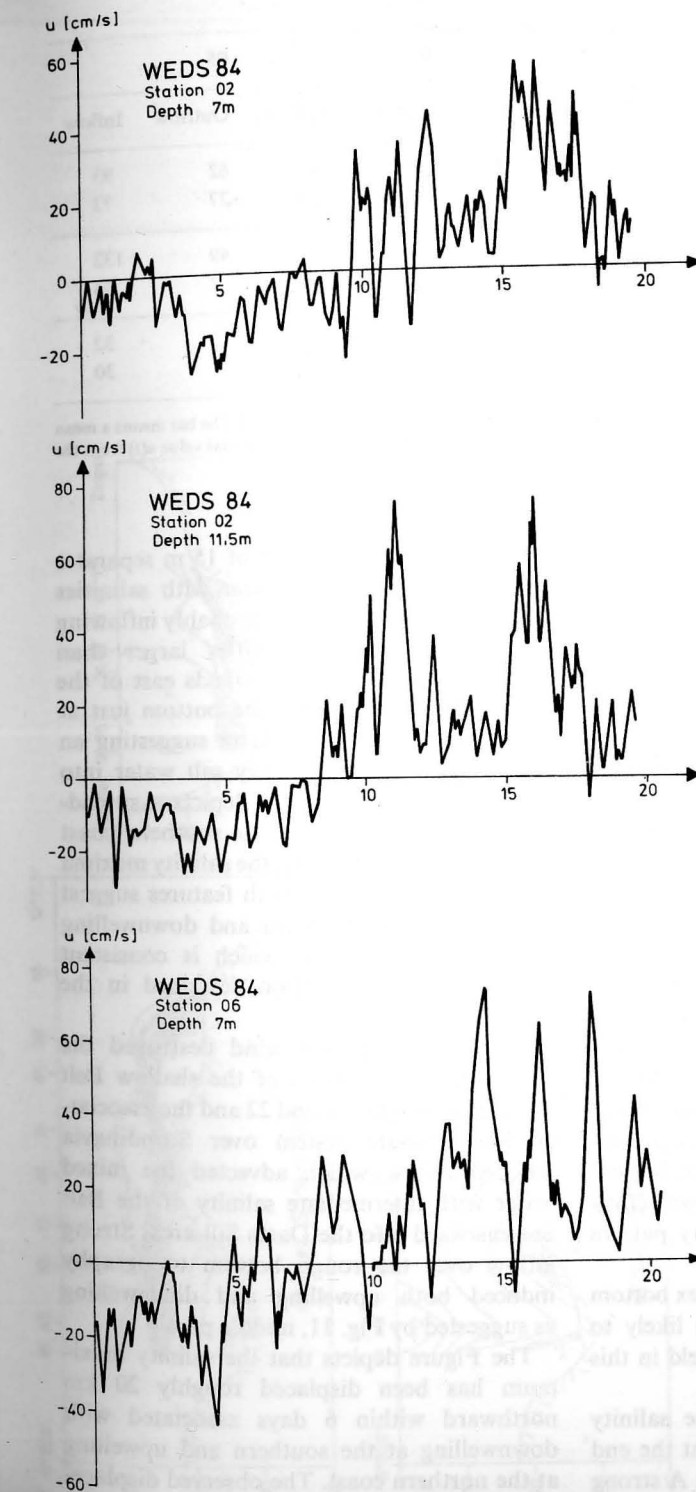


Fig. 10
Time series of the longitudinal current component on station 02 at 7 and 11.5 m depth and on station 06 ($\varphi = 54^\circ 20' \text{ N}$, $\lambda = 11^\circ 56' \text{ E}$) at 7 m depth

Table 1

Depth/Position	06		02		01		05	
	Outflow	Inflow	Outflow	Inflow	Outflow	Inflow	Outflow	Inflow
7 m Eddy	180	415	75,5	174	66	166	62	93
Mean	27	386	46	158	48	108	27	72
11,5 m Eddy	112,5	347	74	228	61	123	49	132
Mean	4,5	200	36	264	41	167	2	54
16,5 m Eddy	54	140	19	66	129	80	12	32
Mean	13	34	20	20	134	157	7	30

Eddy kinetic energy $1/2(\bar{u}^2 + \bar{v}^2)$ and mean kinetic energy $1/2(\bar{u}^2 + \bar{v}^2)$ given in cm^2/s^2 during WEDS 84. The bar means a mean value over one outflow respectively one inflow period of about 8 days. \bar{u}' denotes the deviation of the actual value $u(t)$ from the mean value \bar{u} .

4. The salinity field

The mean salinity distribution in the Belt Sea is determined by the salinity in the Kattegat ($25 \cdot 10^{-3}$), the low salinity in the Baltic ($10 \cdot 10^{-3}$), the mean surface outflow and the mean deep inflow. The corresponding advection processes induce a two layer stratification in the Belt Sea with low salinity in the upper layer and high salinity in the lower layer, which can be modified by vertical mixing due to local winds. In both layers salinity decreases from the Kattegat towards the Baltic.

Due to the high variability of the current field salinity fronts in the Belt Sea discovered by WATTENBERG (1941) move to and fro. (Therefore the actual salinity distribution depends to a large extend from the history of the preceding advection and mixing processes.) Interaction of the currents with bottom topography induce up- and downwelling and can modify the general salinity pattern locally.

The Darss Sill is an area of complex bottom topography and coastlines so it is likely to observe a highly variable salinity field in this area.

Fig. 11, upper part, display the salinity distribution in the Darss Sill area at the end of a roughly 9 day outflow period. A strong

halocline at a mean depth of 15 m separates the outflowing surface water with salinities less than $10 \cdot 10^{-3}$ and the probably inflowing bottom water with salinities larger than $20 \cdot 10^{-3}$. The halocline extends east of the Darss Sill and intersects the bottom just at the edge of the Arkona-Basin suggesting an intermittent inflow of heavy salt water into the Arkona-Basin. Fig. 11 depicts a spreading of the halocline near the southern coast of the Belt Sea, moreover, the salinity maxima are shifted southward. Both features suggest upwelling at the southern and downwelling at the northern coast, which is consistent with the cross circulation described in the preceding section.

Locally strong west wind destroyed the halocline in large parts of the shallow Belt Sea during August 21 and 22 and the associated low pressure system over Scandinavia induced inflow which advected the mixed water with intermediate salinity of the Belt Sea eastward into the Darss Sill area. Strong inflow over the rough bottom topography induced both upwelling and downwelling as suggested by Fig. 11, middle part.

The Figure depicts that the salinity maximum has been displaced roughly 20 km northward within 6 days associated with downwelling at the southern and upwelling at the northern coast. The observed displace-

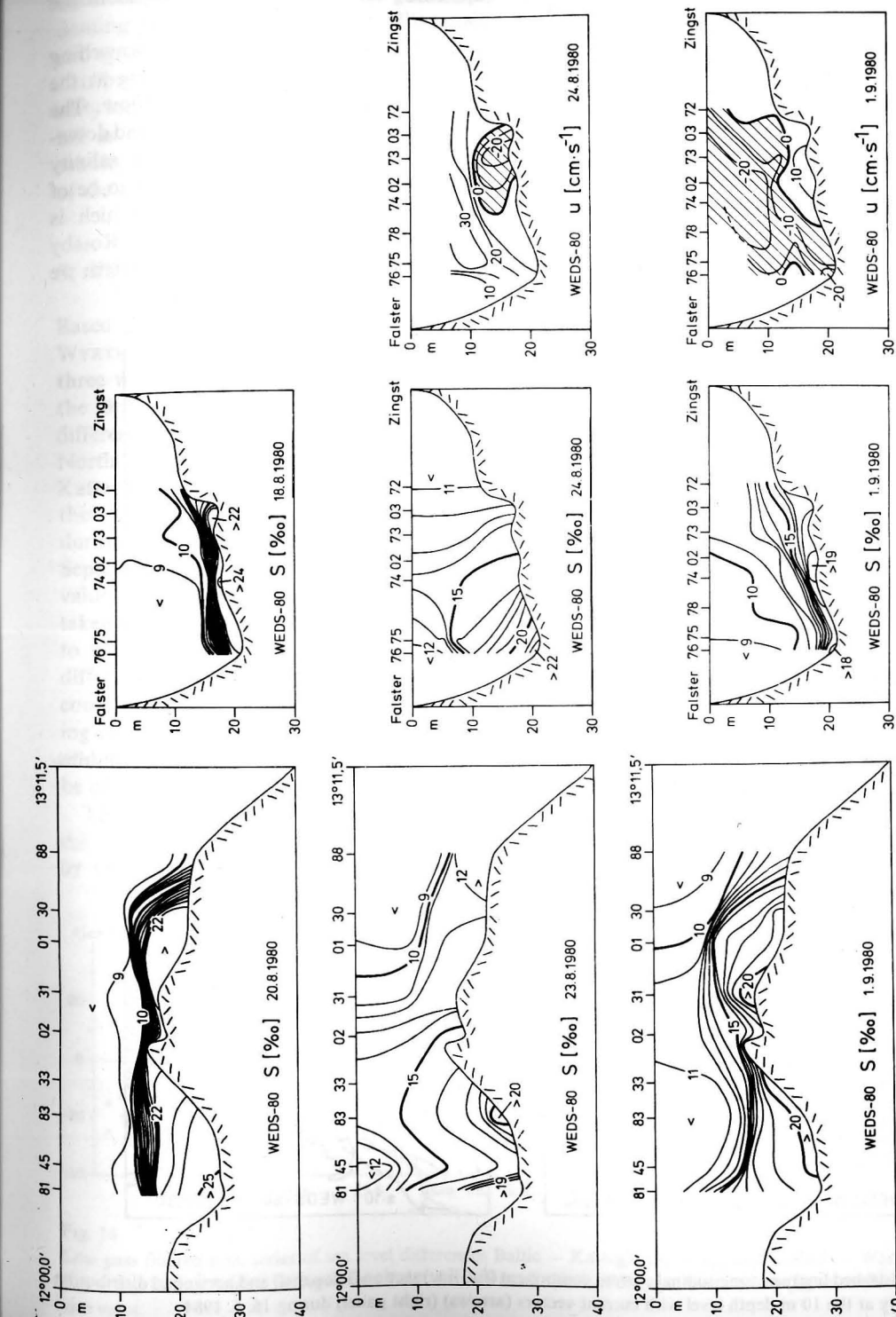


Fig. 11
Salinity and current distributions (longitudinal component) in the Darss Sill area during WEDS-80

ment of the salinity maximum would correspond to a transverse northwestward advection of the order of 5 cm/s near the bottom during inflow.

Fig. 11, lower parts displays the salinity distribution 5 days after the change from the inflow event described in middle part to outflow of high saline bottom water which has reestablished a halocline however being not as homogeneous as those observed two weeks before obviously due to bottom induced

upwelling and downwelling processes in the Darss Sill area.

The Figure again suggests downwelling at the northern coast and upwelling at the southern coast during surface outflow. The cross channel scale of the upwelling and downwelling processes mirrored by the salinity distribution shown in Fig. 11 seems to be of the order of the channel width, which is significantly larger than the baroclinic Rossby radius. Beside the general salinity pattern we

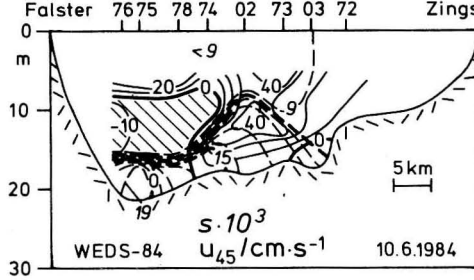


Fig. 12
Salinity (dashed line) and longitudinal current component (full line) section (left panel) and horizontal distribution of salinity at the 10 m depth level with current vectors (arrows) (right panel) during 10. 6. 1984

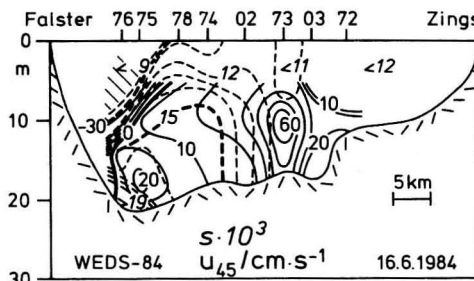


Fig. 13
Salinity (dashed line) and longitudinal current component (full line) section (left panel) and horizontal distribution of salinity at the 10 m depth level with current vectors (arrows) (right panel) during 16. 6. 1984

observed occasionally small scale pattern as doming of salinity associated with locally strong advection events, see Fig. 12, or salinity distribution coupled with an geostrophic eddy located at the northern part of the Darss Sill as shown by Fig. 13. These small scale salinity features emphasize the baroclinicity of the corresponding dynamic processes.

5. The pressure field

Based on the results of KNUDSEN (1899) and WYRTKI (1953) we have to expect the two to three week oscillation of the surface flow in the Belt Sea to be driven by the sea level differences between the Kattegat and the North Sea. Sea level data at Varberg in the Kattegat and at several stations located in the Baltic and the Belt Sea were available during a two month period in August and September 1980. The local two month mean value of sea level at every station has been taken as the common reference level in order to eliminate eustatic sea level changes and differences in the zero levelling of the different countries bordering the Baltic. The remaining error due to long term wind stau effects and the fresh water surplus of the Baltic may be of the order of 1 or 2 cm.

The low pass filtered difference between the mean sea level of the Baltic, calculated by the mean value of sea levels at Hankö,

Helsinki, Ystad and Sassnitz, and the sea level at Varberg in the Kattegat is shown in Fig. 14. This figure reveals that the water level difference Baltic—Kattegat has the same time scale as the coherent fluctuations of the surface current in the Belt Sea and the typical amplitude of this difference is 20 cm at this time scale. Surface inflow corresponds to higher sea level in the Kattegat than in the Baltic and during outflow the inverse sea level difference is observed. A comparison with Fig. 3 suggests that the typical sea level difference between Kattegat and Baltic is associated with a typical surface current of 80 cm/s in the Fehmarn Belt and 40 cm/s at the Darss Sill. Fig. 14 reveals further that the surface current vanishes with vanishing sea level difference between Baltic and Kattegat. All this relations between the sea level differences and the Belt Sea surface currents suggest that the sea level difference is driving the surface current at the two week time scale.

The semigeostrophic relation revealed by JENSEN and SINDING (1945) and LANGE (1975) suggests a relation between the longitudinal and the transverse pressure gradient. Indeed Fig. 14 shows that the sea level difference Gedser—Warnemünde follows the level difference between Baltic and Kattegat with a delay of about 2 days and an amplitude of 10 cm.

Assuming a semigeostrophic balance of the barotropic longitudinal current compo-

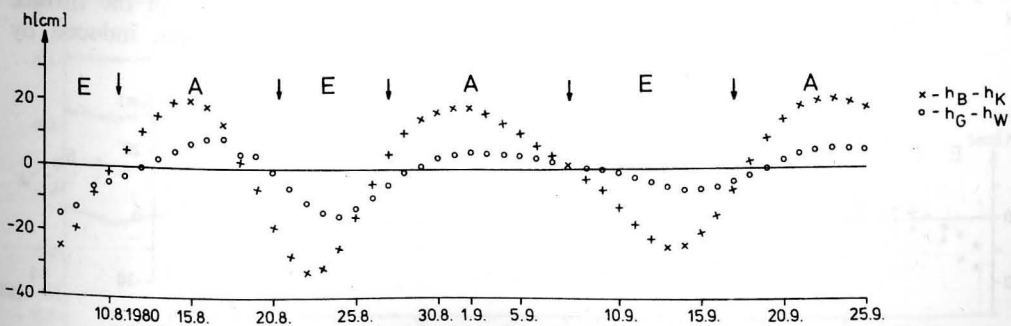


Fig. 14
Low pass filtered time series of sea level differences Baltic — Kattegat ($h_B - h_K$) and Gedser — Warnemünde ($h_G - h_W$) during August to September 1980. Arrows mark times of changes from inflow (E) to outflow (A) and vice versa.

ment between Warnemünde and Gedser, the barotropic volume transport is

$$\bar{M}_u = -\frac{g\bar{H}}{f} (h_G - h_W). \quad (1)$$

Taking gravity $g = 9.81 \text{ m/s}^2$, the Coriolis-frequency $f = 1.18 \cdot 10^{-4} \text{ s}^{-1}$, the mean depth between Gedser and Warnemünde $\bar{H} = 18 \text{ m}$ and the amplitude of the water level difference Gedser—Warnemünde ($h_G - h_W$) $\sim 0.1 \text{ m}$ than the volume transport fluctuations are $\bar{M}_u = 1.5 \cdot 10^5 \text{ m}^3/\text{s}$ which is in good agreement with the directly estimated volume transport by MATTHÄUS et al. (1983) during August—September 1980 at the Darss Sill.

The phase difference between the longitudinal and the transverse sea level difference within the Belt Sea suggests that it takes the geostrophic adaption process two days to adjust the cross channel sea level inclination to the longitudinal surface current driven by the sea level difference between Kattegat and Baltic.

HELA (1944) documented that transport fluctuations in the Danish straits with time scales of 10 days cause significant volume fluctuations of the Baltic at the corresponding time scale. The mass balance equation for the Baltic is

$$\frac{dV}{dt} = F_B \frac{dh_B}{dt} = \iint_0^H dy dz u(y, z) + Q. \quad (2)$$

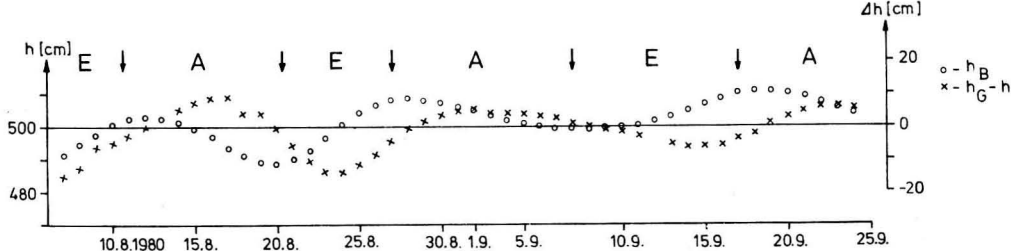


Fig. 15

Low pass filtered time series of sea level difference Gedser — Warnemünde ($h_G - h_W$) and mean sea level of the Baltic h_B during August to September 1980

Using the semigeostrophic balance we get

$$\frac{dh_B}{dt} = -\frac{g\bar{H}}{F_B f} (h_G - h_W) + \frac{Q}{F_B} \quad (3)$$

Assuming the sea level difference $h_G - h_W = \Delta h \sin \omega_0 t$ the integration of (3) leads to

$$h_B(t) = \frac{g\bar{H} \Delta h}{F_B f \omega_0} \cos \omega_0 t + \frac{1}{F_B} \int dt Q(t). \quad (4)$$

With a corresponding period of ω_0 between 14 and 20 days and a surface of the Baltic $F_B = 3.9 \cdot 10^{11} \text{ m}^2$ we get

$$h_B(t) = (0.74 \text{ to } 1.1) \Delta h \cos \omega_0 t + \frac{1}{F_B} \int dt Q(t). \quad (5)$$

Comparing the results of (5) with the low pass filtered sea level difference Gedser—Warnemünde and the low pass filtered mean Baltic sea level shown in Fig. 15 reveals that the largest part of the mean Baltic sea level at a time scale of 2 or 3 weeks can be accounted for by the barotropic volume transport in the Belt Sea at the same time scale.

This has a meaningful implication for the dynamics of the system Kattegat—Baltic because any difference in sea level between both tends to be decreased by the volume transport induced by just those sea level difference.

It has been shown by WYRTKI (1954) that the relation between both the surface and the bottom current in the Belt Sea can be accounted for by the superposition of the surface longitudinal pressure gradient, induced by

the sea level difference between Kattegat and Baltic, and the baroclinic longitudinal pressure gradient, induced by corresponding density differences. While the baroclinic pressure gradient is always directed into the Baltic, slightly oscillating by the advection of water masses in the Belt Sea, the surface pressure gradient changes its direction as it does the sea level difference between Kattegat and Baltic as shown in Fig. 16. Fig. 17 reveals the increasing of the baroclinic longitudinal pressure gradient with depth.

Therefore during inflow both pressure gradients are directed into the Baltic and the amount of the resulting longitudinal pressure gradient increases from the surface to the bottom. This accounts for the inflow in the whole water column as shown in Fig. 7. However, we do not observe a general increase of the longitudinal current component with depth. Should that increase be reduced by bottom friction? That seems to be unlikely because the thickness of the bottom mixed layer in the Belt Sea is of the order of one meter only.

During outflow both pressure gradients have opposite directions and the baroclinic pressure gradient, increasing with depth compensates the surface pressure gradient at a certain depth below which the outflow changes

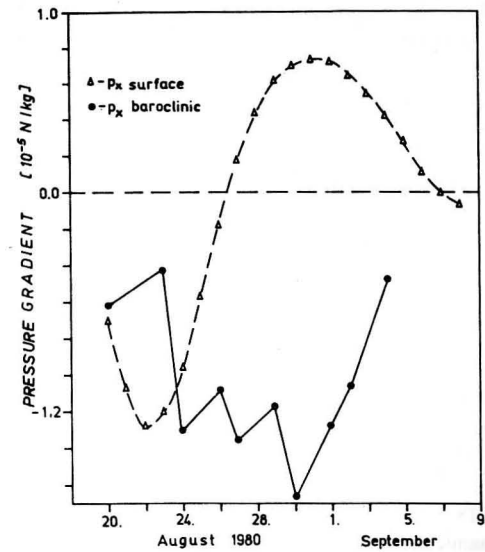


Fig. 16

Time series of longitudinal surface (Δ) and baroclinic pressure gradient (\bullet) at 15 m depth at the Darss Sill area during WEDS-80

to inflow. The feature depicted by Fig. 7 that the outflow tends to start later and to end earlier with increasing depth can be accounted for in terms of the interference of the both longitudinal pressure gradients with its opposite directions.

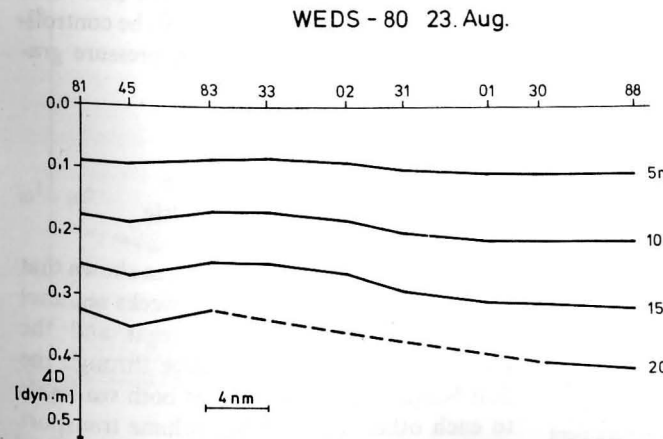


Fig. 17

Dynamic depth anomalies along the axis of the Belt Sea in the Darss Sill area for selected depth levels during WEDS-80

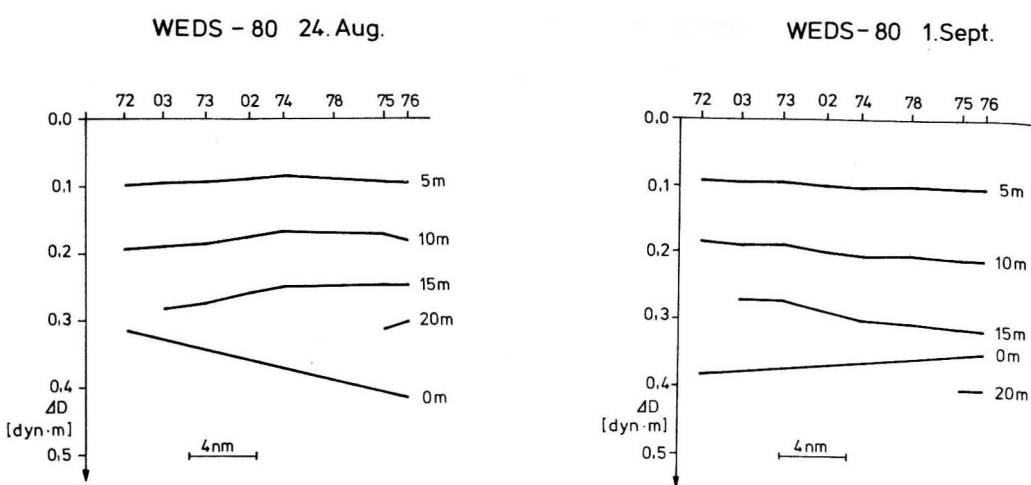


Fig. 18

Dynamic depth anomalies normal to the axis of the Belt Sea in the Darss Sill area for selected depth levels as well as during inflow (24. August) and outflow (1. September) WEDS-80. Sea surface inclination has been included in linearized form.

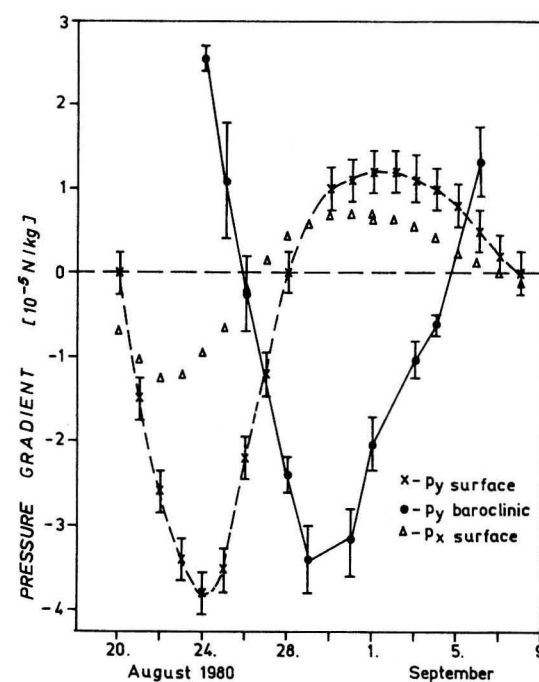


Fig. 19

Time series of the longitudinal surface pressure gradient p_x , and both the surface and baroclinic pressure gradients p_y at the Darss Sill during WEDS-80. The baroclinic pressure gradient p_y has been calculated at a depth of 15 m.

In contrast to the longitudinal pressure gradients the transverse surface and baroclinic pressure gradients have opposite directions as well during inflow (24 August) as during outflow (1 September) (Fig. 18). As shown by Fig. 19 the transverse surface and baroclinic pressure gradients are nearly out of phase during the whole period of observation. Similar relations have been observed by LANGE (1975) in the Fehmarn Belt. This evidently general feature seems to be controlled by the surface longitudinal pressure gradient as suggested by Fig. 19.

6. Forcing of water exchange between Kattegat and Baltic

In the previous sections it has been shown that at a time scale of two to three weeks sea level differences between the Kattegat and the Baltic drive the water exchange through the Belt Sea which tends to adapt both sea levels to each other. Because the volume transport through the Belt Sea is restricted by geometry and friction the adaption process has a low pass filter characteristic. Therefore it is interesting to know the response function of

this process. Sea level differences can be set up as well by sea level variations of the North Sea—Kattegat system as by wind stau effects in the Baltic itself (WYRTKI 1953; LANGE 1975). Because the wind stau effects in the Baltic are most energetic at a time scale of few days, the time scale of the intense weather events, the low frequency forcing of the system is due to the Kattegat sea level variations.

Power spectra of sea level at Varberg (Kattegat) and Saßnitz (Baltic) and the corresponding gain function are shown in Fig. 20. The Kattegat sea level variations are more energetic than the Baltic sea level variations

for periods larger than five days and smaller than 30 hours. There seems to be eigenperiods of the Kattegat at 6.2 h and 4.1 h. The Baltic sea level variations are larger at periods between about 31 hours (the gravest eigenperiod of the Baltic, see WÜBBER, KRAUSS 1979) and about 5 days.

The gain function of the Saßnitz sea level driven by the Varberg sea level is significantly different from zero for periods larger than four days and at the O_2 and M_2 tidal periods. The gain is always smaller than unity and there is no indication of a resonance type response in the gain function. Between the

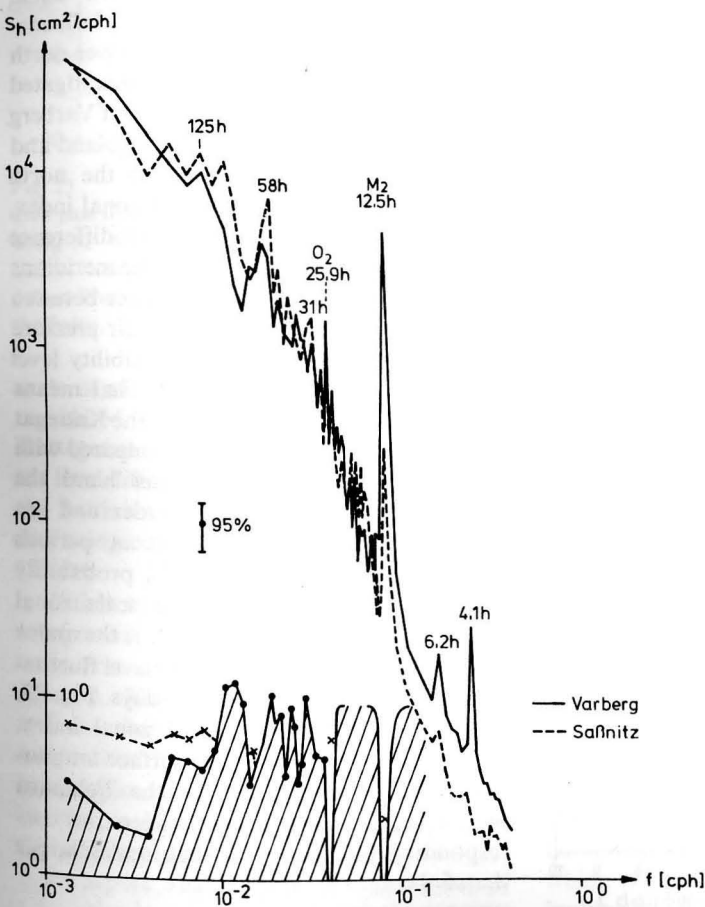


Fig. 20

Power spectra of sea level variations at Varberg (Kattegat) and Saßnitz (Baltic). The gain function (crosses) and the level of significance (dots) at a 95% probability level are estimated after BENDAT and PIERSOL (1966). The linear scale of the gain function is marked on the right hand side of the ordinate.

O_2 tidal period and 4 days the signal to noise ratio is small evidently due to the energetic wind forced sea level variations of the Baltic (see MAGAARD and KRAUSS 1966). For periods larger than a month the gain tends to become one as can be seen by mean monthly sea levels in the Kattegat and Baltic during 1980 as shown in Fig. 21. The phase difference between the sea levels of Varberg and Saßnitz are about 180° around periods of 3 days, about 90° around periods of five to ten days

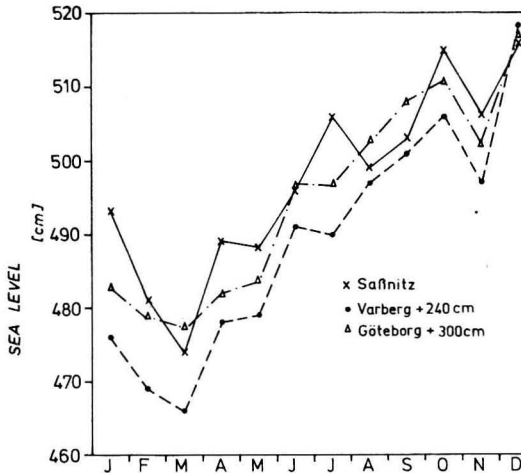


Fig. 21

Mean monthly sea levels at Varberg, Gothenburg (Kattegat) and Saßnitz (Baltic) during 1980

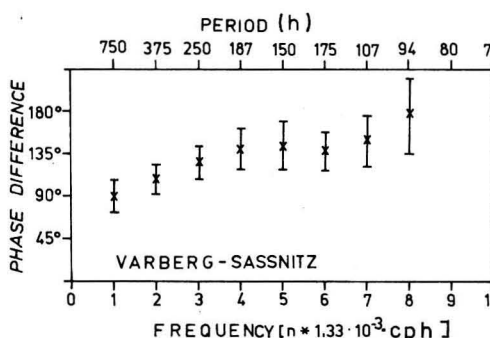


Fig. 22

Phase differences of the sea levels between Varberg (Kattegat) and Saßnitz (Baltic). Positive phase differences mean leading sea level at Varberg.

and approach zero for periods larger than a month as depicted by Figs. 21 and 22.

Obviously the Baltic Sea level and consequently the water exchange is driven mainly at periods larger than about four days by the sea level in the Kattegat and at periods of four days and less additional by the wind forced oscillations of the Baltic sea level.

The question arises which forces govern the Kattegat sea level or more generally the sea level of the North Sea. After WYRTKI (1952) the North Sea level is determined by locally air pressure variations, the wind stress between the British Island and the Jutland peninsula and the sea level of the north east Atlantic, the latter being mainly influenced by large scale weather patterns over north east Atlantic. Therefore we have investigated the coherence between the sea level at Varberg (Kattegat) and air pressure at Helgoland and the large scale zonal wind over the north east Atlantic represented by the zonal index, the mean meridional air pressure difference between 35° N and 65° N along the meridians from 20° W to 40° E. The coherence between Varberg sea level and Helgoland air pressure is not significant at a 95% probability level for periods less than a month. That means that the air pressure influence on the Kattegat sea level in the mean is minor compared with other parameters. On the other hand the coherence between the zonal index and sea level at Varberg is significant at periods larger than 5 days at the 95% probability level, indicating that the large scale zonal wind over the north east Atlantic is the major driving force of the Kattegat sea level fluctuations with periods larger than 5 days. Fig. 23, showing the low pass filtered zonal index, the Varberg sea level and the surface longitudinal current component in the Fehmarn Belt, reveals the causality between the corresponding parameters at time scales larger than 5 days.

7. Conclusions

Large scale fluctuations of the zonal wind component over the NE-Atlantic with a time

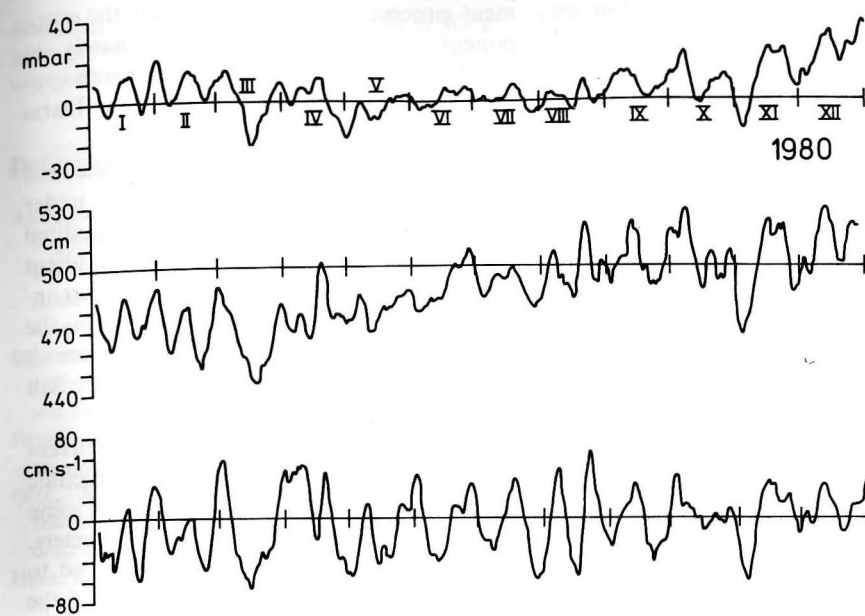


Fig. 23

Low pass filtered time series of zonal index (mean sea surface pressure difference between 35° N and 65° N taken along 20° W to 40° E) (upper panel), sea level at Varberg (Kattegat middle panel) and the surface longitudinal current component in the Fehmarn Belt during 1980 (lower panel). The cut-off period of the used filter was 5 days. Positive values in the upper panel indicate west wind, in the lower panel they indicate current directed into the Baltic.

scale of two to three weeks are significantly correlated with sea level fluctuations in the Kattegat at the same time scale. Subsequently sea level differences between the Kattegat and the Baltic drive longitudinal currents the Belt Sea being coherent over distances of at least 150 km.

Within two days the longitudinal current component is adjusted geostrophically to the transverse sea level differences in the Belt Sea channel. This long adjustment time may indicate that baroclinic processes could be essential in the adjustment process. The pure barotropic adjustment time, the time the barotropic Kelvin wave needs to pass the channel, is of the order of 10 hours.

Transport fluctuations of the order of $1.5 \cdot 10^5 \text{ m}^3/\text{s}$ are associated with the currents induced by the sea level differences. These transport fluctuations account for the mean sea level variations in the Baltic proper at a time scale of two to three weeks. This implies

that the water exchange between the Kattegat and the Baltic forced by sea level variations in the Kattegat can be oscillatory or transient only, because the associated transport through the Belt Sea adjusts the Baltic Sea level to the Kattegat sea level within a certain time.

We observed a strong correlation between the sea level differences between the Kattegat and the Baltic and different baroclinic processes in the Darss Sill area. The intrinsic cross channel scale of this baroclinic processes is larger than the baroclinic Rossby radius and seems to be determined by the scale of the inclined cross channel bottom profile.

We found observational evidence for a baroclinic cross circulation in the Belt Sea which rotates clockwise in the vertical plane looking in downstream direction of the surface current. This cross circulation may be influenced by local winds, however, to a lesser extent than by the longitudinal sea level inclination.

Associated with this cross circulation we observed upwelling at the left hand coast and downwelling at the right hand coast looking downstream at the sea surface. The special features of the up- and downwelling process are governed by the local bottom profile.

This upwelling accounts for the observed higher baroclinic pressure at the left compared with the right hand coast because the upwelling process accumulates heavy bottom water near the left and the downwelling process accumulates light surface water near the right hand coast looking downstream again. Therefore the cross channel water level and baroclinic pressure differences are strong correlated and out of phase. These resulting pressure difference decreases with depth and the geostrophically balanced longitudinal current component decreases with depth too having a similar effect on the longitudinal current component as bottom friction. However, the observed weakening of the longitudinal current component is not symmetrically to the sign of the longitudinal sea level difference in the Belt Sea. This may be due to the interference of both the longitudinal sea level difference and the longitudinal baroclinic pressure gradient. The latter, being caused by the salinity differences between Kattegat and Baltic, is directed always into the Baltic being in a first approximation independent from the sea level difference. During surface inflow both pressure gradients add each other causing an increasing pressure gradient with increasing depth. The above mentioned associated cross circulation at the Darss Sill reduces the inflow from the surface to the bottom so that near the bottom we observe only a weak inflow compared with the upper layers. Bottom friction may contribute to the observed vertical current profile also but can not account for it alone.

During surface outflow both pressure gradients have opposite directions and cancel each other in a certain depth, depending mainly from the amount of the sea level difference. In this case the weakening of the longitudinal current component with increasing depth by the barotropic-baroclinic adjust-

ment process is in such kind that the component reverse its sign approximately at the depth of zero longitudinal pressure gradient and we observe inflow at the Darss Sill from this depth to the bottom.

The cross circulation in the Belt Sea and the subsequent adjustment process under the combined action of both the longitudinal sea surface and baroclinic pressure gradient is not well understood and needs further investigations. It depends essentially on the local bottom topography and therefore it must be studied at different places in the Belt Sea channel.

In addition to the low frequency current variations we observed energetic baroclinic current fluctuations with a time scale of some days and a spatial scale of ten kilometers. These current fluctuations were observed to be associated with baroclinic eddies of the same scale and are more energetic during inflow than during outflow conditions. We can only speculate on a possible generating mechanism of such eddies. But it seems not unlikely that the geostrophically adjusted mass fields along straight coasts and narrow channels advects itself into the open water after passing a strong coastal irregularity. The advected massfield may be unstable in the open water and transform into a stable eddy. This mechanism could shed eddies from the eastern margin of Fehmarn island into Mecklenburg Bight and from Gedser Rev into the Darss Sill area east of Falster during inflow conditions.

Acknowledgements

We are indebted to the crews of the research vessels "A. v. Humboldt" und "Prof. A. Penck" who sailed the ships safely through the dense traffic in the Darss Sill area enabling us to measure at the stations as scheduled during all weather situations. We are grateful to the engineers and technicians of the Institut für Meereskunde Warnemünde who assisted in the CTD and profiling current meter measurements and the deployment and recovering of the current meter moorings. We also gratefully acknowledge the Danish Meteorological Institute, the Institute for Marine Research Helsinki, the Swedish Meteorological and

Hydrological Institute and the Directorate of Water Management-Coast of the GDR who provided us with sea level measurements.

References

- ANONYMUS: Meereskundliche Beobachtungen und Ergebnisse Nr. 42. Beobachtungen auf den deutschen Feuerschiffen der Nord- und Ostsee im Jahre 1980. — Deutsch. Hydrogr. Institut Hamburg, 1981.
- BENDAT, J. S.; PIERSOL, A. G.: Measurement and analysis of random data. — New York: John Wiley and Sons, 1966.
- FENNEL, W.; HELM, R.; STURM, M.: unpublished manuscript, 1984.
- GILL, A. E.: Atmosphere — Ocean Dynamics. International Geophysics Series, Vol. 30. — London: Academic Press 1982.
- HELA, J.: Über die Schwankungen des Wasserstandes in der Ostsee. — Ann. Acad. Sci. Fenn A I. 28 (1944).
- JACOBSEN, T. S.: Sea water exchange of the Baltic, measurements and methods. — Copenhagen: The National Agency of Environmental Protection 1980, 106 pp.
- JENSEN, H.; SINDING, E.: On the difference between the heights of mean sea level at the self recording tidegauges at Korsør and Slipshavn. — Geodätisk Inst. Medd., Nr. 20 (1945).
- KNUDSEN, M.: De hydrografiske forhold i de danske farvande indenfor Skagen i 1894—98. — Komm. for vidensk. Unders. i de danske farvande 2(2) (1899), 19—79.
- KNUDSEN, M.: Ein hydrographischer Lehrsatz. Ann. Hydrogr. mar. Met. 28 (1900), 316—320.
- LANGE, W.: Zu den Ursachen langperiodischer Strömungsänderungen im Fehmarnbelt. — Kieler Meeresforschungen 31 (1975), 65—81.
- LASS, H. U.; FENNEL, W.; HELM, R.; MÖCKEL, F.; STURM, M.; TILL, K.-H.; WIECHERT, H.; WILL, H.: Vorläufige Ergebnisse der Expedition des FS „A. v. Humboldt“ in den äquatorialen Atlantik während des Globalen Wetterexperimentes (FGGE) SOP II, 1979. — Beitr. Meereskunde, H. 44/45 (1980), 87—107.
- LASS, H. U.; MATTHÄUS, W.; FRANCKE, E.; SCHWABE, R.: On the dynamics of water exchange across the Darss Sill based on WEDS-80 data. — Proc. 14th Conf. Baltic Oceanogr. Gdynia 1984, Paper P-8.
- MAGAARD, L.; KRAUSS, W.: Spektren der Wasserstandsschwankungen der Ostsee im Jahre 1958. — Kieler Meeresforschungen 22 (1966), 155—162.
- MATTHÄUS, W.; FRANCKE, E.; LASS, H. U.; SCHWABE, R.: Untersuchung der Wasseraustauschprozesse im Bereich der Darßer Schwelle. — Beitr. Meereskunde, H. 47 (1982), 31—50.
- MATTHÄUS, W.; LASS, H. U.; FRANCKE, E.; SCHWABE, R.: Zur Veränderlichkeit des Volumen- und Salztransports über die Darßer Schwelle. — Gerl. Beitr. Geophys. 92 (1983), 407—420.
- MATTHÄUS, W.; LASS, H. U.; SCHWABE, R.; FRANCKE, E.: Water and salt transport across the Darss Sill in February/March 1982. — Ann. Biol. 39 (1985), 58—61.
- MÖCKEL, F.: Die ozeanologische Meßkette OM-75, eine universelle Datenerfassungsanlage für Forschungsschiffe. — Beitr. Meereskunde, H. 43 (1980), 5—14.
- THIEL, G.: Strombeobachtungen in der westlichen Ostsee im Juli 1936. — Archiv der Deutschen Seewarte 58(7), 1938, 28 pp.
- WATTENBERG, H.: Über die Grenzen zwischen Nord- und Ostseewasser. Ann. Hydrogr. mar. Meteorol. 69(9), 1941, pp. 265—279.
- WITTING, R.: Havsytan, Geoidytan och landhöjningen utmed Baltiska Hafvet. Fennia 39(5), 1918, pp. 346.
- WÜBBER, C.; KRAUSS, W.: The two-dimensional seiches of the Baltic Sea. — Oceanol. Acta 2 (1979), 435—446.
- WYRTKI, K.: Der Einfluß des Windes auf den mittleren Wasserstand der Nordsee und ihren Wasserhaushalt. — D. Hydrogr. Zr. 5 (1952), 245.
- WYRTKI, K.: Die Dynamik der Wasserbewegungen im Fehmarnbelt Teil 1. — Kieler Meeresforschungen 9 (1953), 155—170.
- WYRTKI, K.: Die Dynamik der Wasserbewegungen im Fehmarnbelt Teil 2. — Kieler Meeresforschungen 10 (1954), 162—181. (1954a)
- WYRTKI, K.: Schwankungen im Wasserhaushalt der Ostsee. — D. Hydrogr. Z. 7 (1954), 91—129. (1954b)

Address of the authors:

Dr. sc. HANS ULRICH LASS, Dipl.-Met. REINHARD SCHWABE, Dr. sc. WOLFGANG MATTHÄUS, Dipl.-Met. EBERHARD FRANCKE
Akademie der Wissenschaften der DDR
Institut für Meereskunde
DDR-2530 Rostock-Warnemünde

Received: October 28, 1985

Accepted: January 31, 1986

D. NEHRING, E. HAGEN, A. JORGE DA SILVA, R. SCHEMAINDA, G. WOLF, N. MICHELCHEN,
W. KAISER, L. POSTEL, F. GOSELCK, U. BRENNING, E. KÜHNER, G. ARLT, H. SIEGEL, L. GOHS
und G. BUBLITZ

Results of oceanological studies in the Mozambique Channel in February—March 1980

With 16 figures and 1 table

Abstract: The general structure and the dynamics of the water masses, the influence of seamounts and banks, nearshore upwelling and downwelling as well as short-term oceanological variations on the nutrient distribution and on the primary and secondary production including some meteorological observations and investigations in the sea bottom were studied in the western part of the Mozambique Channel in February to March 1980. The results of these studies are now available (NEHRING et al. 1984). They are briefly summarized in the present publication.

Zusammenfassung: Der vorliegende Beitrag enthält die wichtigsten Ergebnisse von ozeanologischen Untersuchungen, die im Februar—März 1980 im westlichen Teil des Moçambique Kanals durchgeführt und bei NEHRING u. a. (1984) ausführlich diskutiert wurden. Neben dem allgemeinen Aufbau und der Dynamik der Wassermassen betreffen sie den Einfluß submariner Erhebungen und küstennaher Auftriebsprozesse sowie kurzfristiger ozeanologischer Veränderungen auf das Nährstoffregime und die Bioproduktivität, ergänzt durch einige meteorologische Beobachtungen und Untersuchungen am Meeresgrund.

Резюме: Статья содержит самые важные результаты океанологических исследований в западной части Мозамбикского пролива с февраля до марта 1980-го года, которые были представлены раньше (Неринг и др. 1984). Кроме общей стратификации водных масс и их динамики, исследования были направлены на влияние подводных вершин, прибрежного апвеллинга и краткосрочных океанологических изменений, на режим биогенных элементов, а также на биопродуктивность и дополнены некоторыми метеорологическими наблюдениями и исследованиями на морском дне.

1. Introduction

Oceanological investigations based on a programme elaborated by the Institute of Marine

Research of the Academy of Sciences of the GDR and the Institute of Fisheries Development in Maputo were undertaken with the GDR R/V "A. v. Humboldt" in the western part of the Mozambique Channel in February to March 1980. Figs. 1 and 2 show the map with the stations and the bathymetric map respectively of the Mozambique Channel.

Besides the general structure and dynamics of the water masses, the influence of seamounts and banks, nearshore upwelling and downwelling as well as short-term oceanological variations on the nutrient conditions and on the primary and secondary production were investigated including some meteorological observations and investigations into the sea bottom. The results of the studies are discussed in detail by NEHRING et al. (1984). In the following they are briefly summarized.

2. Meteorological observations

At the beginning of the investigations, the large spatial pressure distribution over the southern Africa was almost identical to the long-term mean situation, whereas the core of the anticyclone of the Indian Ocean showed a more extreme position with a pressure which was 17 hPa to high. The large spatial atmospheric pressure variations during the period under investigation were characterized by two distinct periods. At the beginning the transition from the NE-monsoon to the SE-monsoon took place. Later the SE-trade winds, influenced by the SW-monsoon, dominated in the whole area. During both

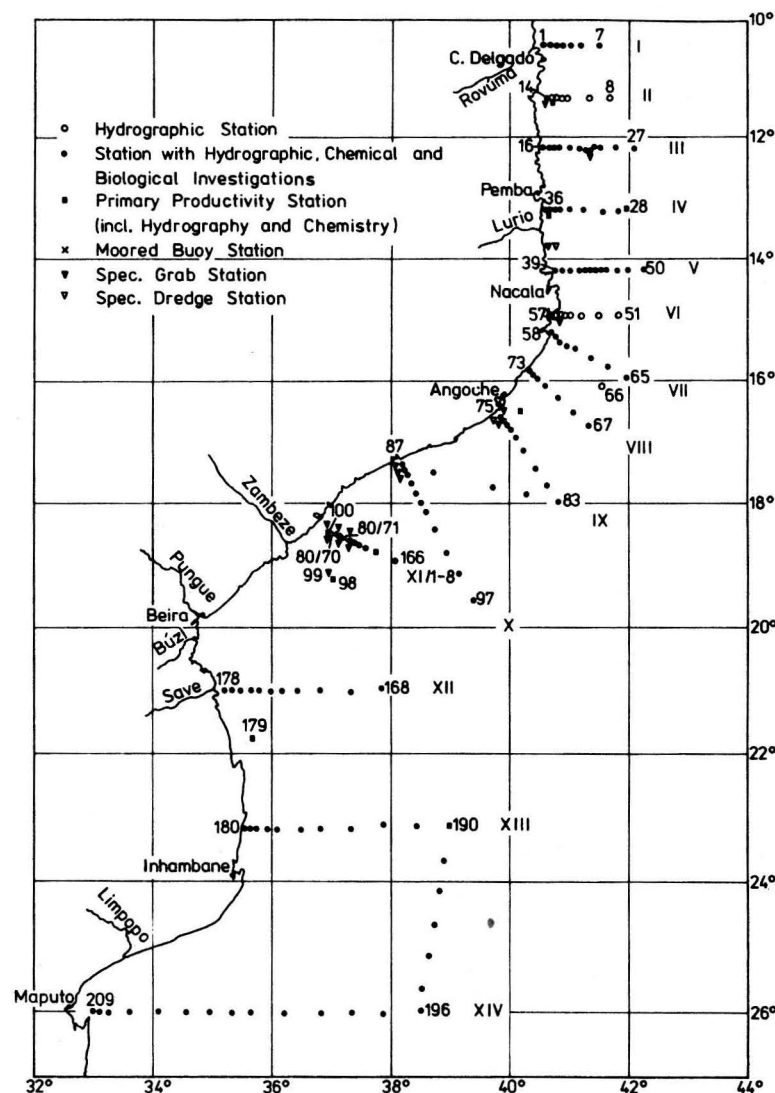


Fig. 1
Map with stations

periods the wind conditions were effected for short times by depressions.

3. Dynamics

In conformity with the large-scale distribution of the wind zones, the geostrophic velocity field of the Mozambique Current at the sea surface clearly consisted of three

parts according to the geostrophical adaption to the mean conditions. Mean geostrophic surface velocities of 51–72 cm s⁻¹ and maximum surface velocities of 82–95 cm s⁻¹ were calculated for the region of the NE-monsoon north of 14° S along the different sections through the Mozambique Current (profiles I–IV) (Fig. 3). The highest surface velocities of, on average 77–135 cm s⁻¹ and maximum values of 112–257 cm s⁻¹

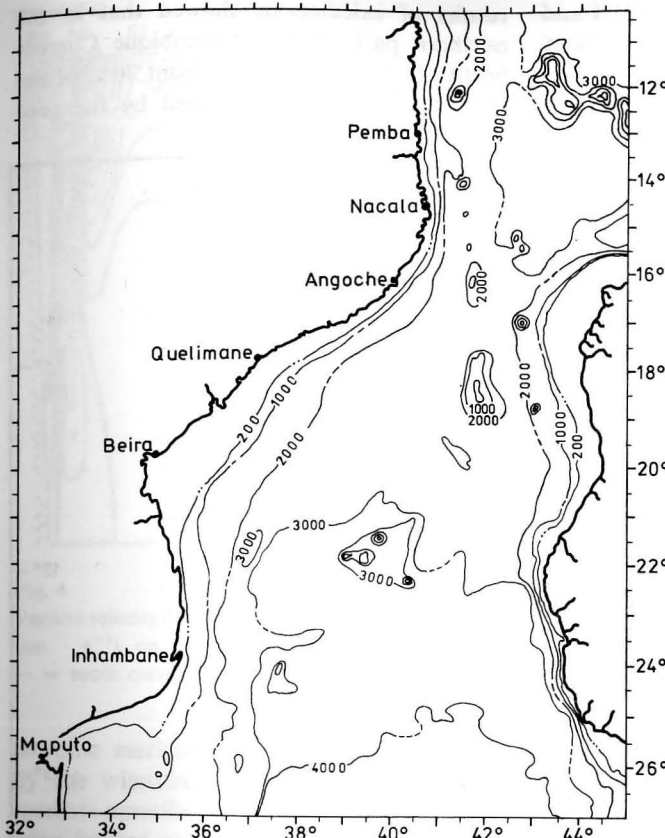


Fig. 2
Bathymetric map of the Mozambique Channel (depth in m)

were found across the profiles V–VII in the doldrums between 14° S and 16° S. Here, the Mozambique Current showed the characteristic features of an oceanic jet stream. In this region near the shelf edge in the layers below the zone of the maximal surface current velocities (at depths greater than 100 m to 150 m), a relatively strong northward flowing countercurrent was observed. Its core with velocities up to 70 cm s⁻¹ in profile VII and up to 35 cm s⁻¹ in section VI was situated at a depth of 250 m (Fig. 4).

South of 16° S in the area of the SE-trade winds the geostrophic surface velocities gradually decreased from north to south. Along profile VIII the mean velocity of the Mozambique Current at the sea surface amounted to 68 cm s⁻¹, and in section XIV it was 24 cm s⁻¹.

In the waters off the large and shallow shelf south of Angoche the geostrophic current field formed a strong cyclonic eddy with its core situated at about 16° 50' S, 39° 57.5' E (Fig. 5).

The broad agreement between the calculated current velocities and the average values of the surface current in February/March based on observations of ships drift for several years permits the conclusion to be drawn that the current velocities of the Mozambique Current are mainly induced by the distribution of mass and pressure during this season (Tab. 1).

To better understand the reasons for the upwelling observed along the northern part of the coast of Mozambique between 10° 30' S and 16° S during the NE-monsoon season, the velocity components of the vertical

currents induced by the windstress curl and forced by the meridional current velocity were estimated for the level of the Ekman "frictional depth" (about 75 m; Fig. 6). The

results of calculations showed that in the northern part of the Mozambique Current north of 14° S on average about 70% of the vertical currents were induced by the geo-

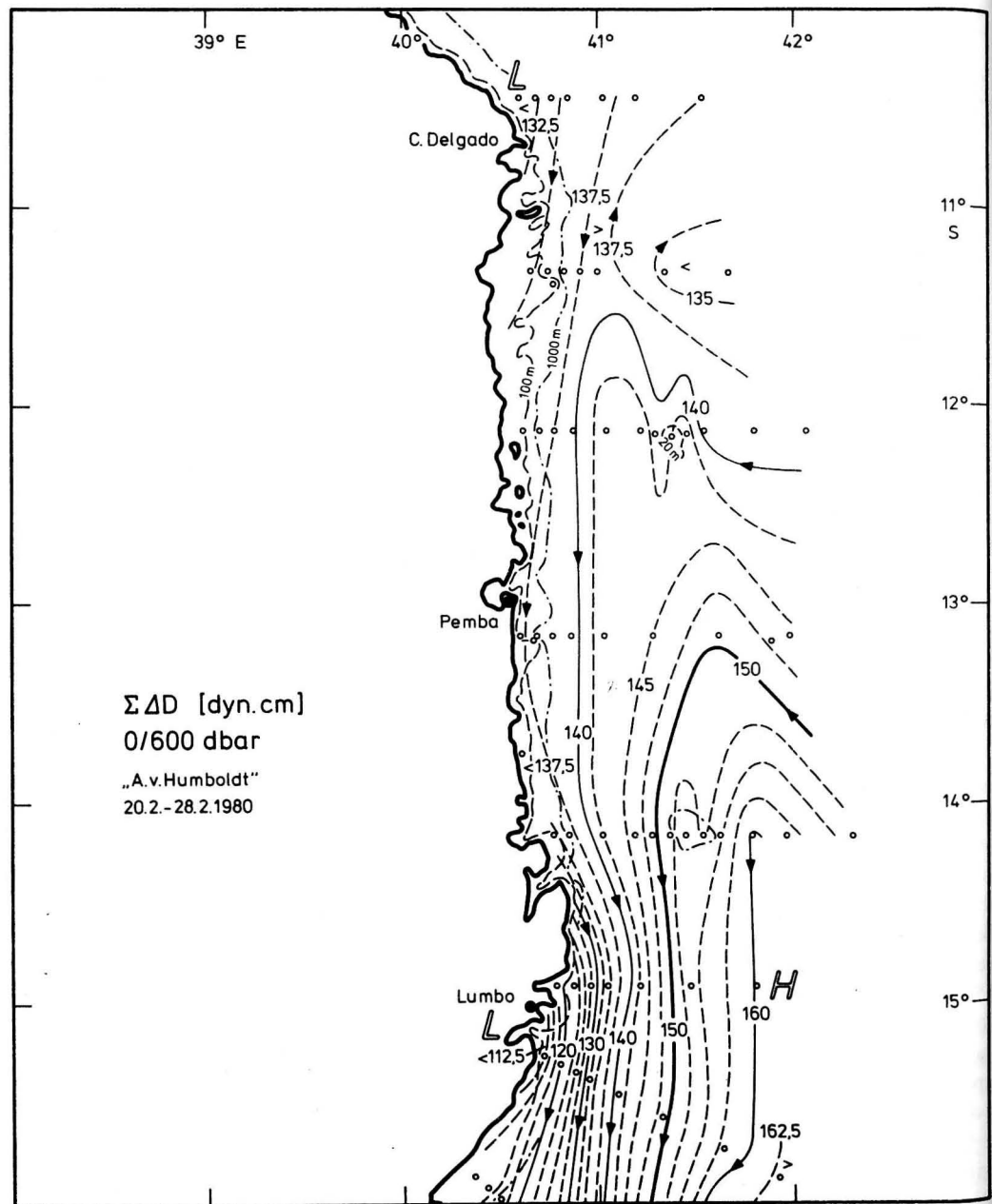


Fig. 3

Dynamical topography of the sea surface relative to the 600 dbar level with geostrophic current arrows within the northern part of the western Mozambique Channel

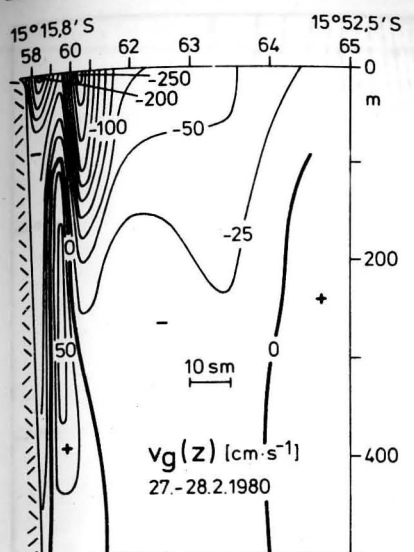


Fig. 4

Vertical velocity distribution of the geostrophic current ($\text{cm} \cdot \text{s}^{-1}$) on section VII (+ = north current; - = south current; reference level 600 dbar)

strophic meridional current and only 30% by the windstress curl. In this area intermediate upwelling occurred seaward the shelf edge limited to the water layers below the level of the Ekman depth. For the doldrums between 14° S and 16° S, where the Mozambique Current showed the characteristic features of an oceanic jet stream, the mean part

Table 1

Maximum and mean surface velocities ($\text{cm} \cdot \text{s}^{-1}$) in the Mozambique Channel in February/March according to the "Monthly Charts" of the Deutsches Hydrographisches Institut, Hamburg, and from investigations by the R/V "A. v. Humboldt"

Sea area	"Monthly Charts"		"A. v. Humboldt"	
	February/March	\bar{v}	February/March	\bar{v}_g
10° S–16° S	229	77	258	79
16° S–26° S	—	51	105	49

of the vertical current component caused by the meridional current velocity at the level of the Ekman depth was calculated to 80%, the portion of the wind induced vertical current component to 20% (Fig. 7). On the strength of the high meridional velocities of the Mozambique Current, the area with intermediate ascending water movements at the Ekman level extended here close to the shelf edge and the intermediate upwelling processes came nearly up to the sea surface.

In the region of the SE-trade winds south of 16° S the vertical current component forced by the windstress curl amounted to about 75%, the vertical current component from the velocity of the geostrophic meridional current only to 25%. As a result of the strong Ekman onshore transport in this area off the coast downwelling predominated. An exception to this rule was the cyclonic eddy of Angoche. Here the change in relative vorticity caused topographically produced strong upward vertical currents in the core of the eddy.

The results of analyses verify our hypothesis that north of 16° S during the NE-monsoon season vertical currents are primarily induced by the velocity field of the Mozambique Current (intermediate upwelling) and its counter-currents (intermediate downwelling), whereas south of this region they are mainly caused by the wind field.

The mean TS-characteristics of the area under investigation show only small variations and a strict TS-relation (300 m to 600 m) in the Indian Central Water. Z-shaped TS-profiles within the Ekman layer (about 75 m) were often found. A salinity minimum above the Ekman depth and a maximum at about 30 m depth were the main feature of wind-driven cross-circulation (Fig. 8). Along the main axis of the Mozambique Current there was no minimum in salinity. The maximum was always caused by upwelling processes.

Temporal variations of oceanological fields in the area of the Sofala Bank were studied on a rerun section (section XI) which was repeated 8 times during 12 days, and by means of 3 current meter moorings over the shelf

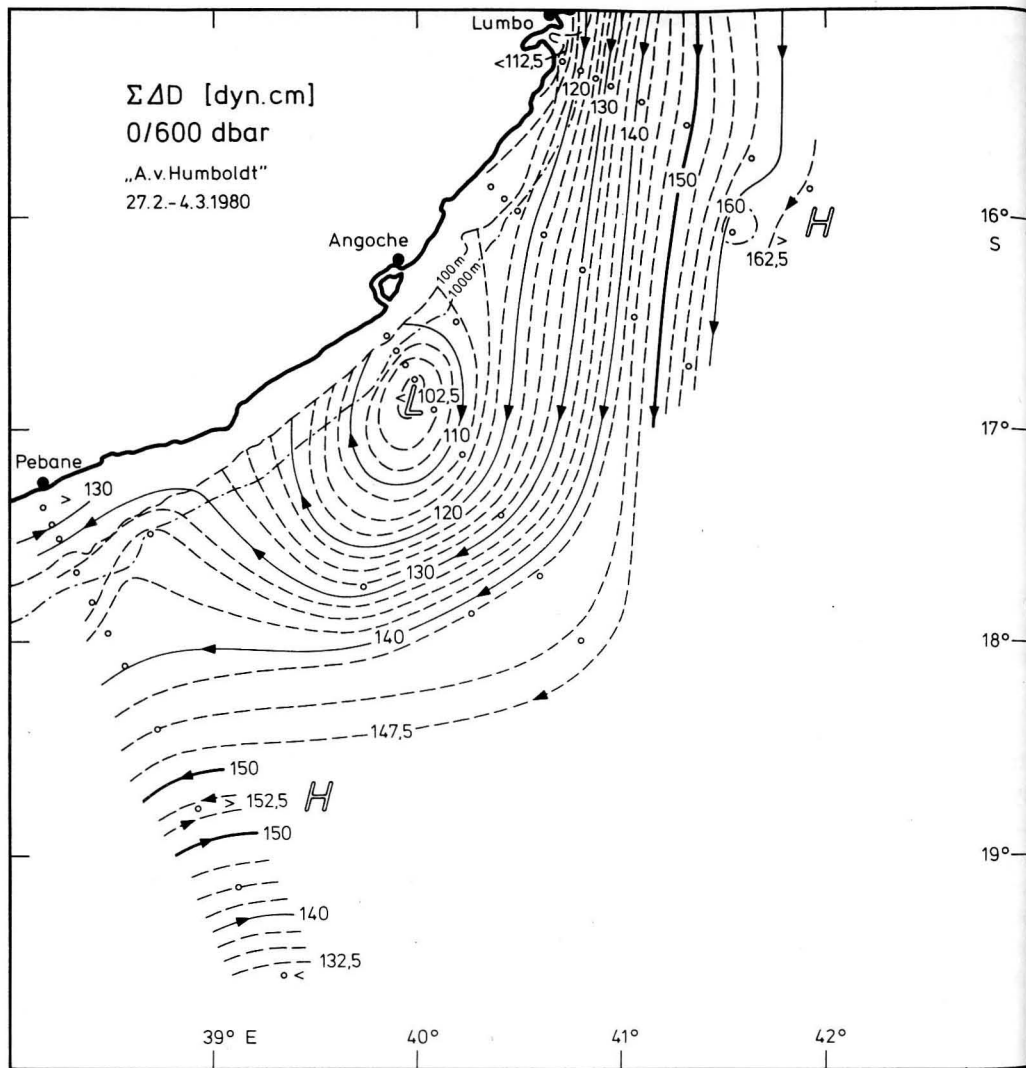


Fig. 5

Dynamical topography of the sea surface relative to the 600 dbar level ($1 \text{ dyn} \cdot \text{cm} = 10^{-1} \text{ m}^2 \text{ s}^{-2}$) with geostrophic current arrows for the middle part of the western Mozambique Channel

and on the shelf edge. These variations were in substance determined by the large-scale offshore dynamics. They reflected rhythmical atmospheric disturbances and shift with a velocity of about 8.5 km h^{-1} zonally from the sea to the coast.

The atmospheric disturbances were superimposed on the U_w -component of the wind. The cycle was $T = 260 \text{ h}$ and the same as that of the currents at buoy station 80/70

(Fig. 9), whereas the cycle at buoy station 80/71 was $T = 310 \text{ h}$. Between the two stations an oceanological front was observed.

At all stations along the rerun section XI distinct temporal TS-variations were observed at depths down to 300 m over a length of 150 km. It was therefore deduced that large-scale offshore dynamics are the cause of these variations.

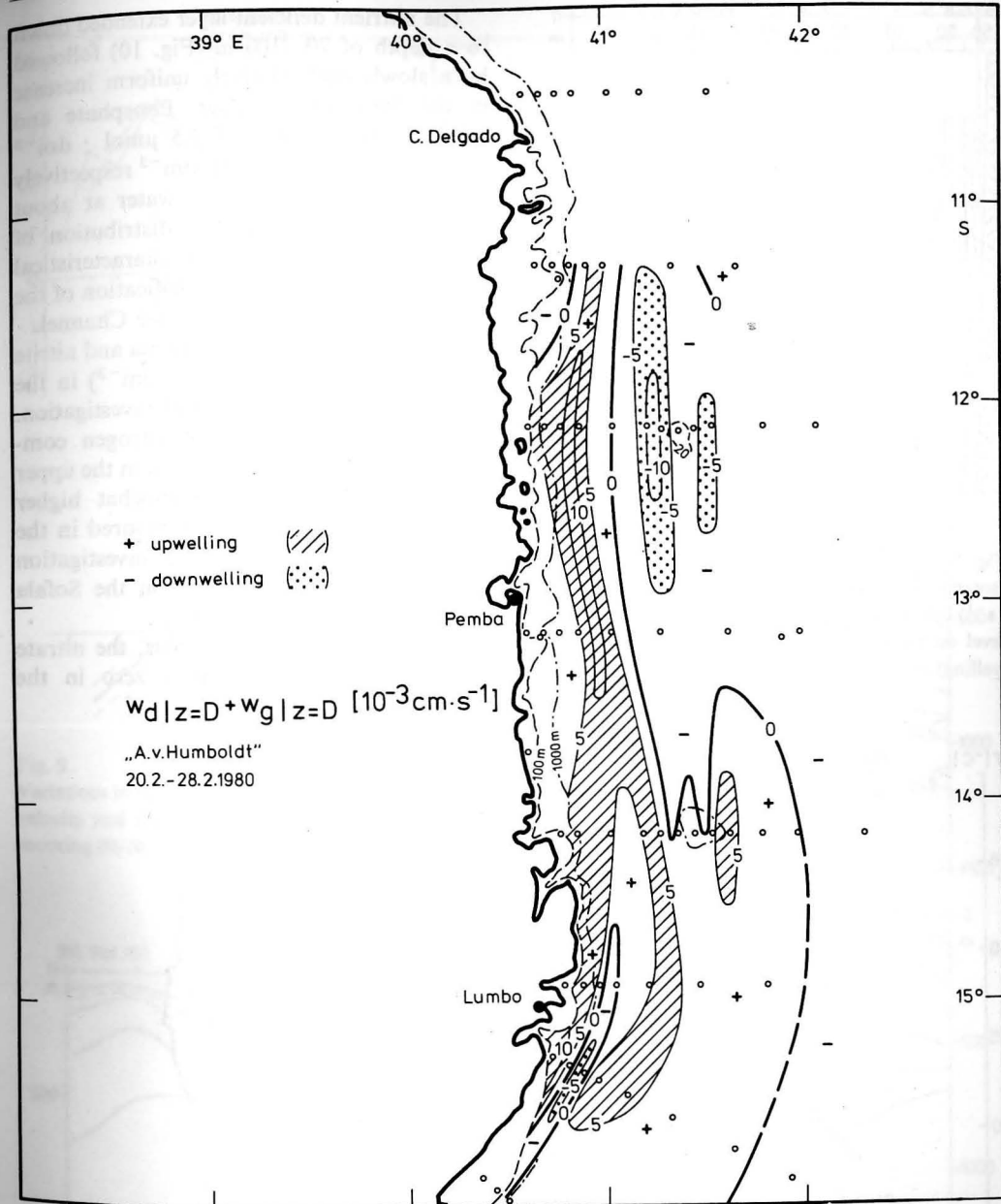


Fig. 6

Isotachs of the wind and current induced vertical currents at the Ekman level $z = D$ (70–83 m)

4. Nutrient response

The phosphate concentrations in the euphotic layer of the western Mozambique Channel were generally smaller than $0.2 \mu\text{mol} \cdot \text{dm}^{-3}$,

but decreased only rarely to below $0.1 \mu\text{mol} \cdot \text{dm}^{-3}$. In contrast, the nitrate concentrations were mostly below $0.1 \mu\text{mol} \cdot \text{dm}^{-3}$ and often reached the limit of analytical detection.

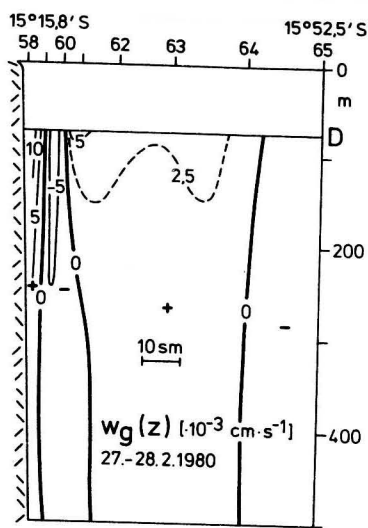


Fig. 7

Isotachs of the geostrophic vertical current ($10^{-3} \text{ cm} \cdot \text{s}^{-1}$) below the Ekman depth relative to the 600 dbar level on section VII (+ = upwelling; - = downwelling)

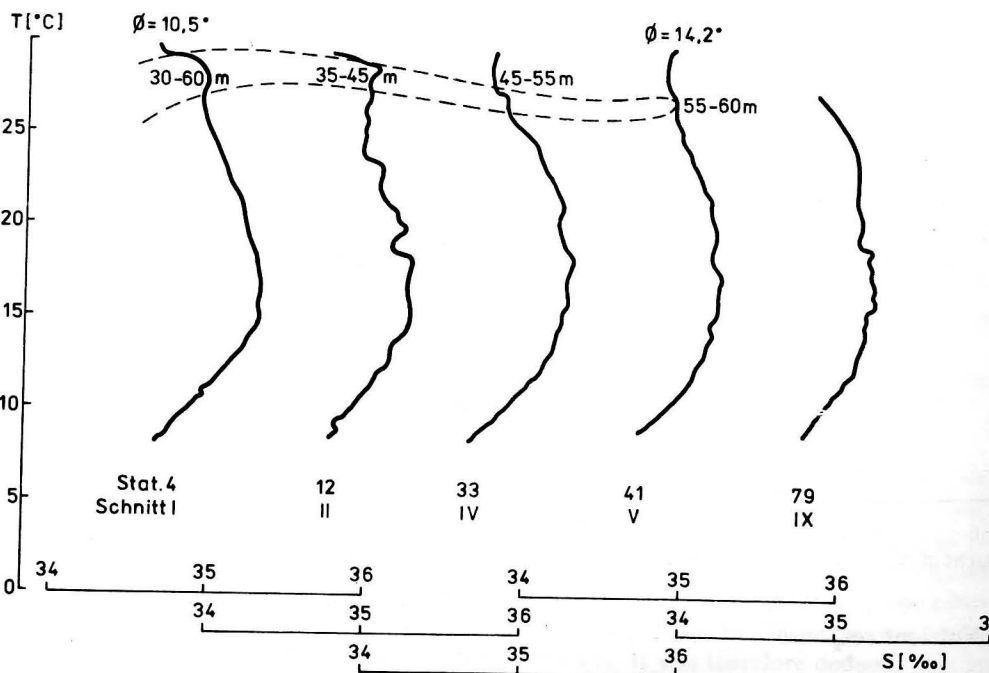


Fig. 8

TS-profiles from the main axes of the current as shown in Figs. 3 and 5

The nutrient deficient layer extended down to a depth of 70–100 m (Fig. 10) followed by a slowly and relatively uniform increase in the discontinuity layer. Phosphate and nitrate concentrations of $2.5 \mu\text{mol} \cdot \text{dm}^{-3}$ and between 32 to $33 \mu\text{mol} \cdot \text{dm}^{-3}$ respectively were measured in the deep water at about 100 m depth. The vertical distribution of these nutrients was related to characteristic water types found by the classification of the water masses in the Mozambique Channel.

The concentrations of ammonia and nitrite were very low (0 – $0.2 \mu\text{mol} \cdot \text{dm}^{-3}$) in the northern part of the area under investigation. Small enrichments of these nitrogen compounds were frequently observed in the upper part of the pycnocline. Somewhat higher amounts of ammonia were measured in the southern part of the area under investigation (0.2 – $0.7 \mu\text{mol} \cdot \text{dm}^{-3}$) and on the Sofala Bank (0.2 – $2 \mu\text{mol} \cdot \text{dm}^{-3}$).

Due to the phosphate surplus, the nitrate to phosphate ratio was near zero in the

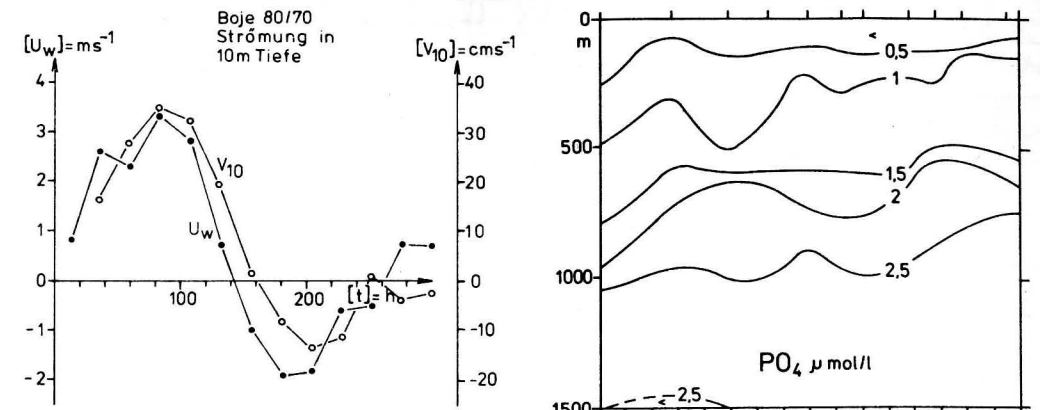


Fig. 9

Variations in time of the wind (U_w) and current (V) velocity and their regression in 10 m depth at the mooring 80/70

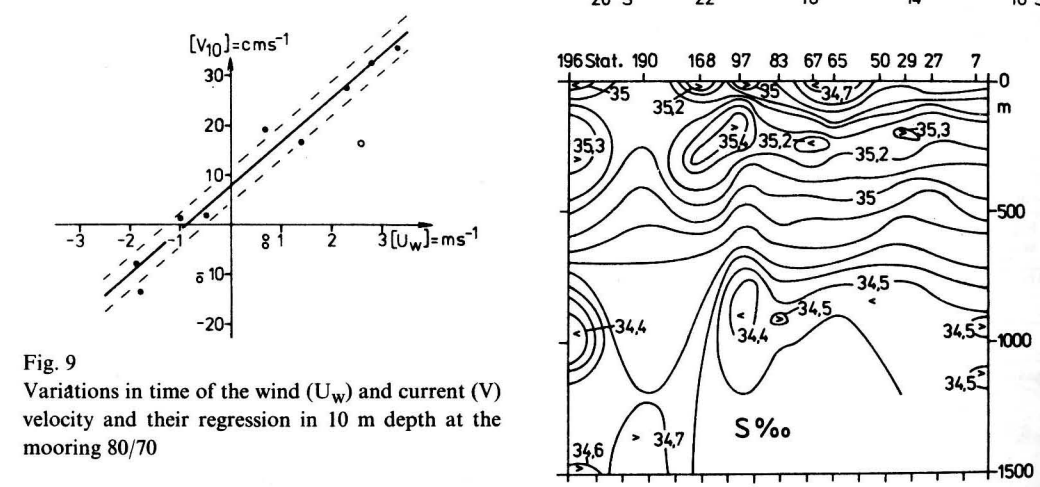


Fig. 10

Vertical distribution of selected oceanological parameters along a meridional section through the Mozambique Channel

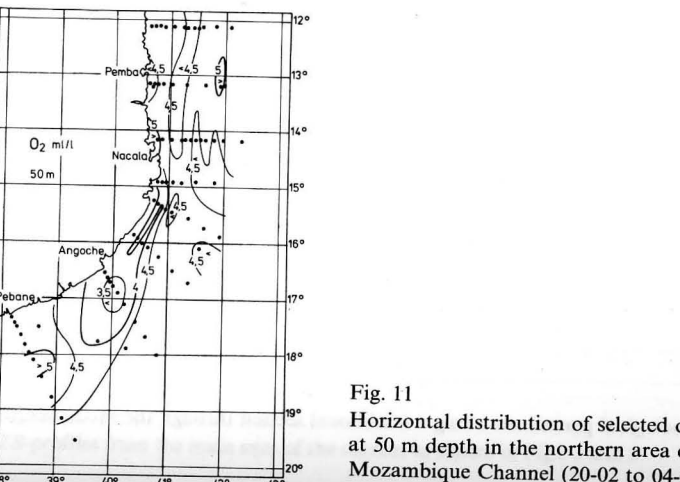
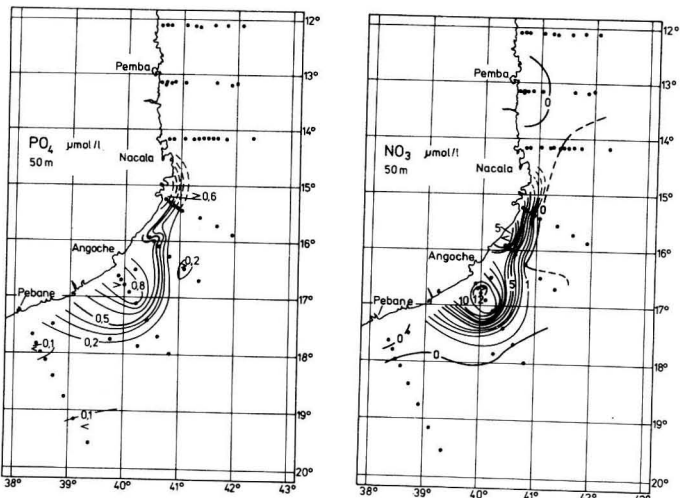
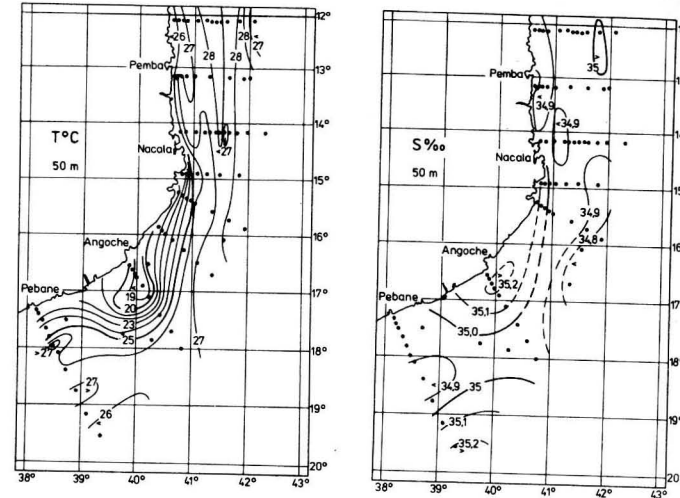


Fig. 11

Horizontal distribution of selected oceanological parameters at 50 m depth in the northern area of the western Mozambique Channel (20-02 to 04-03-1980)

nutrient deficient surface layer. The ratio increased in the discontinuity layer and was characterized by an intermediary maximum of over 14:1 in the layer of the Indian Central Water. It decreased again in the Antarctic Intermediate Water and below it reaching values of 12 to 13:1.

Depending on the dynamically forced upwelling processes south-east of Nacala and by the significant eddy in the area off Angoche, cold deep water rich in nutrients was transported almost to the surface, thus reducing the thickness of the nutrient depleted surface layer from about 100 m to 20–30 m (Fig. 11). Disturbances in the current and mass fields due to the St. Lazarus Bank are also reflected

in the nutrient distribution. The depth of the nutrient discontinuity layer in the southern part of the area under investigation was obviously modified by cyclonic and anti-cyclonic gyres.

5. Biological response

Very low chlorophyll concentrations were found on sections I to IV in the northern region (Fig. 12) and XII to XIV in the southern region (Fig. 13) in the western Mozambique Channel. In the area of the cyclonic eddy (about 16° S) larger amounts of phytoplankton were measured. The reason for the greater

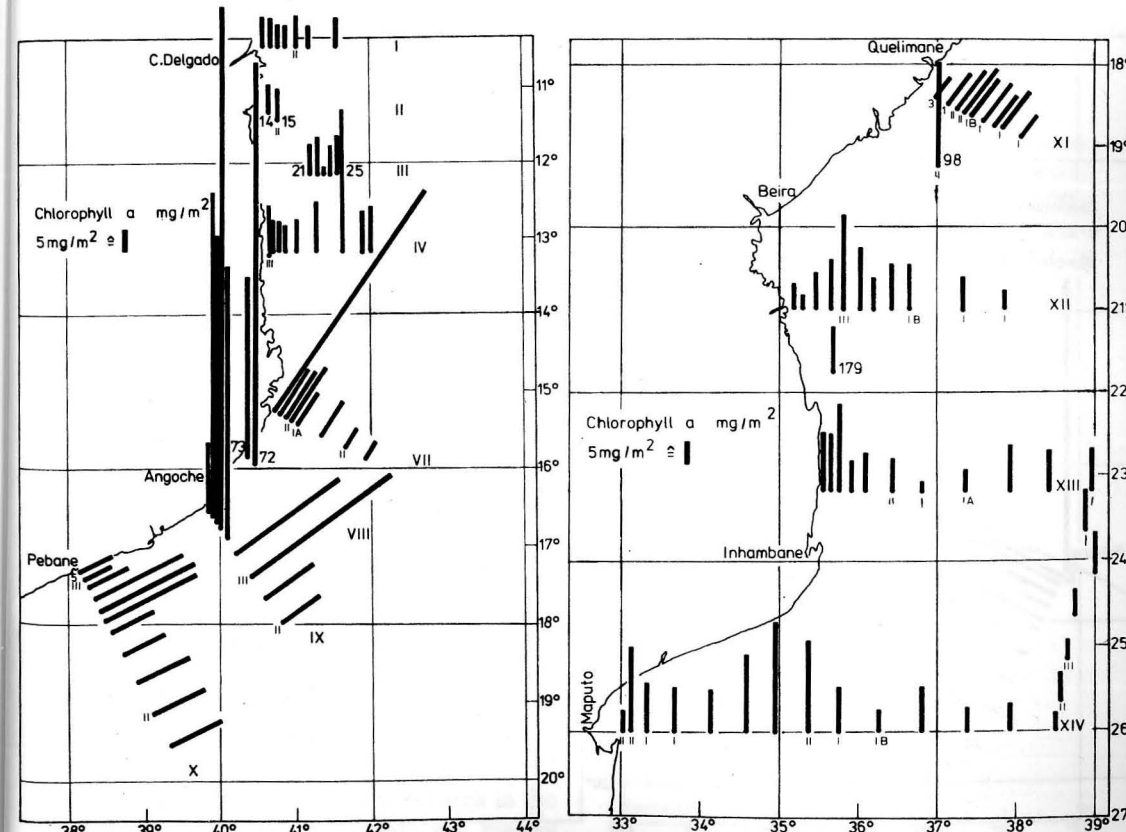


Fig. 12

Column concentrations of chlorophyll a (0–75 m) in the northern area of the western Mozambique Channel (20-02 to 04-03-1980)

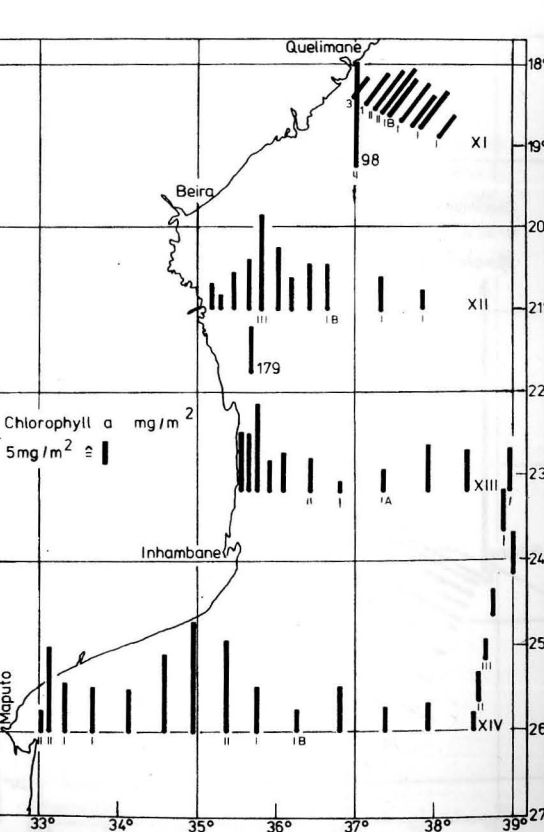


Fig. 13

Column concentrations of chlorophyll a (0–75 m) in the southern area of the western Mozambique Channel (23-03 to 30-03-1980)

productivity was the better nutrient supply resulting from an upward mass transport.

The distribution of chlorophyll in the whole area was in conformity with the phytoplankton cell numbers. *Rhizosolenia hebetata* f. *semispina*, *Rh. alata*, *Nitzschia pungens* var. *atlantica*, *N. delicatissima*, *Cylindrotheca closterium* and *Asterionella japonica* were observed in high frequency, but only *Rh. hebetata* f. *semispina* showed signs of a mass development with up to $2 \cdot 10^5$ cells · dm³ at station 91 (section X).

The zooplankton biomass was lower in the northern region (Fig. 14) and higher in the southern region (Fig. 15). The most productive part of the area under investigation was the southern edge of the cyclonic eddy.

But the highest value (275 mg · m⁻³ dry weight) was measured on the St. Lazarus Bank (station 23). Like the productivity of the phytoplankton, the zooplankton biomass was higher in the onshore areas than offshore.

According to the qualitative and quantitative zooplankton investigations the northern area is only of low productivity. The zooplankton community was typical of tropical seas with stable stratification. At the onshore stations in the southern area zooplankton was present in high abundances, this indicating highly productive communities.

The whole northern region studied and the offshore part of the southern region were assessed as oligotrophic areas. Better conditions for the primary and secondary produc-

tion were identified in the area of the cyclonic eddy, on the Sofala Bank, and in the southern onshore region.

On section XI (Sofala Bank area), which was repeated 8 times during 12 days, higher chlorophyll concentrations and zooplankton biomass were generally measured near the shore than offshore. The variations in time of the chlorophyll and phosphate concentrations were greater parallel to the coast whereas the variability of the zooplankton biomass and ecological efficiency were greatest in the across-shelf direction.

The optical water types defined by JERLOV coincided with the distribution of the biological parameters on the rerun section XI, especially with the chlorophyll concentration (Fig. 16). The half-day sums of the global irradiance measured at some primary productivity stations were higher in the morning (mean 1073.1 J/cm²) than in the afternoon (mean 885.8 J/cm²).

concentrations (up to 10.1%, w/w) were found on the shelf between Quelimane and Beira. The small number of samples, however, does not allow generalisations to be made regarding the occurrence and distribution of specific types of sediment.

Some few investigations concerned the distribution of the macro- and meiobenthos on the shelf area studied.

Reference

NEHRING, D. (Editor); HAGEN, E.; JORGE DA SILVA, A.; SCHEMAINDA, R.; WOLF, G.; MICHELCHEN, N.; KAISER, W.; POSTEL, L.; GOSELCK, F.; BRENNING, U.; KÜHNER, E.; ARLT, G.; SIEGEL, H.; GOHS, L.; BUBLITZ, G.: The oceanological conditions in the western part of the Mozambique Channel in February—March 1980. — Geod. Geoph. Veröff. R. IV, H. 39 (1984), 163 S.

Addresses of authors:

Prof. Dr. sc. DIETWART NEHRING, Dr. sc. EBERHARD HAGEN, Dr. RUDOLF SCHEMAINDA, GERHARD WOLF, NORBERT MICHELCHEN, Dr. WOLFGANG KAISER, LUTZ POSTEL, HERBERT SIEGEL, Dr. LUDWIG GOHS, GÜNTHER BUBLITZ
Akademie der Wissenschaften der DDR
Institut für Meereskunde
DDR-2530 Rostock-Warnemünde

Dr. FRITZ GOSELCK, Dr. sc. ULLRICH BRENNING, Dr. sc. EUGEN KÜHNER, Dr. sc. GÜNTHER ARLT
Wilhelm-Pieck-Universität Rostock
Sektion Biologie
DDR-2500 Rostock, Wismarsche Str. 7—8

Dr. ANTÓNIO JORGE DA SILVA*)
Instituto de Desenvolvimento Pesqueiro
Maputo
PR Moçambique

*) Present address:
Instituto Hidrográfico
Rua das Trinas, 49
P-1296 Lisboa
Portugal

Received: August 30, 1985

Accepted: January 20, 1986

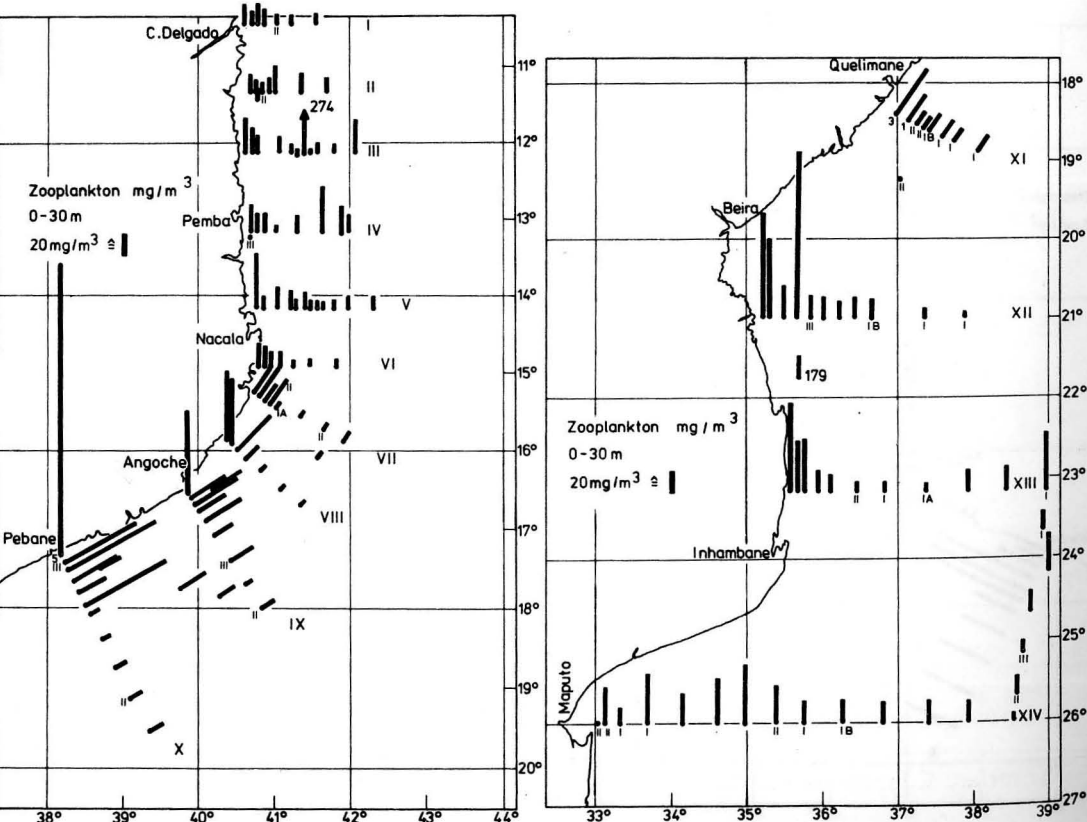


Fig. 14

Zooplankton biomass (dry weight; 0–30 m) in the northern area of the western Mozambique Channel (20-02 to 04-03-1980)

Fig. 15

Zooplankton biomass (dry weight; 0–30 m) in the southern area of the western Mozambique Channel (23-03 to 30-03-1980)

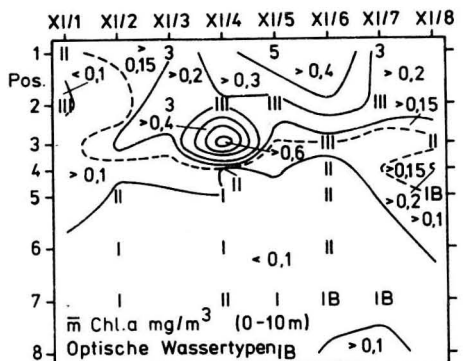


Fig. 16

Optical water types (I, IB, II, III by Jerlov) related to the mean chlorophyll a concentrations in the surface layer (0–10 m) on the rerun section XI

6. Investigations into the sea bottom

The surface sediments of the shelf area in the western Mozambique Channel are mainly of a sandy-silty nature and contain only small amounts of heavy-minerals. Higher

HARTMUT PRANDKE und ADOLF STIPS

Zur unterschiedlichen Ausprägung der Mikrostruktur von Temperatur und Salzgehalt in thermohalinen Sprungschichten

Mit 4 Abbildungen und 2 Tabellen

Zusammenfassung: Die unterschiedlich starke molekulare Diffusion von Temperatur und Salzgehalt bewirkt einen schnelleren Abbau mikromästablicher Schichtungsstrukturen der Temperatur als der des Salzgehaltes. Dies kann zu einer im Mittel stärkeren Ausprägung der Mikrostruktur des Salzgehaltes gegenüber der Temperatur in thermohalinen Sprungschichten führen. Dieser Effekt wurde am Beispiel der sommerlichen Temperatur/Salzgehaltssprungschicht der westlichen Ostsee untersucht. Während bei der Ausprägung der Stufenstruktur der Sprungschicht (vertikale Skala 0,2 ... 0,3 m) keine Unterschiede zwischen Temperatur und Salzgehalt festgestellt wurden, tritt im Bereich aktiver Mikrostruktur (vertikale Skala kleiner 0,15 m) eine signifikant stärkere Ausprägung der Mikrostruktur des Salzgehaltes gegenüber der Temperatur auf. Ausgehend von der unterschiedlichen Wirkung der molekularen Diffusion auf die Mikrostruktur der Temperatur und des Salzgehaltes wurde ein mittleres Alter der Stufenstruktur von ca. 2 Tagen und der Mikrostrukturpatch von ca. 10 Stunden abgeschätzt.

Abstract: The different coefficient of molecular diffusion of temperature and salinity leads to a more rapidly weakening of microscale stratification elements of temperature than of salinity. As a result of this process, a stronger pronounced microstructure of salinity than of temperature can appear. This effect was investigated for the temperature/salinity pycnocline (summertime stratification) in the western Baltic.

In contrast to the step-like structure of the pycnocline (vertical scale 0.2 ... 0.3 m), we found in the microstructure patches (internal vertical scales smaller 0.15 m) a significant stronger pronounced microstructure of salinity than of temperature. Based on the different effect of the molecular diffusion on the microstructure of temperature and salinity, we estimated a mean age of the step-like structure of about

2 days and a mean age of the microstructure patches of about 10 hours.

Резюме: Различная интенсивность молекулярной диффузии температуры и солености вызывает более быстрый распад микромасштабных структур температурных слоев, чем слоёв солености. Это может привести в среднем к более интенсивному проявленную микроструктуры солености сравнивательно с микроструктурой температуры в термохалинных слоях скачков. Такой эффект исследовался на примере летнего слоя скачка температуры/солености в западной части Балтийского моря. Если при образовании ступенчатой структуры слоя скачка (вертикальная шкала 0,2 ... 0,3 м) разница между температурой и соленостью не отмечается, то в зоне активной микроструктуры (вертикальная шкала менее 0,15 м) проявляется значительно большее образование микроструктуры солености, чем температуры. Исходя из различного действия молекулярной диффузии на микроструктуру температуры и солености оценочно определен средний возраст ступенчатой структуры около 2 дней и пятен микроструктуры около 10 часов.

1. Einleitung

Mikromästabliche Schichtungsstrukturen im Meer entstehen hauptsächlich durch Scherungsinstabilitäten, brechende interne Wellen und seegangsbedingte Vermischung. Diese Prozesse erzeugen vertikal und horizontal begrenzte Gebiete mit aktiver Turbulenz, die auch als Mikrostrukturpatch (aktive Mikrostruktur) bezeichnet werden. Nach Absterben der aktiven Turbulenz entstehen Wasserschichten mit geringeren mittleren Gradienten als im Wasserkörper oberhalb und

unterhalb. Die horizontale Ausdehnung dieser Schichten (Layer) kann dabei wesentlich größer sein als die horizontale Ausdehnung der Mikrostrukturpatche. Dies ist durch intrusive Prozesse bedingt (KUDIN und ABRAMJAN 1984). Die Layer sind nach oben und unten durch dünne Schichten mit stärkeren Temperatur- bzw. Salzgehaltsänderungen (Sheets) begrenzt. In ihrer Gesamtheit erzeugen die Sheets und Layer einen stufenförmigen Aufbau der Dichteschichtung (passive Mikrostruktur), der auch für die Sprungschichten der Ostsee typisch ist (PRANDKE und STIPS 1984a).

Eine an einem Ort zu einem bestimmten Zeitpunkt entstandene Mikrostruktur wird durch advektive und konvektive Vorgänge, interne Wellen und Stromscherungen in der Folgezeit modifiziert, wobei die in der Mikrostruktur-Schichtung enthaltene potentielle Energie erniedrigt wird (Glättung des Mikrostrukturprofiles). Zusätzlich zu diesen dynamischen Vorgängen wirkt die molekulare Diffusion von Temperatur- und Salzgehalt (WOODS und WILEY 1972). Dabei ist der molekulare Diffusionskoeffizient der Temperatur ca. 2 Größenordnungen größer als der des Salzgehaltes. Der große Unterschied zwischen thermischen und halinen Diffusionskoeffizienten lässt in thermohalinen Sprungschichten, wie sie im Sommer für die westliche Ostsee typisch sind, einen unterschiedlich starken Abbau thermischer und haliner Mikrostruktur erwarten. Als Folge davon muß auch eine unterschiedlich starke Ausprägung der Mikrostruktur der Temperatur und des Salzgehaltes auftreten. Der Abbau kleinskaliger Schichtungsstrukturen durch molekulare Diffusion bewirkt somit im Gegensatz zu der Wirkung der dynamischen Prozesse eine Verringerung der Kohärenz von Temperatur und Salzgehalt. Aus der Literatur sind bisher jedoch keine quantitativen Angaben bzw. experimentelle Untersuchungen dieses Effektes bekannt.

Neben der Glättung von Mikrostrukturprofilen führt die molekulare Diffusion von Temperatur und Salzgehalt unter bestimmten Schichtungsverhältnissen zu Doppeldif-

fusionsvorgängen („Salzfinger“), die einen erheblichen Beitrag zum Vertikaltransport von Masse und Energie im Meer leisten können (s. z. B. TURNER 1967). Dieser Effekt soll hier nicht betrachtet werden.

Ziel der durchgeföhrten Untersuchung ist es, die durch unterschiedliche molekulare Diffusionsgeschwindigkeit bedingten Unterschiede in der Ausprägung der Mikrostruktur von Temperatur und Salzgehalt in thermohalinen Sprungschichten qualitativ und quantitativ zu erfassen. Insbesondere soll untersucht werden, unter welchen Bedingungen und in welchem Skalenbereich der Mikrostruktur signifikante Unterschiede in der Ausprägung von Temperatur- und Salzgehaltsmikrostruktur auftreten.

Die experimentellen Untersuchungen wurden am Beispiel der sommerlichen thermohalinen Sprungschicht der westlichen Ostsee durchgeföhr. Diese Sprungschicht zeichnet sich durch große Temperatur- und Salzgehaltsgradienten aus und weist eine ausgeprägte Mikrostruktur auf. Die haline Sprungschicht der offenen Ostsee wurde wegen der geringen Ausprägung der Mikrostruktur (PRANDKE und STIPS 1984b) nicht berücksichtigt.

2. Zur Wirkung der molekularen Diffusion

Ausgehend von der Diffusionsgleichung für einen Parameter P

$$\frac{\partial P}{\partial t} - K_p \nabla^2 P = 0 \quad (1)$$

(∇ — Nablaoperator, K_p — molekularer Diffusionskoeffizient) erhält man bei Abhängigkeit nur von der Tiefe z und der Zeit t durch Fouriertransformation bezüglich z als Lösung der Differentialgleichung mit der Anfangsbedingung $P(z, 0) = P_0(z)$:

$$\tilde{P}(k, t) = \tilde{P}_0(k) \cdot e^{-K_p k^2 t} \quad (2)$$

($k = \frac{2\pi}{z}$ — Wellenzahl). Aus der Gleichung (2) ist erkennbar, daß ein gegebenes Anfangs-

spektrum bedingt durch die Wirkung der molekularen Diffusion zu hohen Wellenzahlen abfällt und eine zeitliche Dämpfung auftritt. Für einen Abfall des Spektrums auf die Hälfte seines ursprünglichen Wertes erhält man:

$$t_{1/2} = \frac{\ln 2}{K_p \cdot k^2}. \quad (3)$$

Für die Wirkung der molekularen Diffusion auf einen idealen scharfen Sprung des Parameters P am Ort $z_0 = 0$ zur Zeit $t = 0$ erhält man aus Gleichung (1) im Orts- und Zeitbereich für $t > 0$ nach LANDAU und LIFSHITZ (1966) die Lösung

$$P(z, t) = \frac{1}{\sqrt{2\pi}} \int_{-\infty}^{\infty} e^{-\frac{z^2}{2}} dz \\ = \frac{1}{2} + \text{erfc}\left(\frac{z}{\sqrt{2K_p t}}\right) \quad \text{für } z \geq 0, \quad (4)$$

welche gerade das Fehlerintegral ist. In der Abbildung 1 ist die Wirkung der molekularen Diffusion anschaulich dargestellt. Zur Charakterisierung der Schärfe des Sprunges wird im allgemeinen die Halbwertsbreite h ver-

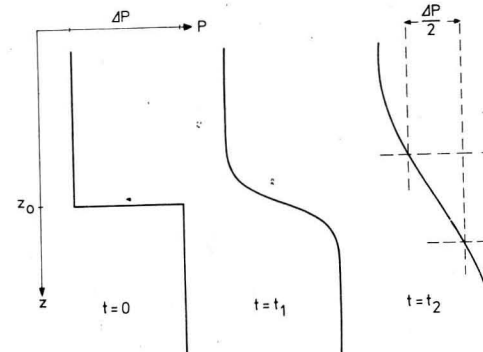


Abb. 1

Zur Wirkung der molekularen Diffusion auf einen idealen Sprung im Vertikalprofil des Parameters P . Die charakteristische Halbwertsbreite der Sprungschicht ist mit h gekennzeichnet.

wendet. Aus Gleichung (4) erhält man für h die Beziehung

$$h = \sqrt{0,91 K_p t_{1/2}}. \quad (5)$$

Der funktionale Zusammenhang zwischen $t_{1/2}$ und h ist in Abb. 2 für die Temperatur, $K_T = 2,9 \cdot 10^{-4} \text{ cm}^2/\text{s}$, und den Salzgehalt, $K_S = 5,8 \cdot 10^{-6} \text{ cm}^2/\text{s}$ (molekulare Diffusionskoeffizienten nach STOMMEL und FEDOROV 1967) dargestellt. Hieraus sind die großen Unterschiede in der Wirkung der molekularen Diffusion auf einen Sprung im Temperatur- und Salzgehaltsprofil erkennbar. Weiterhin ist sichtbar, daß die Wirkung der molekularen Diffusion besonders bei kleinen vertikalen Skalen von Bedeutung ist.

3. Meß- und Auswertemethoden

Für die hier dargelegten Untersuchungen standen ca. 150 Mikrostrukturondierungen der T/S-Sprungschicht der westlichen Ostsee mit der frei fallenden Mikrostrukturonde MSS zur Verfügung. Aufbau und Funktion sowie Meßfehler dieser Sonde, ebenso die angewendeten Verfahren der Datavalidation (dynamische Korrektur) sind von PRANDKE, KRÜGER und ROEDER (1985) ausführlich diskutiert worden. An dieser Stelle sei daher

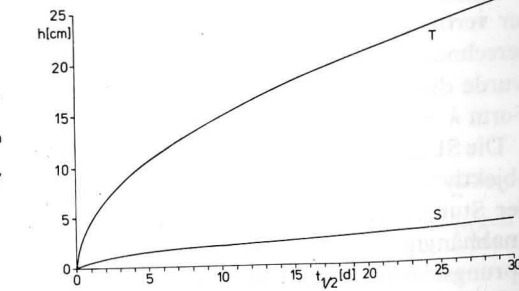


Abb. 2

Darstellung des Zusammenhangs zwischen der Halbwertsbreite h und dem Alter $t_{1/2}$ eines Sprunges im Vertikalprofil der Temperatur (T) und des Salzgehaltes (S)

nur auf einige wesentliche Parameter der Sonde hingewiesen. Mit der MSS werden Vertikalprofile der Temperatur und der elektrischen Leitfähigkeit in ausgewählten Tiefenbereichen (Sprungschicht) registriert. Die Sonde sinkt unbeeinflußt von den Rollbewegungen des Schiffes mit einer mittleren Sinkgeschwindigkeit von ca. 0,5 m/s. Die Ansprechzeit beider Sensoren beträgt 40 ms. Bei Anwendung einer dynamischen Korrektur sind somit vertikale Meßwertauflösungen von ca. 2 mm möglich.

Die Untersuchung des Einflusses unterschiedlicher molekularer Diffusionsgeschwindigkeiten auf die Ausprägung der Temperatur- und Salzgehaltsmikrostruktur erfolgte auf der Grundlage folgender Analysen:

- Analyse der Gradientenspektren von Temperatur und Salzgehalt sowie der Kohärenz zwischen den Gradientenprofilen von Temperatur und Salzgehalt
- Analyse der Ausprägung der Sheet-Layer-Struktur der Sprungschicht auf der Grundlage der SL-Zahl
- Analyse der Häufigkeit des Auftretens und der Eigenschaften aktiver Schichtungsbereiche (Mikrostrukturpatche).

Mittlere Gradientenspektren der Temperatur und des Salzgehaltes wurden aus 10 ausgewählten typischen Mikrostrukturprofilen der T/S-Sprungschicht berechnet. Ebenfalls aus diesen ausgewählten Profilen wurde die mittlere Kohärenz zwischen Temperatur- und Salzgehaltsgradienten in Abhängigkeit von der vertikalen Wellenzahl bestimmt. Bei der Berechnung der Spektren und der Kohärenz wurde die Wellenzahl k grundsätzlich in der Form $k = 1/\lambda$ (λ — Wellenlänge) benutzt.

Die SL-Zahl ist ein direktes und weitgehend objektives Maß für die Stärke der Ausbildung der Stufenstruktur der Sprungschichten, das unabhängig vom mittleren Gradienten der Sprungschicht ist und nicht durch willkürlich festgelegte Parameter wie Mittelungsweiten u. a. beeinflußt wird. Die SL-Zahl eines Ensembles von Sprungschichten ist definiert als das Verhältnis der mittleren Gradienten der Sheets zu den mittleren Gradienten der Layer. Die mittleren Gradienten

der Sheets und der Layer wurden aus den Beiträgen der Gradienten der entsprechenden Tiefenbereiche berechnet. Für die Bestimmung der SL-Zahl der Temperatur und des Salzgehaltes wurde ein Ensemble von 30 charakteristischen Profilen ausgewertet. Insgesamt wurden ca. 200 Sheets und Layer sowohl für die Temperatur als auch für den Salzgehalt bestimmt.

Die Identifikation aktiver Schichtungsbereiche erfolgte durch die Auszählung der Nulldurchgänge (NDG) der Gradienten von Temperatur und Salzgehalt in jeweils 20 cm dicken Tiefenintervallen der registrierten Profile. Einzelne isolierte Tiefenintervalle mit NDG wurden als aktiver Bereich betrachtet, wenn mindestens 2 NDG aufraten. Tiefenintervalle mit einem NDG wurden nur dann als aktiv betrachtet, wenn sie Teile ausgedehnter aktiver Schichtungsbereiche sind. Die Dicke eines aktiven Schichtungsbereiches ist die Summe der zusammenhängenden aktiven Tiefenintervalle. Als Maß für das Auftreten von aktiven Schichtungsbereichen wurde der mittlere aktive Teil der Sprungschicht bestimmt. Diese Größe ist der proportionale Anteil der Summe aller aktiven Tiefenbereiche an der Summe der Sprungschichtdicken des untersuchten Ensembles von Sprungschichten. Aus der mittleren Anzahl der NDG pro Meter in den aktiven Schichtungsbereichen wurde durch Kehrwertbildung die mittlere Separationslänge als charakteristisches Maß für die vertikale Ausdehnung der Strukturelemente innerhalb der aktiven Bereiche bestimmt.

Für die Analyse der aktiven Schichtungsbereiche wurden alle zur Verfügung stehenden Mikrostruktursondierungen der T/S-Sprungschicht der westlichen Ostsee herangezogen.

4. Meßergebnisse und Diskussion

4.1. Kohärenz zwischen Temperatur und Salzgehalt

In den Sprungschichten des offenen Ozeans tritt i. allg. zwischen der Temperatur und dem Salzgehalt nur im Bereich sehr kleiner Wellen-

zahlen ($k = 0,02\text{--}0,05 \text{ m}^{-1}$) ein kohärenter Verlauf auf, während bei größeren Wellenzahlen keine Kohärenz vorhanden ist (RODEN 1971). In der T/S-Sprungschicht der westlichen Ostsee konnten wir jedoch auch im Bereich sehr großer Wellenzahlen noch eine Kohärenz zwischen den Temperatur- und Salzgehaltsgradienten nachweisen. Aus Abb. 3 ist erkennbar, daß bei $k = 1 \text{ m}^{-1}$ und $k = 12 \text{ m}^{-1}$ deutliche Maxima im Kohärenzspektrum auftreten, die die 90%-Signifikanzschwelle überschreiten. Das Maximum bei $k = 1 \text{ m}^{-1}$ korrespondiert zu vertikalen Schichtungsstrukturen von ca. 50 cm Dicke. Dies ist gerade die mittlere vertikale Ausdehnung einer Stufe (Sheet + Layer) der Sheet-Layer-Struktur der untersuchten Sprungschicht. Das Maximum bei $k = 12 \text{ m}^{-1}$ korrespondiert zu Schichtungsstrukturen von ca. 4 cm Dicke. Strukturen mit diesen vertikalen Abmessungen sind für aktive Schichtungsbereiche charakteristisch.

Im Feinstrukturbereich ($k < 1 \text{ m}^{-1}$) wurde keine Kohärenz von Temperatur- und Salzgehaltsschichtung festgestellt. Dies ist damit zu erklären, daß die Schichtungsstrukturen im Feinstrukturbereich hauptsächlich durch advektive Vorgänge (salzarmes Ostseewasser über salzreichem Wasser aus dem Kattegat) entstehen. Die T-S-Eigenschaften dieser Wasserkörper sind nicht durch lokale Prozesse in

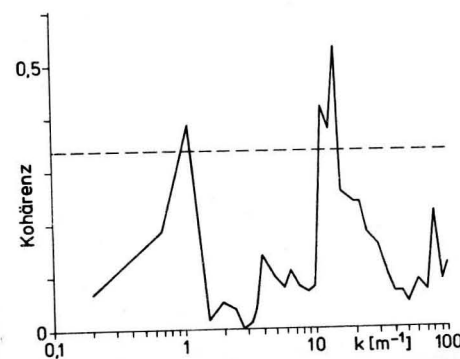


Abb. 3
Mittleres Kohärenzspektrum von Temperatur- und Salzgehaltsgradienten der T/S-Sprungschicht der westlichen Ostsee. Die 90%-Signifikanzschwelle ist gestrichelt eingezeichnet.

der westlichen Ostsee, sondern in entfernter Seegebieten, unabhängig voneinander, entstanden.

Die Kohärenz zwischen Temperatur und Salzgehalt im Skalenbereich der Sheet-Layer-Struktur und der Strukturen innerhalb der aktiven Bereiche zeigt, daß die Mikrostruktur von Temperatur und Salzgehalt durch Prozesse erzeugt wird, die auf beide Parameter gleichermaßen wirken. Diese Prozesse dominieren gegenüber der molekularen Diffusion, die auf Temperatur und Salzgehalt in unterschiedlichem Maße wirkt und somit eine Verringerung der Kohärenz erzeugt.

4.2. Spektren

Aus den Gradientenspektren der Temperatur und des Salzgehaltes (Abb. 4) ist zu erkennen,

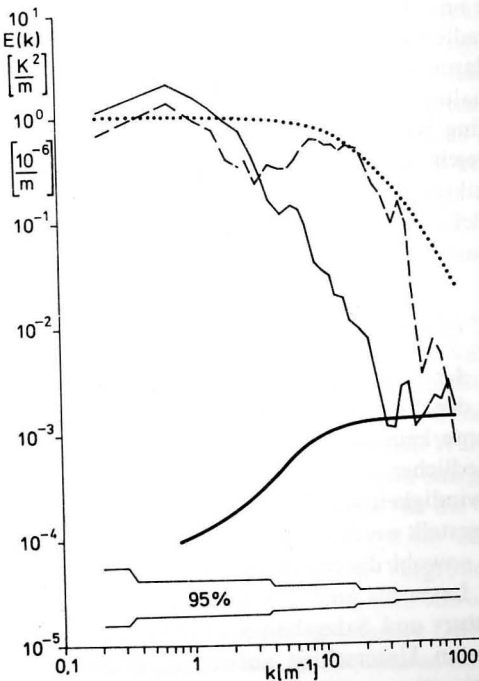


Abb. 4
Mittlere Gradientenspektren der Temperatur (durchgehende Linie) und des Salzgehaltes (gestrichelte Linie) der T/S-Sprungschicht der westlichen Ostsee. Dicke Linie: mittleres geglättetes Rauschspektrum; gepunktete Linie: Übertragungsfunktion des Meßsystems

daß in der *T/S*-Sprungschicht der westlichen Ostsee eine stärkere Ausprägung der Salzgehaltsmikrostruktur gegenüber der der Temperatur auftritt. Während im Bereich kleiner Wellenzahlen ($k < 3 \text{ m}^{-1}$) die Gradientenspektren von Temperatur und Salzgehalt einen parallelen Verlauf aufweisen, tritt im viskos-konvektiven Bereich ($k > 3 \text{ m}^{-1}$) eine signifikant stärkere Ausprägung der Mikrostruktur des Salzgehaltes in Erscheinung. Im Vergleich zur Temperatur liegt der cutoff (steiler Abfall des Spektrums) beim Salzgehalts-Gradientenspektrum bei größeren Wellenzahlen. Die cutoff-Wellenzahl (Beginn des steilen Abfalles des Spektrums) des Temperatur-Gradientenspektrums liegt bei ca. 20 m^{-1} , beim Salzgehalt liegt sie bei ca. 50 m^{-1} .

Ebenso wie die unterschiedliche Ausprägung des viskos-konvektiven Bereiches sind die unterschiedlichen cutoff-Wellenzahlen im Gradientenspektrum mit der geringeren molekularen Diffusionsgeschwindigkeit des Salzgehaltes zu erklären. Dadurch bleiben kleine haline Schichtungsstrukturen im Zentimeterbereich länger erhalten als entsprechende Strukturen im Temperaturprofil, die durch die molekulare Diffusion wesentlich schneller abgebaut werden.

4.3. Sheet-Layer-Struktur

Bei der Ausprägung der Sheet-Layer-Struktur der Temperatur- und Salzgehaltsprofile konnte kein signifikanter Einfluß der unterschiedlichen molekularen Diffusionsgeschwindigkeit von Temperatur und Salzgehalt festgestellt werden. Aus Tab. 1 ist zu erkennen, daß sowohl die mittleren Dicken der Sheets und Layer als auch die SL-Zahlen der Temperatur- und Salzgehaltsprofile keinen signifikanten Unterschied aufweisen. Dieses Ergebnis stimmt mit der aus der Analyse der Gradientenspektren gewonnenen Aussage überein, daß bei Schichtungsstrukturen größer $0,17 \text{ m}$ ($k < 3 \text{ m}^{-1}$) kein Unterschied in der Ausprägung der Mikrostruktur von Temperatur und Salzgehalt auftritt.

Tabelle 1

Zusammenstellung mittlerer Größen zur Charakterisierung der Sheet-Layer-Struktur von Temperatur und Salzgehalt in der *T/S*-Sprungschicht der westlichen Ostsee. $\bar{\Delta}L$ — mittlere Dicke der Layer, $\bar{\Delta}S$ — mittlere Dicke der Sheets. Die Zahlenangaben in den Klammern sind die 95%-Konfidenzintervalle (einseitig).

Parameter	$\bar{\Delta}L$ m	$\bar{\Delta}S$ m	SL-Zahl
Temperatur	0,29 (0,012)	0,18 (0,007)	4,84 (0,34)
Salzgehalt	0,31 (0,018)	0,18 (0,01)	5,17 (0,41)

4.4. Aktive Schichtungsbereiche

Im Gegensatz zur passiven Mikrostruktur (Sheet-Layer-Struktur) wurden bei der Häufigkeit und den Eigenschaften aktiver Schichtungsbereiche signifikante Unterschiede zwischen Temperatur und Salzgehalt festgestellt. Aus Tab. 2 ist ersichtlich, daß die Häufigkeit (mittlerer aktiver Teil der Sprungschicht) aktiver Salzgehaltsschichtung in der *T/S*-Sprungschicht der westlichen Ostsee ca. 1 Größenordnung über der Temperatur liegt. Die mittlere vertikale Abmessung der aktiven Schichtungsbereiche des Salzgehaltes ist ca. doppelt so groß wie bei der Temperatur. Der

Tabelle 2

Zusammenstellung mittlerer Größen zur Charakterisierung aktiver Schichtungsbereiche der Temperatur und des Salzgehaltes in der *T/S*-Sprungschicht der westlichen Ostsee. AT — mittlerer aktiver Teil der Sprungschicht, \bar{L}_p — mittlere Dicke der aktiven Schichtungsbereiche, \bar{L}_s — mittlere Separationslänge. Die Zahlenangaben in den Klammern sind die 95%-Konfidenzintervalle (einseitig).

Parameter	AT %	\bar{L}_p m	\bar{L}_s m
Temperatur	3,7	0,42 (0,043)	7,7 (0,48)
Salzgehalt	30,5	0,73 (0,047)	6,7 (0,22)

Vergleich dieser beiden Parameter (Häufigkeit und Patchdicke) zeigt, daß der größere mittlere aktive Teil der Sprungschicht beim Salzgehalt im wesentlichen durch eine größere Anzahl von Mikrostrukturpatchen, und nicht durch eine größere vertikale Ausdehnung dieser Schichtungsbereiche bedingt ist. Die größere Häufigkeit von Mikrostrukturpatchen im Salzgehalt gegenüber der Temperatur ist damit zu erklären, daß durch die wesentlich größere molekulare Diffusionsgeschwindigkeit der Temperatur die lokalen Gradienten dieses Parameters in den aktiven Schichtungsbereichen verhältnismäßig schnell abgebaut werden und somit im Gegensatz zum Salzgehalt nicht mehr den notwendigen Wert aufweisen, um bei der Auszählung der Null-durchgänge in Erscheinung zu treten.

Auch die charakteristischen vertikalen Skalen innerhalb der aktiven Bereiche zeigen einen signifikanten Einfluß der unterschiedlichen molekularen Diffusionsgeschwindigkeit von Temperatur und Salzgehalt. Während die mittlere Separationslänge beim Salzgehalt 6,7 cm beträgt, wurden für die Temperatur 7,7 cm bestimmt.

4.5. Abschätzung von Zeitskalen

Aus dem unterschiedlich starken Abbau kleinskaliger Schichtungsstrukturen des Salzgehaltes und der Temperatur durch molekulare Diffusion läßt sich das mittlere Alter dieser Strukturen abschätzen. Derartige Abschätzungen wurden für die Sheet-Layer-Struktur und die aktiven Schichtungsbereiche durchgeführt. Dabei wurde von folgenden Voraussetzungen ausgegangen:

1. Temperatur- und Salzgehalts-Mikrostruktur sind durch dynamische Vorgänge gleichzeitig und mit gleichen vertikalen Skalen entstanden. Molekulare Diffusionsvorgänge spielen bei der Entstehung aktiver Schichtungsbereiche (Zeitskale nach Woods und WILEY (1972) einige Minuten) keine Rolle.
2. Bedingt durch die geringe molekulare Diffusion, werden die kleinskaligen Schichtungsstrukturen des Salzgehaltes als konstant betrachtet.

3. Die in der Einleitung genannten dynamischen Vorgänge, die zur Modifizierung einmal entstandener Mikrostruktur führen, beeinträchtigen nicht die Wirkung der molekularen Diffusion und erzeugen keine neue aktive Vermischung.

Sheet-Layer-Struktur

Die mittlere Dicke der Sheets sowohl der Temperatur als auch des Salzgehaltes beträgt ca. $18 (\pm 1) \text{ cm}$ (s. Tab. 1). Wenn durch molekulare Diffusion der Temperatur ein signifikanter Unterschied in der Dicke der Sheets und damit in der Ausprägung der Sheet-Layer-Struktur der Temperatur und des Salzgehaltes auftreten soll, müßte sich die Dicke der Temperatur-Sheets um ca. $2,5 \text{ cm}$ vergrößern. Bei der Anfangsdicke eines Temperatursprunges von 18 cm ist dafür eine Zeitdauer für das Wirken der molekularen Diffusion von ca. 4 Tagen notwendig. Da zwischen der thermischen und der halinen Sheet-Layer-Struktur keine signifikanten Unterschiede festgestellt wurden, muß das mittlere Alter dieser Strukturen deutlich kleiner als 4 Tage sein.

Aktive Schichtungsbereiche

Bei der mittleren Separationslänge wurde zwischen der Temperatur und dem Salzgehalt ein signifikanter Unterschied festgestellt, der auf unterschiedliche molekulare Diffusionsgeschwindigkeit zurückzuführen ist. Während die mittlere Separationslänge beim Salzgehalt $6,7 (\pm 0,22) \text{ cm}$ beträgt, wurde für die Temperatur ein Wert von $7,7 (\pm 0,48) \text{ cm}$ ermittelt. (s. Tab. 2). Für die Vergrößerung einer Struktur im Temperaturprofil von $6,7 \text{ cm}$ Dicke auf $7,7 \text{ cm}$ durch molekulare Diffusion ist eine Zeitdauer von ca. 15 Stunden notwendig. Dies ist somit auch das mittlere Alter der in der *T/S*-Sprungschicht der westlichen Ostsee registrierten Mikrostrukturpatche.

Diese Abschätzungen sind konsistent mit der Abschätzung von Zeitskalen aus dem unterschiedlichen Verlauf der Temperatur- und Salzgehaltsgradientenspektren. Bei der

für aktive Schichtungsbereiche charakteristischen Wellenzahl $k = 10 \text{ m}^{-1}$ ist das Gradientenspektrum der Temperatur gegenüber dem des Salzgehaltes etwa um eine Größenordnung abgefallen. Modifiziert man Gleichung (3) entsprechend einem Abfall auf 10% und setzt den Wert $k = 10 \text{ m}^{-1}$ ein, so ergibt sich für die aktiven Schichtungsbereiche ein charakteristisches Alter von ca. 6 Stunden.

5. Schlußfolgerungen

Aus den durchgeföhrten Untersuchungen zum Einfluß der molekularen Diffusion von Temperatur und Salzgehalt auf die Ausprägung der Mikrostruktur in der T/S-Sprungschicht der westlichen Ostsee lassen sich folgende Schlußfolgerungen ziehen:

1. Im vertikalen Skalenbereich der Sheet-Layer-Struktur und der aktiven Schichtungsbereiche tritt eine signifikante Kohärenz zwischen Temperatur- und Salzgehaltsgradienten auf. Dies zeigt, daß die Temperatur- und Salzgehaltsmikrostruktur durch gleiche dynamische Prozesse erzeugt wird, die gegenüber der molekularen Diffusion dominieren.
 2. Ein meßbarer Einfluß der unterschiedlich starken molekularen Diffusion von Temperatur und Salzgehalt auf die Ausprägung der Mikrostruktur konnte nur bei vertikalen Skalen kleiner 17 cm (Skalenbereich aktiver Mikrostruktur) festgestellt werden. Hier tritt eine signifikant stärkere Ausprägung der Mikrostruktur des Salzgehaltes gegenüber der der Temperatur auf. Dies muß bei der Bestimmung der Mikrostruktur der Dichte, insbesondere bei der Abschätzung des durch lokale Turbulenz bedingten Vertikaltransports durch thermohaline Sprungschichten berücksichtigt werden.
 3. Aus der durch molekulare Diffusion bedingten unterschiedlich starken Ausprägung von Temperatur- und Salzgehaltsmikrostruktur lassen sich charakteristische Zeitskalen für das mittlere Alter von mikromästablichen Schichtungsstruk-
- turen abschätzen. Die Sheet-Layer-Struktur der T/S-Sprungschicht der westlichen Ostsee hat ein mittleres Alter von ca. 2 Tagen, das mittlere Alter der Mikrostrukturpatchs beträgt ca. 10 Stunden.

Literatur

- KUDIN, A. M.; ABRAMIAN, T. O.: Ob odnom fizičeskom mechanizme formirovania tonkoj struktury vod okeana. — Dokl. AN SSSR **276** (1984), 1464—1466.
- LANDAU, L. D.; LIFSHITZ, E. M.: Lehrbuch der theoretischen Physik, Bd. 6, Hydrodynamik, S. 222. — Berlin: Akademie-Verlag 1966.
- PRANDKE, H.; KRÜGER, S.; ROEDER, W.: Aufbau und Funktion einer frei fallenden Sonde zur Untersuchung der Mikrostruktur der thermohalinen Schichtung im Meer. — Acta Hydrophysica **29** (1985) H. 2/3, 165—210.
- PRANDKE, H.; STIPS, A.: The step-like structure of the Baltic pycnoclines. — Proceedings of the XIV Conference of Baltic Oceanographers, Gdynia, 28. Sept.—2. Oct. 1984, (1984a), 359—369.
- PRANDKE, H.; STIPS, A.: Microstructure patches in the Baltic pycnoclines. — Proceedings of the XIV Conference of Baltic Oceanographers, Gdynia, 28. Sept.—2. Oct. 1984, (1984b), 343—357.
- RODEN, G. I.: Spectra of North Pacific temperature and salinity perturbations in the depth domain. — J. phys. Oceanography **1** (1971), 25—33.
- STOMMEL, H.; FEDOROV, K. N.: Small scale structure in temperature and salinity near Timor and Mindanao. — Tellus **19** (1967), 306—325.
- THORPE, S. A.: Turbulence and mixing in a Scottish Loch. — Philos. Trans. royal Soc. London **A 286** (1977), 125—181.
- TURNER, J. S.: The influence of molecular diffusivity on turbulent entrainment across a density interface. — J. fluid Mechanics **33** (1968), 639—656.
- WOODS, J. D.; WILEY, R. L.: Billow turbulence and ocean microstructure. — Deep-Sea Research **19** (1972), 87—121.

Anschrift der Autoren:

Dr. HARTMUT PRANDKE
Dipl.-Phys. ADOLF STIPS
Akademie der Wissenschaften der DDR
Institut für Meereskunde
DDR-2530 Rostock-Warnemünde

Eingereicht: 25. Juli 1985

Zur Veröffentlichung angenommen: 31. Januar 1986

HERBERT SIEGEL

On the relationship between the spectral reflectance and inherent optical properties of oceanic water

With 10 figures

трацию хлорофилла и желтого вещества из коэффициента отражения без *in situ*-измерений.

1. Introduction

The spectral reflectance of seawater is produced and modified by the scattering and absorbing properties of pure seawater and of the material dissolved and suspended in it. The composition of these materials and their concentration can vary in dependence on the biological production in the water and on coastal influence, and in that connection also the spectral reflectance is a variable parameter.

To understand the effect of each component on the spectral reflectance it is necessary to carry out model calculations on this relationship as for instance by MOREL and PRIEUR (1977), OKAMI et al. (1982), LOKK and PURGA (1982), BUKATA et al. (1983).

The first step are calculations for ocean case 1 water, where the optical properties are determined by the pure sea water and the phytoplankton and its derivative products.

2. Calculations of spectral reflectances

One of the most important parameters for the determination of optical properties of seawater from remote measurements is the spectral reflectance.

In general the spectral reflectance represents the ratio of the upward irradiance E_u and the downward irradiance E_d just below the sea surface. If the radiance distribution just below the surface is given at a wavelength λ as

Резюме: Были проведены некоторые модельные расчеты о связи между коэффициентом диффузного отражения морской воды и собственными оптическими характеристиками. С помощью простого отношения можно изучить влияние оптических характеристик различных взвешенных и растворенных веществ на коэффициент отражения. Вычисленные коэффициенты для "случая-1 воды" хорошо совпадают с измерениями в Восточном Центральном Атлантическом Океане. Предлагается метод, с помощью которого можно определить концен-

$L(\Theta, \Phi, 0)$ the spectral reflectance can be written in the following form

$$R_w(0) = \frac{E_u(0)}{E_d(0)} \\ = \frac{\int_0^{2\pi} \int_{\pi/2}^{\pi} L(\Theta, \Phi, 0) \cos \Theta \sin \Theta d\Theta d\Phi}{\int_0^{2\pi} \int_0^{\pi/2} L(\Theta, \Phi, 0) \cos \Theta \sin \Theta d\Theta d\Phi} \quad (1)$$

where Θ is the zenith distance and Φ the azimuth.

Different models for the solving of the radiative transfer equation are used for the discussion the relation between the spectral reflectance and the inherent optical properties of seawater especially the backscattering coefficient b_b and the absorption coefficient a . The first way which was gone by different authors is the use of the two stream model as an approximating solution of the radiative transfer equation.

PREISENDORFER (1976) got the following expression

$$R_w(z) = \frac{b_{bd}(z)}{a_u(z) + b_{bu}(z) + K_u(z)}. \quad (2)$$

In this equation $b_{bd}(z)$ and $b_{bu}(z)$ are the backscattering coefficients for diffuse down- and upward radiation fluxes, a_u and K_u the absorption and attenuation coefficients for upward irradiance.

Equation (2) is an exact solution of the two stream model, but b_{bd} and b_{bu} are difficult to determine.

JOSEPH (1950) already used the two stream model and got the following expression after some approximations.

$$R_w(z) = \frac{\left(1 + \frac{2b_b}{a}\right)^{1/2} - 1}{\left(1 + \frac{2b_b}{a}\right)^{1/2} + 1} \approx \frac{b_b}{2a + b_b} \approx \frac{1}{2} \frac{b_b}{a}. \quad (3)$$

Many authors obtained nearly the same expression. GORDON et al. (1975) performed the complete solution of the radiative transfer equation using the Monte Carlo technique

for different inherent optical properties and radiation conditions. By regression analyses of the results they got the following polynom for R_w

$$R_w = \sum_0^3 r_n x^n, \quad x = \frac{b_b}{a + b_b}. \quad (4)$$

The term of 1. order provides the dominant contribution. The factor r_1 was found to be between 0.32 for solar illumination from near the zenith and 0.37 for total diffuse illumination.

KIRK (1981) applied also the Monte Carlo technique and got a linear relationship between R_w and b_b/a . For sun heights between 90° and 45° the coefficient varied between 0.328 and 0.391.

MOREL and PRIEUR (1977) obtained the relation

$$R_w = 0.33 \frac{b_b}{a} (1 + \Delta) \quad (5)$$

for the ratio $b_b/a < 0.3$ by using the successive order of scattering method.

The second order term Δ depends on the volume scattering function and the radiance distribution. For different cases they got a typical value $\Delta < \pm 5\%$. For practical purposes this value may be neglected.

This simple equation is in a good agreement with the relation from KIRK (1981) and GORDON et al. (1975). Its practical usefulness was shown for some cases.

For remote sensing studies it seems to be not necessary to use a more complicated relationship until a better knowledge of the absorbing and scattering properties of the dissolved and suspended material in seawater will be achieved (GORDON and MOREL 1983).

In the following the equation (5) is used for the study of the influence of the inherent optical properties of different materials in ocean water on the spectral reflectance. The backscattering coefficient b_b can be calculated from measurements of the volume scattering function $\beta(\gamma)$

$$b_b = 2\pi \int_{\pi/2}^{\pi} \beta(\gamma) \sin \gamma dy. \quad (6)$$

The total absorption and backscattering coefficients consist of the following components:

$$a = a_w + a_{ph} + a_y + a_x \quad (7)$$

$$b_b = b_{bw} + b_{bp}.$$

The indices denote pure seawater w, phytoplankton ph, dissolved organic substances (yellow substance) y, particles p and other constituents x.

In this paper the calculations of the relationship between the spectral reflectance and the inherent optical properties will be carried out for case 1 water (see MOREL and PRIEUR 1977). In case 1 water the inherent optical properties are determined by the pure sea water and the phytoplankton and its derivative products. Therefore the main components which influence the spectral reflectance are b_{bw} and a_w as well as a_{ph} , a_y and b_{bp} .

The actual absorption coefficient can be obtained from the concentration of the constituent and the specific absorption coefficient per volume unit. The spectral dependence of the absorption coefficient of pure seawater a_w as well as of the specific absorption coefficients of chlorophyll-a ($10 \text{ mg} \cdot \text{m}^{-3}$) and yellow substances ($1 \text{ mg} \cdot \text{dm}^{-3}$) are shown in Fig. 1. The specific absorption for natural phytoplankton was taken from LORENZEN

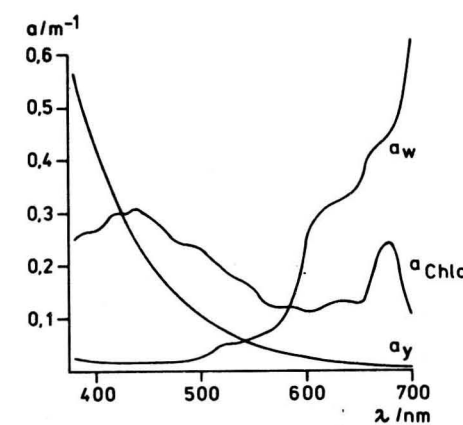


Fig. 1
Spectral absorption coefficients for pure seawater, chlorophyll a ($10 \text{ mg} \cdot \text{m}^{-3}$) and yellow substances ($1 \text{ mg} \cdot \text{dm}^{-3}$)

(1972) and for yellow substances from HØJERSLEV (1980) with the following spectral dependence

$$C_y = 4.72 a_y(\lambda) e^{0.0140(\lambda - 450)}. \quad (8)$$

For the spectral backscattering properties the equation from MOREL and PRIEUR (1977) was used in the following form.

$$b_b(\lambda) = b_{bw}(\lambda_0) \left(\frac{\lambda}{\lambda_0}\right)^{n_w} \\ + (b_b(\lambda_0) - b_{bw}(\lambda_0)) \left(\frac{\lambda}{\lambda_0}\right)^{n_p}. \quad (9)$$

The wavelength dependence of the molecular backscattering can be expressed by a power law. Usually the exponent $n_w = -4.3$ is used. From theoretical investigations for polydisperse particles with a Junge distribution and an exponent $-m$ it can be assumed to be $n_p = 3 - m$ with $m = 4$ for the most actual cases. The wavelength $\lambda_0 = 633$ was chosen

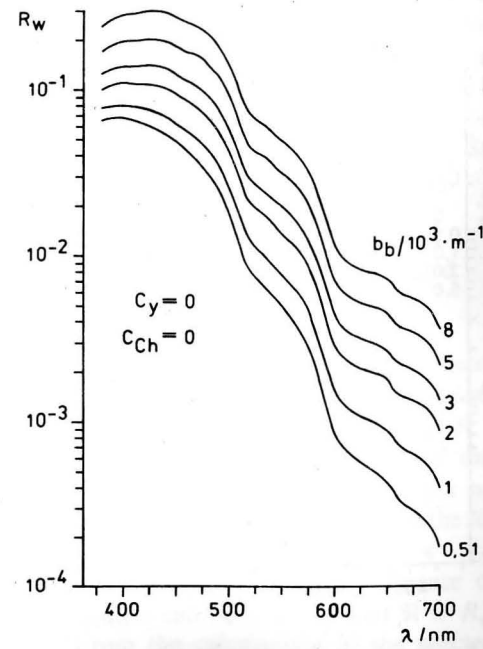


Fig. 2
Dependence of calculated reflectances on different backscattering coefficients ($C_y = 0, C_{Ch} = 0$)

for the spectral calculation of the backscattering coefficient. At this wavelength $\beta(\gamma)$ was measured.

To study the influence of each parameter the spectral reflectances were calculated according to equation (5) for different combinations of chlorophyll-a concentrations C_{ch} and of yellow substances C_y and with different backscattering coefficients. Fig. 2 shows the increase of the spectral reflectance in the spectral range between 380 nm and 700 nm with increasing backscattering coefficients for $C_y = 0$ and $C_{ch} = 0$. An increase of the concentrations C_{ch} and C_y and by this of the absorption leads to a decrease of the spectral reflectance in the shorter wavelength range (Fig. 3 and Fig. 4). The influence of the C_y variation is more significant than the influence of the C_{ch} variation. Fig. 5 describes the influence of $1 \text{ mg} \cdot \text{m}^{-3} C_{ch}$ in the presence of different C_y concentrations as possible in a case 1 water. The higher the C_y concentration the lower is the influence of $1 \text{ mg} \cdot \text{m}^{-3}$ chlorophyll-a.

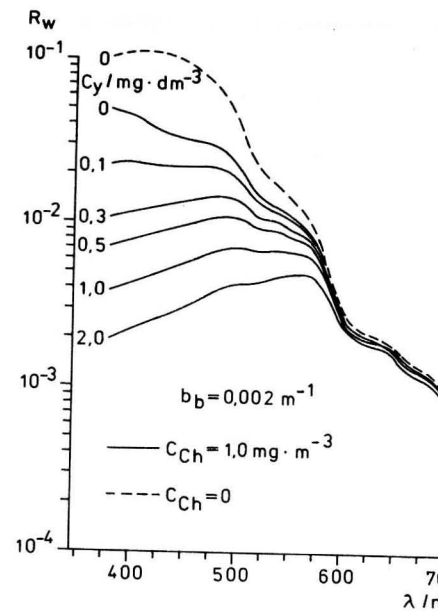


Fig. 4
Dependence of calculated reflectances on different concentrations of yellow substances ($b_b = 0.002 \text{ m}^{-1}$, $C_{ch} = 1.0 \text{ mg} \cdot \text{m}^{-3}$)

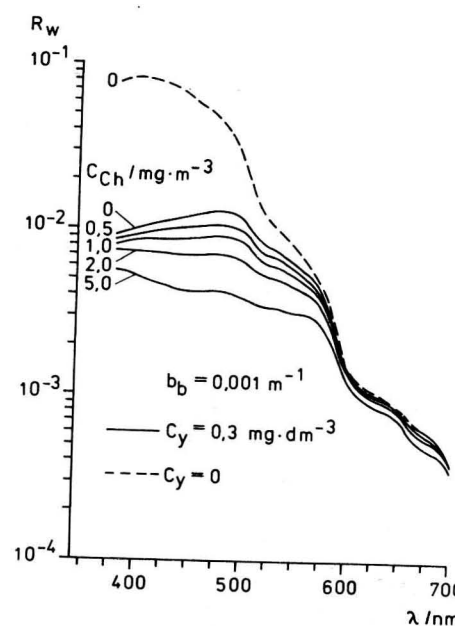


Fig. 5
Dependence of calculated reflectances on different concentrations of yellow substances ($b_b = 0.002 \text{ m}^{-1}$, $C_{ch} = 0$ and $1.0 \text{ mg} \cdot \text{m}^{-3}$)

In oceanic case 1 water an increase of the concentration of chlorophyll-a is correlated with increasing phytoplankton concentration, consequently the concentration of the

suspended matter and by this the scattering properties must be higher. From measurements in case 1 water we obtained an empirical relationship between the chlorophyll-a concentration and the backscattering coefficient. The dependence of the spectral reflectance from C_{ch} is shown in Fig. 6, where b_b was taken into account corresponding to this empirical correlation and $C_y = 0$. But in case 1 water C_y varies also. If the dissolved organic substances are derivative products of the phytoplankton then there must be a connection between C_{ch} and C_y . The variation of C_y in dependence of C_{ch} was approximately determined by measurements and fixed in Fig. 7. The spectral behaviour of the reflectance in dependence of the three parameters can be studied for their typical range for case 1 water on the basis of Fig. 6 and Fig. 7. In the short wavelength range the reflectances are governed by the absorption properties of chlorophyll-a and yellow substances. Low concentrations of C_{ch} and C_y lead to high reflectances. In the range between 520 nm and 560 nm there is an inter-

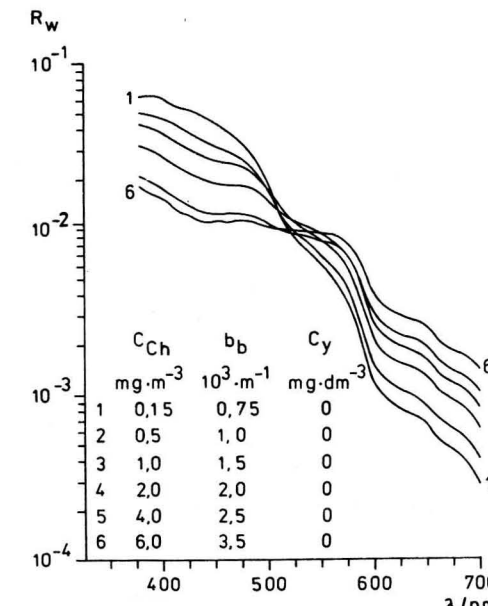


Fig. 6
Calculated reflectances for increasing b_b and C_{ch} as in case 1 water ($C_y = 0$)

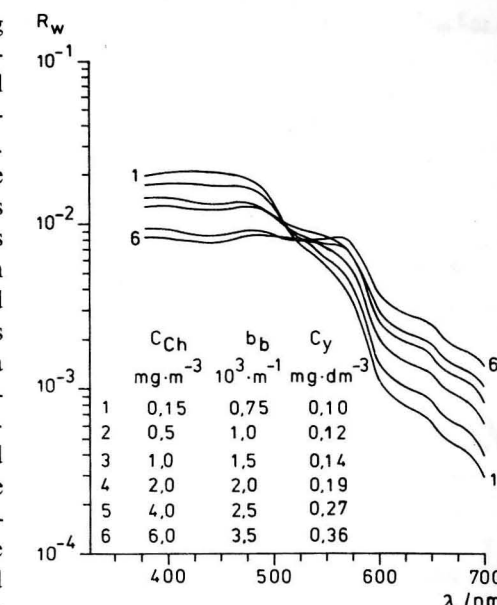


Fig. 7
Calculated reflectances for increasing b_b , C_{ch} and C_y as in case 1 water

section of the reflectance curves. This means that the height of the reflectance is determined by backscattering at longer wavelengths. The spectral reflectances presented in Fig. 7 are similar to the measured curves from the Eastern Central Atlantic Ocean (see SIEGEL, BROSIN 1986).

3. Comparison between calculated and measured reflectances

In the following we want to compare the calculated reflectances R_w with measured reflectances R . The reflectances R were determined from measurements of the upward radiance L_u just below the sea surface and downward irradiance E_G above the surface according to the relation $R = \pi \cdot L_u / E_G$. For an ocean without any influence of the bottom it can be assumed that $R \approx R_w$.

From the calculations of the spectral reflectances R_w it is possible to approximate the relationship between the backscattering coefficient b_b and the reflectance R_w at three

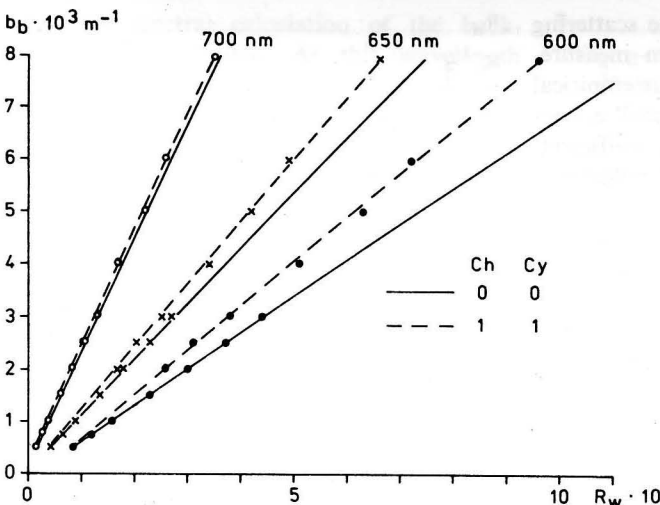


Fig. 8
 b_b (633 nm) determined from calculated reflectances

wavelengths (600, 650, 700 nm) as shown in Fig. 8. The reason of this relation is the dominating influence of backscattering on R_w in that spectral range. Using Fig. 8 the backscattering coefficient was determined from four examples of measured reflectances displayed in Fig. 9. From those b_b and measured C_{ch} and C_y the spectral reflectances were calculated. Fig. 10a-d show a good agreement between measured and calculated reflectances.

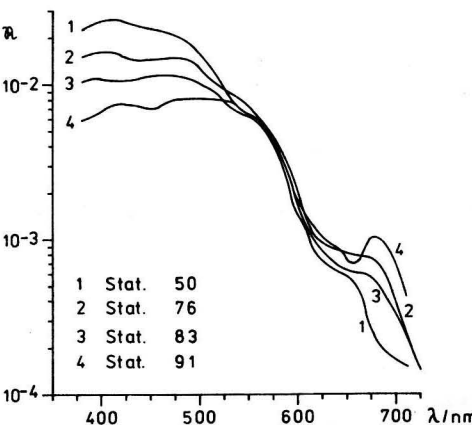


Fig. 9
 Measured reflectances for different stations in the Eastern Central Atlantic Ocean.

These results give the possibility to develop a method for the determination of composition and concentration of C_{ch} and C_y in oceanic case 1 water. Using the typical range of the values of C_{ch} and C_y as well as b_b for case 1 water we calculated the spectral reflectances R_w and collect them in a catalogue. b_b was chosen as the primary parameter in the catalogue. For each b_b -value and the typical C_{ch} - and C_y -values the reflectance curves were collected. Using Fig. 8 it is possible to determine b_b from measured reflectances. According to the b_b -value we compare the measured spectral curve with the calculated one. A good agreement gives us the concentration of C_{ch} and C_y from the parameters of the calculated reflectance. This method allows us to approximate the composition of C_{ch} and C_y in oceanic case 1 water from reflectance measurements using the total visible spectrum and not only a few wavelength as mentioned in chlorophyll algorithms for remote sensing studies.

4. Concluding remarks

The simple relation between the spectral reflectance and inherent optical properties of

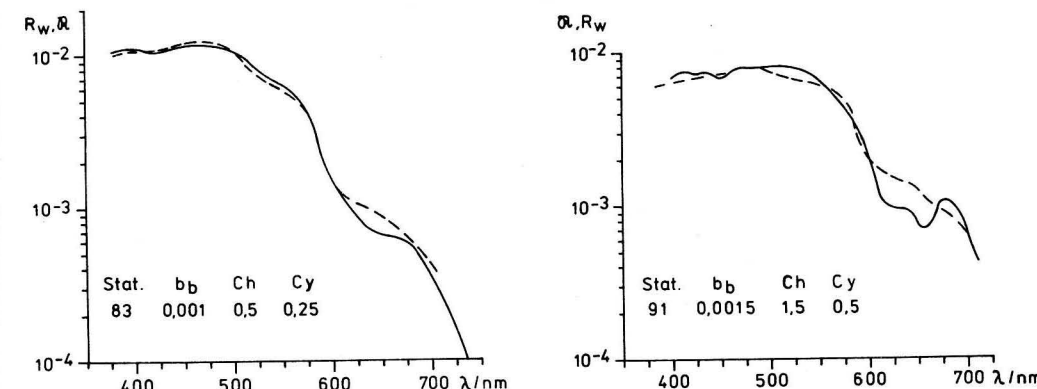
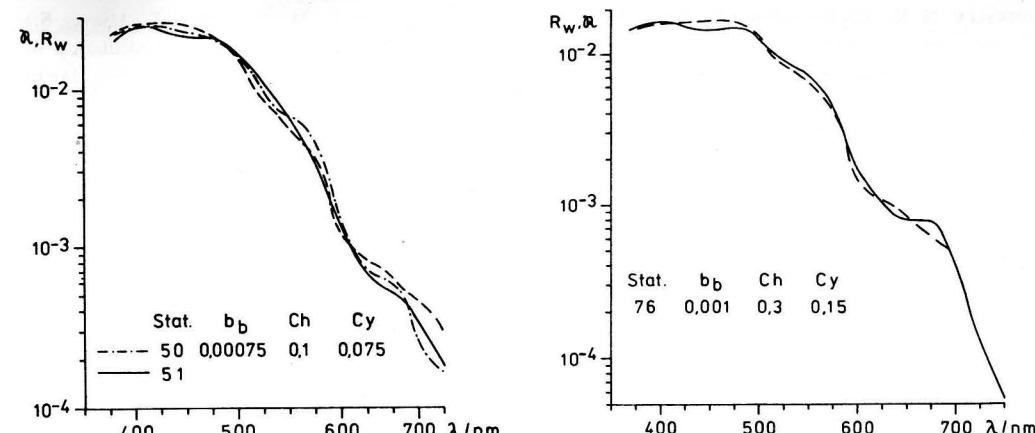


Fig. 10
 Comparison of measured (—) and calculated (---) reflectances

ocean water as suggested by MOREL and PRIEUR (1977) allows to study this relationship for case 1 water, where the optical properties are determined by the pure seawater and the phytoplankton and its derivative products.

Good correlations were found between measured and calculated reflectances.

It is possible to approximate the combination and concentration of chlorophyll-a and yellow substances from reflectance measurements from systematical investigations of this relationship and with a catalogue of calculated R_w curves for different b_b as well as C_{ch} and C_y .

References

- BUKATA, R. P.; BRUTON, J. E.; JEROME, J. H.: Use of chromaticity in remote measurements of water quality. — *Remote Sensing of Environment* 13 (1983), 161–177.
- GORDON, H. R.; MOREL, A.: Remote assessment of ocean color for interpretation of satellite visible imagery, a review. In: *Lecture notes in coastal and estuarine studies*. — New York: Springer-Verlag 1983, 111 pp.
- GORDON, H. R.; BROWN, O. B.; JACOBS, M. M.: Computed relationships between the inherent and apparent optical properties of a flat homogeneous ocean. — *Appl. Opt.* 14 (1975), 417–427.

- HØJERSLEV, N. K.: On the origin of yellow substance in marine environment. — Rep. Inst. Phys. Oceanogr. Univ. Copenhagen 42 (1980), 39—56.
- JOSEPH, J.: Untersuchungen über Ober- und Unterlichtmessungen im Meere und über ihren Zusammenhang mit Durchsichtigkeitsmessungen. — Dt. Hydrogr. Z. 3 (1950), 324—335.
- KIRK, J. T. O.: Monte Carlo study of the nature of the underwater light field in, and relationships between optical properties of, turbid yellow waters. — Aust. J. Mar. Freshwater Res. 32 (1981), 517—532.
- LOKK, J.; PURGA, A.: Water quality study of the Baltic Sea by optical remote sensing methods. In: Hydrodynamics of semi-enclosed seas, ed. by J. C. J. NIHOUL. — 1982, pp. 523—530.
- LORENZEN, C. J.: Extinction of light in the ocean by phytoplankton. — J. Cons. Int. Explor. Mer 34 (1972), 262—267.
- MOREL, A.; PRIEUR, L.: Analysis of variations in ocean color. — Limnology and oceanography 22 (1977) 4, 709—722.

- OKAMI, M.; KISHINO, M.; SUGIHARA, S.; UNOKI, S.: Analysis of ocean color spectra I. Calculation of irradiance reflectance. — J. Oceanogr. Soc. Japan 38 (1982) 4, 208—214.
- PREISENDORFER, R. W.: Hydrologic Optics. Vol. 5. Vol. 5. (US-Department of Commerce, National Oceanic and Atmospheric Administration, Honolulu 1976.
- SIEGEL, H.; BROSIN, H.-J.: Regional differences in the spectral reflectance of sea water. — Beitr. Meereskunde, H. 55 (1986), 71—77.

Address of the author:

Dipl.-Phys. HERBERT SIEGEL
Akademie der Wissenschaften der DDR
Institut für Meereskunde
DDR-2530 Rostock-Warnemünde

Received: July 12, 1985

Accepted: January 31, 1986

Beitr. Meereskd., Berlin 56 (1987) S. 81—82 (Wissenschaftliche Kurzmitteilung)

HERBERT FRANCK, WOLFGANG MATTHÄUS, RUDOLF SAMMLER

Major Baltic inflows during this century

With 2 figures and 1 table

The major inflows of saline water into the Baltic Sea have been investigated for the first time for the period from 1897 to 1976 using the daily salinity measurements at the light vessel "Gedser Rev". This analysis of the major Baltic inflows was carried out by means of a method suggested by WOLF (1972) and modified by the authors.

The general conditions for inflow events in the Darss Sill area (l/v "Gedser Rev") were defined by WOLF as follows:

1. The stratification coefficient $G = 1 - S_0/S_b$ (S_0 = surface salinity) must be ≤ 0.2 for at least 5 consecutive days, and
2. the bottom salinity S_b must be $\geq 17 \cdot 10^{-3}$. Further conditions have been specified as criteria to decide whether or not single days before, after or between detected inflow events may be added to the inflow period. The major Baltic inflows have been categoriz-

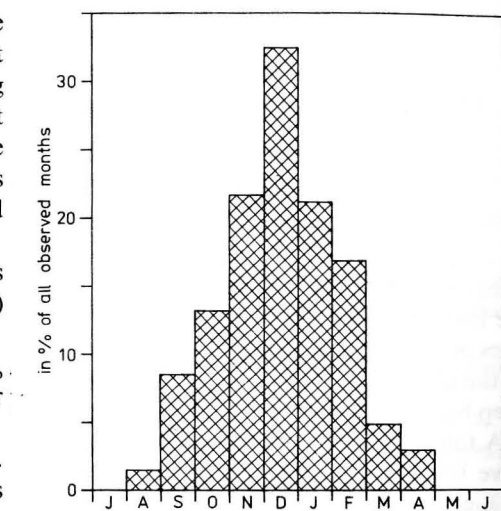


Fig. 2

Seasonal frequency distribution of the major Baltic inflows between 1897 and 1976

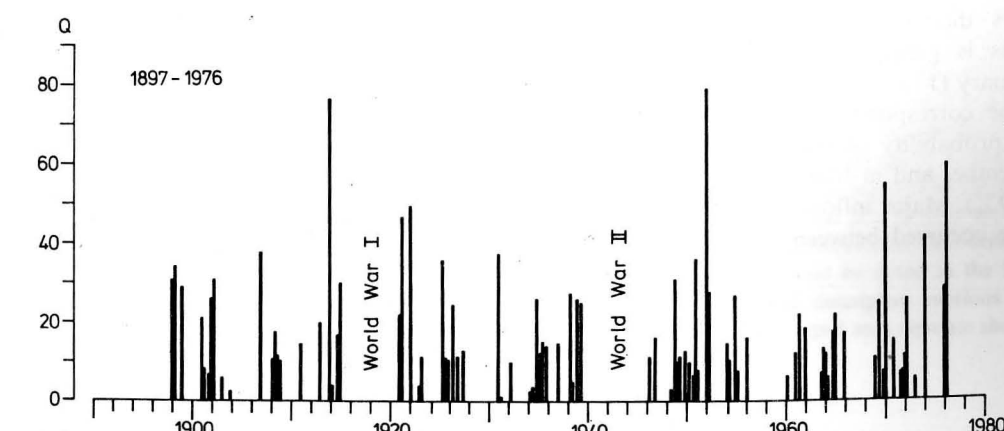


Fig. 1

Major inflows of saline water into the Baltic Sea between 1897 and 1976

Table 1

The most intensive Baltic inflows between 1897 and 1976

No.	Period	Q	k days	$S_p \cdot 10^3$	T_p °C	G_p
1	25. XI.—19. XII. 51	79.1	25	22.5	7.5	0.06
2	18. XI.—16. XII. 13	76.6	29	21.0	7.7	0.04
3	22. XII. 75—14. I. 76	60.0	24	20.1	4.1	0.03
4	29. X.—25. XI. 69	54.8	28	18.2	9.4	0.04
5	16. XII. 21—6. I. 22	49.4	22	19.2	4.0	0.04
6	17. I.—31. I. 21	46.6	15	20.7	3.4	0.10
7	13. XI.—29. XI. 73	41.4	17	19.4	6.6	0.04
8	26. XI.—13. XII. 06	38.0	18	18.7	6.8	0.05
9	10. XI.—20. XI. 30	37.3	11	20.5	8.4	0.03
10	28. IX.—15. X. 50	35.9	18	18.4	13.3	0.04

ed by means of an intensity index, Q , calculated from the length and mean salinity of the inflow period. This index, which characterizes the intensity of the inflows at the Darss Sill, does not always correspond to the magnitude of the effects such inflows have on the Baltic deep basins.

A total of 90 major inflows of saline water have been identified for 1897–1976 period. In Fig. 1 the distribution of the major inflows in time are given and characterized by the corresponding intensity indexes. This long-term study shows that major inflows occur in groups which are sometimes separated by long periods without inflow events. The seasonal frequency distribution in Fig. 2 shows that the frequency of such inflow events is greatest between November and February (17–32%; referred to the number of the corresponding observation months). The probability of such events in August/September and in March/April is only small (2–9%). Major inflows of saline water have never occurred between May and July.

In Table 1 the ten most intensive Baltic inflows classified according to Q are listed together with the duration of inflow k , the mean vertical salinity S_p , the mean vertical temperature T_p , and the mean stratification coefficient G_p of the inflow period. These inflow events occurred between 28 September and 31 January.

Reference

WOLF, G.: Salzwassereinbrüche im Gebiet der westlichen Ostsee. — Beitr. Meereskunde, No. 29 (1972), 67–77.

Address of the authors:

Dr. rer. nat. HERBERT FRANCK,
Dr. sc. nat. WOLFGANG MATTHÄUS,
RUDOLF SAMMLER
Akademie der Wissenschaften der DDR
Institut für Meereskunde
DDR-2530 Rostock-Warnemünde

Received: June 9, 1986

Accepted: June 16, 1986

Note to Contributors:

Manuscripts should be typed in double-spacing and submitted in three copies on white paper of size A4 (297 × 210 mm). Only one side of each sheet should be used. The margins should be 3.5 cm wide at the left side and 2.5 cm wide at the top. Manuscripts should not be longer than 20 pages (including figures). Authors will receive one proof copy for correction. Belated insertions or major changes to the text can not be considered.

Authors are requested to pay special attention to the subsequent notes regarding the preparation of the manuscripts. The following sequence should in general be used:

Title: Full name(s) of the author(s). Below it the complete title of the contribution in English, German and Russian.

Abstract, Zusammenfassung, Résumé: A brief but cogent summary in English, German and Russian must precede each contribution. It should contain informations regarding the methods used and the most important conclusions reached by the author.

Text: Pages belonging to the manuscript must be numbered consecutively. The contribution should be clearly arranged, and the chapters should be consecutively numbered.

The following print instructions are to be inserted by the author (in pencil!): spaced print: underlined with dashes; small print: vertical line in the left margin; italics: underlined with undulating line. The names of all authors cited must be written in capitals with the year of publication in brackets after the name. The recommendations given in

the IAPSO-SUN report should be taken into account when presenting measured data (S.I. units). Mathematical symbols, formulae and letters that cannot be typed must be entered carefully and clearly by hand.

Abbreviations should be used only if required repeatedly in the text and should, if necessary, be explained separately at the end of the contribution.

References: The authors cited in the text should be listed alphabetically at the end of the contribution in the following way:

Books: LEBLOND, P. H.; MYSAK, L. A.: Waves in the Ocean. — Amsterdam: Elsevier 1978.

Journals: VERONIS, G.; MORGAN, G. W.: A study of the time-dependent wind-driven ocean circulation. — Tellus 7 (1955) 2, 232–247.

Abbreviations for journal titles should conform to the procedure of libraries; for non-periodicals, add "No." (of the issue) to avoid confusions.

Author's address: The date on which the contribution was concluded, the full name(s) of the author(s) and their affiliation should be typed at the end of the manuscript.

Figures, tables, legends: Figures must be submitted in printable form drawn on tracing paper with black Indian ink or as photographic copies (black and white). Figures and tables should be numbered according to their sequence in the text and identified on the reverse side by their appropriate number and the author's name. Their desired position in the text should be noted in the left margin. All tables and descriptive captions to figures and tables to be typed on a separate sheet.

Инструкция для авторов:

Машинописные статьи следует высыпать в трех экземплярах на белой бумаге формата А4 (297×210 мм) с полями в 3,5 см (слева) и 2,5 см (вверху) соответственно при письме только на одной стороне листа через два интервала. Объем статьи, по возможности, не должен превышать 20 страниц (включая рисунки). Для разовой корректуры автору передается корректурный оттиск статьи, поэтому дополнительные вставки или значительные изменения текста исключаются.

В ходе оформления статьи просим учесть следующие указания и принять такую последовательность частей рукописи:

Название: Имя (имена) и фамилия (фамилии) автора(ов), под ними: полное название статьи на немецком, английском и русском языках.

Резюме, Zusammenfassung, Abstract: Предположить каждой статье краткое, но содержательное резюме на русском, немецком и английском языках. Оно должно содержать информацию о применяемых методах исследований и основные выводы автора.

Текстовая часть: Следует нумеровать страницы статьи по порядку. Статья должна обладать четкой структурой с нумерацией глав по порядку.

Автор должен внести в рукопись следующие заметки (карандашом!): разрядка — ломаная линия, мелкий шрифт — вертикальная линия с левого края, курсив — волнистая линия.

Фамилии цитируемых авторов писать прописными буквами, а год публикации — в скобках.

Приводя данные измерений, автор должен принять во внимание рекомендации Междуна-

родной системы единиц (СИ). Математические символы, формулы, а также буквы, которые не могут быть напечатаны на машинке, должны быть тщательно и четко внесены от руки. Сокращения в тексте допускаются только в случае повторов и, при необходимости, объяснены в конце статьи.

Литература: Список цитируемых в тексте авторов, должен быть приведен согласно образцу в алфавитном порядке:

Книги: LEBLOND, P. H.; MYSAK, L. A.: Waves in the Ocean. — Amsterdam: Elsevier 1978.

Журналы: VERONIS, G.; MORGAN, G. W.: A study of the time-dependent wind-driven ocean circulation. — Tellus 7 (1955) 2, 232—247.

Сокращать названия журналов можно только так, как принято в библиотеках. С целью избежания недоразумений рекомендуется добавить к названиям журналов, выходящих непериодично, № выпуска.

Адрес автора: В конце рукописи следует указать: дату окончания работы, полные имя (имена) и фамилию(и) автора(ов), адрес института(ов) или организаций(и).

Рисунки, таблицы, условные обозначения: Рисунки должны быть четкими и оформлены на кальке (черной тушью) или фотобумаге (черно-белой). Рисунки и таблицы должны быть пронумерованы по порядку, а на обороте следует написать, фамилию автора и номер рисунка или таблицы. Их местонахождение в тексте следует пометить на левом поле. Таблицы, заголовки таблиц и подписи к рисункам (условные обозначения) должны быть написаны отдельно.

Hinweise für Autoren:

Die Manuskripte sind in Maschinenschrift (zwei-zeilig) auf weißem, einseitig beschriebenem Papier im A4-Format (297×210 mm) mit jeweils 3,5 cm (links) und 2,5 cm (oben) breiten Rändern sowie in dreifacher Ausfertigung einzureichen. Der Umfang eines Beitrags sollte 20 Manuskriptseiten (einschließlich Abbildungen) nicht überschreiten. Dem Autor wird zur einmaligen Korrektur ein Umbruch-Exemplar seines Beitrags zugesandt; nachträgliche Einfügungen oder größere Textveränderungen sind daher nicht möglich.

Bei der formellen Gestaltung des Beitrags wird um die Beachtung folgender Richtlinien und um die Einhaltung der Abfolge nachstehend aufgeführter Details des Manuskripts gebeten:

Titel: Vor- und Zuname(n) des Autors (der Autoren). Darunter: Vollständiger Titel des Beitrags in deutscher, englischer und russischer Sprache.

Zusammenfassung, Abstract, Резюме: Jedem Beitrag ist eine kurzgefaßte, aber aussagekräftige Zusammenfassung in deutscher, englischer und russischer Sprache voranzustellen. Sie sollte Informationen über die angewandten Untersuchungsmethoden sowie die wichtigsten Ergebnisse und Schlußfolgerungen beinhalten.

Textteil: Die Seiten des Manuskripts sind fortlaufend zu numerieren. Der Beitrag sollte eine klare Gliederung mit fortlaufend nummerierten Kapitelüberschriften aufweisen.

Folgende Auszeichnungen sind vom Autor (mit Bleistift!) vorzunehmen: Sperrdruck: unterbrochene Linie; Kleindruck: senkrechte Linie am linken Rand; kursiv: Wellenlinie.

Zitierte Autorennamen werden grundsätzlich in Großbuchstaben und das Jahr der Publikation in Klammern angegeben. Für die Wiedergabe von Meßwerten sind die Empfehlungen des IAPSO-

SUN Reports (SI-Einheiten) zu beachten. Mathematische Symbole, Formeln und Buchstaben, die nicht in Maschinenschrift ausgeführt werden können, sind sorgfältig und deutlich lesbar mit der Hand einzutragen.

Abkürzungen sollten nur bei wiederholtem Gebrauch im Text verwendet und erforderlichenfalls am Ende des Beitrags gesondert erläutert werden.

Literaturverzeichnis: Die im Textteil zitierten Autoren werden nach folgendem Muster in alphabetischer Reihenfolge aufgeführt:

Bücher: LEBLOND, P. H.; MYSAK, L. A.: Waves in the Ocean. — Amsterdam: Elsevier 1978.

Zeitschriften: VERONIS, G.; MORGAN, G. W.: A study of the time-dependent wind-driven ocean circulation. — Tellus 7 (1955) 2, 232—247.

Die Abkürzung der Zeitschriftentitel ist wie in Bibliotheken üblich vorzunehmen. Bei nichtperiodisch erscheinenden Zeitschriften sollte „H.“ (Heft) ergänzt werden, um Verwechslungen zu vermeiden.

Anschrift des Autors: Am Ende des Manuskripts sind das Abschlußdatum der Arbeit, der (die) vollständige(n) Name(n) des Autors (der Autoren) sowie die Anschrift der Institution(en) anzugeben.

Abbildungen, Tabellen, Legenden: Abbildungen sind in reproduktionsfähigem Zustand auf Transparentpapier (in schwarzer Tusche) oder auf Fotopapier (schwarz-weiß) einzureichen. Abbildungen und Tabellen müssen durchlaufend nummeriert und auf der Rückseite mit dem Namen des Autors und der Abbildungs-/Tabellennummer versehen werden. Ihre gewünschte Plazierung im Text ist jeweils auf dem linken Rand anzugeben. Tabellen, Tabelleüberschriften sowie Abbildungsunterschriften (-legenden) sind grundsätzlich gesondert als Manuskript zu schreiben.